Characterisation of Uncured Carbon Fibre Prepreg

Erland, Samuel

Award date:
2017

Awarding institution:
University of Bath

Characterisation of uncured carbon fibre composites

submitted by

Samuel Erland

for the degree of Doctor of Philosophy

of the

University of Bath

Department of Mechanical Engineering

October 2016

ABSTRACT

The weight saving benefits of carbon fibre composites have been keenly adopted by civil aviation, with over 50% of the weight of modern designs coming from the carbon fibre components. The rapid rise in demand for this new material has led to the development of fully automated manufacturing techniques, improving rate of production and repeatability of manufacture. However, this rapid development, combined with a constant drive for increased rate of manufacture from industry can result in the formation of critical defects in the more complicated structural components.

Manufacturing complex aeronautical structures from carbon fibre leads to a number of interesting mechanical problems. Forcing a multi-layered laminate to conform to a curved geometry requires individual layers to move relative to one another in order to relieve various forming-induced stresses. If the layers are constrained the dissipation of these stresses in the form of interply shear is prevented and a wide range of defects can occur, compromising the integrity of the final component. One of the most important of these is fibre wrinkling, which is effectively the buckling of one or more layers within an uncured laminate. This buckle results in a localised change in fibre orientation, which can result in a significant knockdown in part strength.

A large amount of research has been conducted on carbon fibre in its cured state, when it exists as elastic fibres in an elastic matrix. Manufacturing occurs when the material is uncured however, with modern processes typically using fibres which are pre-impregnated with resin in order to reduce void content and aid fibre placement. A ply of uncured material therefore consists of stiff elastic fibres suspended in a very weak liquid viscoelastic material, whose properties are hugely influenced by temperature and rate of deformation.

This thesis builds a better understanding of the mechanics involved in forming, using a series of characterisation techniques developed drawing from techniques in the literature. Part of the process involves the fitting of a one-dimensional viscoelasto-plastic model to experimental test data in order to represent the material response when

shearing two plies about their interface. This model shows the material response to be dominated by the viscoelastic resin at low temperatures, before becoming frictional and fibre dominated at higher temperatures. In terms of optimum formability, a region exists in the transition from the viscous to frictional behaviour at which resistance to forming is minimised. With this data alone, optimum forming parameters such as rate of deformation, pressure and temperature can be suggested based on the material being used, along with design parameters such as stacking sequence.

Another important characteristic which must be understood when considering ply wrinkling is the bending stiffness of uncured prepreg, both as a single ply and when combined to form a small laminate. A wrinkle is in effect the buckling of a single or small number of plies within a laminate, therefore by understanding the bending stiffness and process-induced loading we can begin to predict whether or not wrinkles are likely to occur for a particular manufacturing regime. In order to assess bending stiffness, a modified Dynamic Mechanical Analysis process is employed, replacing the standard Engineers Bending Theory calculations with a Timoshenko element to capture the large degree of intraply shear experienced in the bending of uncured prepreg.

Finally, a small laminate scale demonstrator is considered in which a 24-ply laminate is consolidated into a female tool in such a way as to induced maximum shear strain between the plies, in order that the optimum forming parameters predicted by the characterisation tests might be validated. A simple energy minimisation model is used to predict the variation in consolidation strain around the part due to resistance to shear, using material parameters from the model describing the inter-ply shear test data. These parameters are also used to inform a novel modelling technique which has been developed parallel to this thesis, which is validated against the experimental results, and shows how the characterisation techniques can be used to advance simulation methods aimed at reducing the development time for new carbon fibre components.

This work provides a set of tests and methodologies for the accurate characterisation of the behaviour of uncured carbon fibre during forming. The models developed alongside these tests allow for a detailed interrogation of the results, providing valuable insight into the mechanics behind the observed material behaviour and enabling informed decisions to be made regarding the forming process in order that the occurrence of defects might be minimised. The primary aim has been to provide a set of vital input parameters for novel, complex process modelling techniques under development, which has been achieved and validated experimentally.

ACKNOWLEDGEMENTS

Firstly I would like to thank Dr. Timothy Dodwell who has provided a huge amount of tutelage and supervision through my whole PhD. Equally I would like to thank Prof. Richard Butler for agreeing to take on a Civil Engineering graduate for a PhD in mixed Mechanical Engineering and Materials Science! Hopefully it paid off...

Special mention must be given to a number of people, especially the technical staff at the University of Bath, namely Steve Thomas and Clare Ball, for listening to my ideas then making them a reality in the labs. I would also like to thank Kevin Johnson for letting me make use of some of his test data, and without whom the final chapter of the thesis could not have been achieved. In a similar vein, I would like to thank Prof. Oana Ghita from the University of Exeter for allowing me the use of her Dynamic Mechanical Analysis rig. Special mention must be given to Chris Jones for first hiring me on an EngD with GKN Aerospace and the University of Surrey then facilitating my transferral to the University of Bath when that arrangement broke down, and for his friendship throughout. On that note I would also like to thank GKN Aerospace for providing me with the opportunity to conduct this research and the financial support without which I could not have eaten!

Finally, I would like to thank my parents who have constantly supported me throughout the whole process without question.

CONTENTS

LIST OF FIGURES

LIST OF TABLES

NOMENCLATURE

Coordinates, dimensions and angles

s_{pre}	Pre-debulk arclength
s_{post}	Post-debulk arclength
h	Two ply thickness
θ	Tool angle
θ_x	Timoshenko rotation
r	Tool radius
ϕ	Ply angle
ϕ_μ	Angle of internal friction
R	Rate of displacement
T	Time
A	Area
ℓ	DMA sample length
b	DMA sample width
t	DMA sample thickness

Material Properties

η	Coefficient of viscosity
μ	Coefficient of friction
K	Initial stiffness
K_t	Post-yield stiffness
E	Young's modulus
E_c	Combined modulus
j	Joint strength
H	Work hardening parameter
S	Rate independent shear modulus

G	Shear modulus
I	Second moment of area
f	Fibre volume fraction
V	Volume
C	Consolidation coefficient

Energy

W	Total potential energy functional
U_S	Energy in shear
U_C	Energy in consolidation
w_q	Work done by the bag

Loads, amplitudes and wavelengths

P	Load
τ	Shear stress
τ_c	Critical shear stress
γ	Shear strain
γ_c	Critical shear strain
$\gamma_v e$	Viscoelastic shear strain
γ_p	Plastic shear strain
γ_{form}	Forming induced shear strain
$\gamma_{cons.}$	Consolidation induced shear strain
σ	Stress
σ_n	Normal stress or pressure
ω	Frequency
δ	Phase difference
w	DMA applied deformation
Δ	Deformation
ν	Consolidation strain
q	Applied pressure

Miscellaneous

N	Number of layers

α	Percentage consolidation
β	Shear modifier
y_t	Time series
T_t	Time independent component
S_t	Time dependent component
$_{lam}$	Laminate parameter
$_{ply}$	Ply parameter
$_{int}$	Interface parameter
$_{s}$	Spring parameter
$_{d}$	Dashpot parameter
$\dot{}$	Differentiation with respect to time
$_{e}$	Elastic parameter
$_{v}$	Viscous parameter
$_{f}$	Fibre parameter
$_{max}$	Maximum value of parameter
$_{phi}$	Parameter of ply angle ϕ
$_{0}$	Parameter of 0° ply

Abbreviations

AFP	Automatic Fibre Placement
ATL	Automated Tape Laying
DDF	Double Diaphragm Forming
DMA	Dynamic Mechanical Analysis
HDF	Hot Drape Forming
IPS	Inter-ply shear
PJN	Pin-jointed Net
UD	Unidirectional

CHAPTER 1

INTRODUCTION

Whilst the basic advantages of composite materials are well proven, they are often compromised by high costs, long development time, and poor quality due to manufacturing defects. This is particularly the case for the complex structures found in large aerospace applications built from unidirectional prepreg, which is preferred in automated deposition processes but significantly harder to form. The problem begins with a lack of depth of understanding surrounding the fundamental mechanisms behind the forming of certain defects. Whilst the causes for defects and even the mechanisms themselves have been identified across various bodies of work, little has been done to accurately characterise the behaviour of uncured unidirectional prepreg, and those bodies of work which have attempted this regularly apply significant assumptions regarding the nature of the material. The difficulty with characterising uncured prepreg lies in its highly heterogeneous nature (Fig. 1-1), comprised as it is of stiff fibres and very weak, fluid resin.

The significant contrast between the stiffness of carbon fibre and uncured resin is further complicated by the former acting as a purely elastic solid, whilst the latter acts as a viscoelastic fluid whose properties are hugely influenced by temperature and rate of deformation. The challenge therefore is to determine which component of the composite is dominant in responding to various loading scenarios. As a basic example, tensile loading along the fibre orientation clearly results in a fibre dominated response, whereas loading orthogonal to the fibre invokes a resin dominated response. The loading scenarios which give rise to defect formation are significantly more complex, invoking mixed responses from the constituent materials which must be separated if they are to be understood. If a viable characterisation regime is to be established the mechanisms governing formability and defect generation must be identified and

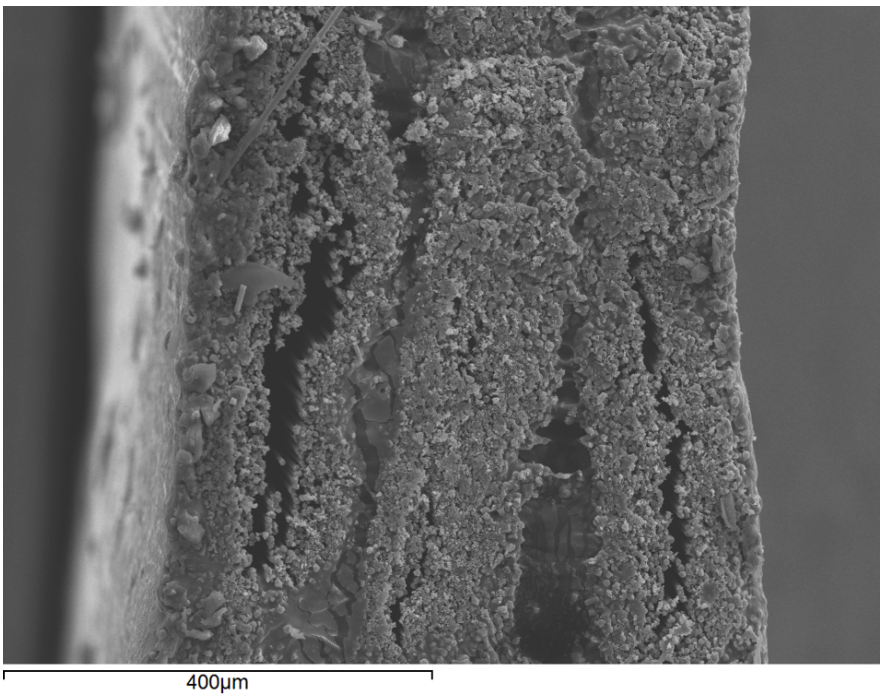

Figure 1-1: *Cross-sectional image of three uncured unidirectional plies of 8552/AS4 taken at 300x magnification. Distinct regions of fibre, resin and air can be seen, which contribute to the material behaviour in very different ways when under the influence of heat, pressure and deformation.*

investigated. From observation, two key mechanisms exist in the forming of complex composite components; (1) the shearing at the interface of the plies as the laminate conforms to curved geometries, and (2) the bending stiffness of the plies, which is vital in resisting buckling under the influence of end loading.

1.1 The motivation for this thesis

Commercially viable process modelling of the manufacturing process for large composite components is currently hindered in two areas. Firstly, current modelling techniques require prohibitively fine meshing in order to capture the contrast between the stiff fibres and the weak uncured resin, meaning components up to tens of metres in length must be modelled with elements of just a few microns in size. This problem is the motivation for a new form of model being developed at the Universities of Bath and Exeter based on Cosserat principles, which is capable of representing fine scale effects on a coarse mesh via the use of additional rotational degrees of freedom not commonly considered. The second area holding back modelling efforts, including this novel technique, is the lack of accurate material characterisation techniques, particu-

larly for unidirectional materials. The intent of this work is therefore to attain a deeper understanding of the mechanisms at play during forming processes, and develop characterisation methods capable of providing the modelling parameters required to inform the novel process model being developed. These parameters will also provide a metric by which the formability of a material might be assessed, allowing material suppliers to present customers with a clear set of data describing the suitability of the material for the manufacturing process being considered.

1.2 Outline of this thesis and principal results

Chapter 2: Literature review

In the literature review, the history of the development of carbon fibre prepreg is briefly discussed before investigating manufacturing induced defects and the mechanisms governing their formation, i.e. intraply shear and interply slip, and how these mechanisms are induced by various forming techniques. Current characterisation techniques are considered, principally those developed for woven prepregs such as the picture frame and bias extension techniques, and their limitations when applied to unidirectional material are discussed. Finally, process modelling techniques are briefly discussed to give some context to the motivation behind the work.

Chapter 3: Interply slip in unidirectional carbon fibre prepreg

In Chapter 3 a method for characterising interply slip is introduced. Interply slip typically occurs as the weak interface between two plies yields, allowing the plies within a laminate to reposition relative to one another under the influence of forming induced stresses (Fig. 1-2). Understanding the interply shear behaviour of uncured carbon fibre prepreg is fundamental to avoiding process-induced defects during manufacturing of large-scale components. A methodology capable of determining the parameters of temperature, rate and pressure required for minimum resistance to movement of a prepreg is presented, and a heuristic one-dimensional viscoelasto-plastic model for interply shear is derived.

Extensive testing is carried out on a second generation prepreg, AS4/8552, and the model applied to the results in order to allow for a thorough investigation of the mechanisms behind interply shear. By breaking the response into the individual viscoelastic resin and frictional, elastic, fibrous responses we show that friction actually increases with temperature contrary to previous work, and that the new value of joint strength, describing the adhesive nature of the resin, is dominant at lower temperatures. Rate

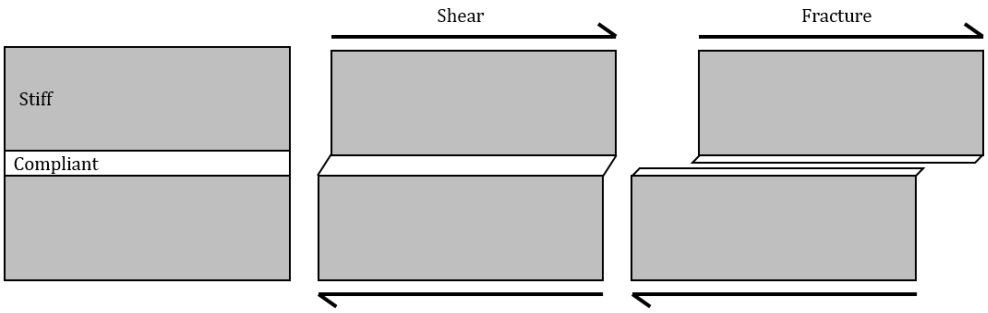

Figure 1-2: *Showing the progression towards interply slip following some initial interply shear in a layered media comprised of stiff and weak layers under the influence of shear loading.*

dependent variables are strongly linked to the resin behaviour, confirming the need for a viscoelastic model. The chapter concludes with some simple application scenarios, along with proposals for future work.

The key highlights of this chapter are:

(1) The interply shear response **cannot be be simply represented** using Coulomb friction or a classic viscoelastic model, rather a constitutive approach must be considered.

(2) The interply shear response is **highly dependent upon a wide range of forming parameters**, of which temperature is the most critical.

This work has been presented at ECCM 16 and appears in Composites Part A.

S. Erland, T. J. Dodwell and R. Butler. *Characterisation of interply shear in uncured carbon fibre pre-preg*, Composites Part A, 2015. 77:210-218

S. Erland, T. J. Dodwell and R. Butler. *Inter and intraply shearing of uncured carbon fibre laminates*, ECCM $16-16^{th}$ European Conference on Composite Materials, Seville, Spain, $22-26^{th}$ June, 2014.

Chapter 4: The influence of angled interfaces on interply shear

In this chapter the methodology developed in Chapter 3 is applied to samples of varying fibre orientation, in order that the effects of the angled interface might be better understood. This requires minimal alterations to the existing technique, and although not perfectly representative of the expected deformation mechanism, the test results again provide an insight into the mechanisms governing the interfacial behaviour. Increasing the mismatch in interface angle results in an increase in the initial stiffness of the response, offset by a decrease in the post-yield stiffness, whilst the yield point itself remains unchanged. This is due to the manner in which stress is transferred

from the fibrous region to the interface as a function of the effective surface roughness of the fibrous region increasing with interface angle. In the post-yield response, this same behaviour results in a reduction in fibre-fibre contact, as well as preventing the intermingling of the plies, which is thought to play a large part in the hardening behaviour, leading to a reduction in hardening. The primary output of these results is the improved applicability of the parameters derived in Chapter 3, allowing for the modelling of laminates with realistic stacking sequences. On a more simplistic level, stacking sequences can now be optimised to promote inter-layer mobility, much as with the previous parameters of temperature, rate and pressure.

The key highlight of this chapter is that **interface angle has a significant effect on the interply shear response**. This means that stacking sequence can now be added to the list of parameters which might be tailored in order to improve formability.

This work has yet to be published, but has been presented in various forms at both ICCM 20 and ECCM 17

S. Erland, T. J. Dodwell and R. Butler. *Viscoelastic interply slip in uncured laminates: Experimental characterisation and modelling*, ICCM $20-20^{th}$ International Conference on Composite Materials, Copenhagen, Denmark, $19-24^{th}$ July, 2015.

S. Erland, T. J. Dodwell and R. Butler. *The influence of fibre angle and resin properties on uncured interply shear*, ECCM $17-17^{th}$ European Conference on Composite Materials, Munich, Germany, $26-30^{th}$ June, 2016.

Chapter 5: The interactions of intra- and inter-ply shear in uncured laminate bending

The in-plane shear response of a flat laminate has been shown to localise to the weak interfacial region as interply slip, however in the bending of a ply of prepreg some intraply shear, that is to say shear within the fibrous region, must exist if deformation is to occur. Existing methods for characterising bending behaviour, such as the Peirce cantilever test are often lacking in accuracy, and require extensive data analysis to determine useful parameters. Dynamic Mechanical Analysis is investigated as an alternative, providing a readily available, highly repeatable and accurate test platform. In order to adapt the existing methodology to account for the large amount of shear expected in the specimen the original Engineers Bending Theory approach adopted by the DMA is modified with the addition of a Timoshenko shear modifier. This changes the behaviour from one which is infinitely stiff in shear to one which allows layers to slip or shear relative to one another, creating a shape commonly termed as a 'bookend' [60] (Fig. 1-3).

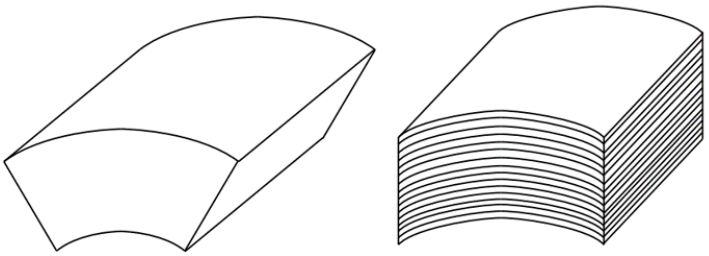

Figure 1-3: *(Left) Bending of a material that is infinitely stiff in shear as per EBT assumptions vs. (Right) bending of a material in which shear occurs at the interfaces between the constituent layers. Image taken from [60]*

This results in the calculation of an intraply shear stiffness value an order of magnitude greater than the interply shear stiffness previously calculated, as expected. It is also possible to derive a rough estimate of the initial interply shear stiffness from multi-layered samples, providing confidence in both methodologies. The new results complicate the simple prediction of the optimum forming temperature, as an increased temperature improves mobility, which is desirable, but also reduces resistance to buckling. This coupling effect is similar to that experienced when attempting to determine the optimum forming pressure, and thus requires a more in depth examination. An interesting output of this chapter is the possibility of applying the technique used to allow the investigation of bending stiffness to other deformation modes supported by the DMA. The chapter concludes by showing the theory behind unravelling the tensile modulus of a [0,90,0] laminate, although in practice the clamping technique currently used renders the DMA unsuitable to tensile methods and is considered an area of future interest.

The key highlights of this chapter are:

(1) By utilising a Timoshenko shear modifier, standard Dynamic Mechanical Analysis results can be **adapted to consider specimens which shear in bending**.

(2) **Intraply shear modulus can now be experimentally derived** for a material, which is a vital characteristic for process modelling.

(3) The initial interply shear modulus can also be backcalculated for multilayered samples, allowing **verification of results across both the test methodologies proposed in this thesis**.

A revision of this work which considers a new shear modifier is being prepared for submission to Composites Part A: Applied Science and Manufacturing.

Chapter 6: Modelling coupled parameters and laminate scenarios

Coupled parameters exist when modifying a parameter to achieve one desirable outcome results in a separate, negative effect. For the results presented in Chapters 3 and 5 these are pressure; the reduction of which promotes mobility but also reduces the driving force for consolidation, and temperature, which improves ply mobility when elevated but also reduces resistance to bending. Of the two parameters pressure is more readily investigated, as modelling of buckling requires the consideration of more complex instabilities. In this chapter a fairly simple energy minimisation approach is used to determine whether the consolidation of a laminate into a curved female tool is improved or restrained with additional pressure. The model is compared against an experimental validation program developed at the University of Bath and presented at ECCM 17 in Munich [54]. From the results it becomes clear that the simple consolidation law used is not suitable, and whilst there is some evidence of the expected shear behaviour, it is somewhat masked by the prediction of excessive consolidation across the part.

The key highlights of this chapter are:

(1) Coupled parameters such as temperature and pressure **prevent simple prediction of optimum processing conditions**.

(2) **Simple modelling techniques** can be employed to assess the dominant result of changing a process parameter allowing the optimum value for manufacture to be prescribed, however the accuracy of the results is highly dependent upon the models describing the mechanisms involved in the deformation.

This work has yet to be published, however it has been presented at ECCM 17. K. Johnson, S. Erland and R. Butler. *The influence of fibre angle and resin properties on consolidation of curved laminates*, ECCM $17-17^{th}$ European Conference on Composite Materials, Munich, Germany, $26-30^{th}$ June, 2016.

CHAPTER 2

LITERATURE REVIEW

2.1 Material development

Natural composite materials occur in both plants and animals, with wood and bone being prime examples (Fig. 2-1). In wood, cellulose fibres are held together by a matrix material called lignin. The cellulose fibres in wood are very similar to those found in cotton, however the addition of the binding lignin matrix makes wood rigid, and significantly stronger. Bone is formed from a hard, brittle material called hydroxyapatite and a much softer material called collagen. In their individual form, neither material would be fit for purpose, hydroxyapatite would be too brittle to cope with the everyday wear and tear a skeleton is subject to, and collagen would be too flexible to provide an adequate structure for the body. Together however they create a material that is both stiff enough to provide structure, and sufficiently flexible to allow it to take some impact loading without shattering.

Early man made composites are typically found in engineering applications. One of the earliest examples of these is the mud brick. Mud can be easily moulded and dried into a shape suitable for constructing basic structures, and has good compressive strength. Its tensile strength is poor however, as mud is typically composed of tiny grains of material with minimal interlocking. This was remedied with the inclusion of straw, which has a comparatively high tensile strength, but little compressive strength due to the length to width ratio. By combining two materials with different strengths, it is possible to make one with the best aspects of both.

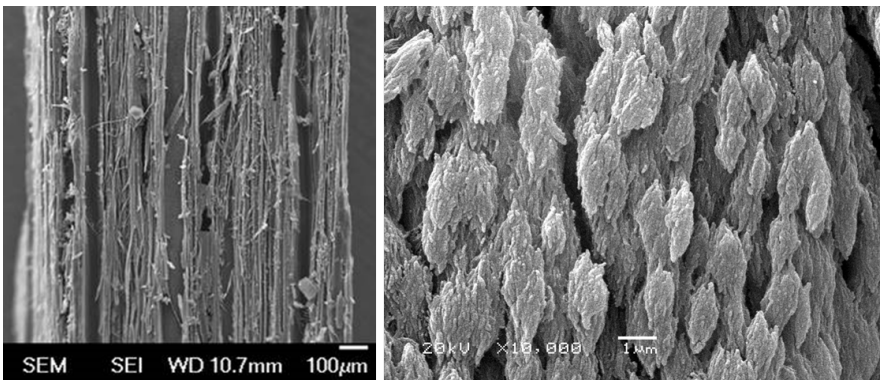

Figure 2-1: *(Left) Secondary Electron Microscopy (S.E.M.) of wood, a fibre reinforced composite, and (Right) bone, a particulate reinforced composite.*

2.1.1 Composites in aerospace

The basic principle behind the mud brick is identical to that used in modern aerospace composites; a matrix material with good compressive strength holds and aligns a fibrous reinforcement architecture which is good in tension. The first aircraft were constructed from both natural and man made composites, with light, rigid wooden frames and skins made of doped fabric. Doped fabric is particularly interesting, as it is the first recognisable modern aerospace composite. The material consists of some form of cotton fabric, draped over a structure provided by wooden spars and ribs, then impregnated with a cellulose nitrate dope. This dope acts to airproof the material as well as give it rigidity, forcing air to flow around rather than through the wing, allowing it to generate lift whilst being an order of magnitude lighter than a similar solid wing section. As aircraft became faster however the strength of the doped fabric proved insufficient and designs switched to using stressed aluminium.

The development of glass fibre reinforced polymers in the 1930's led to the creation of a composite that was strong, rigid, light and weather resistant. The separate materials in this composite were both breaking edge technology at the time. Whilst glass had been around for centuries, the first method for creating ultra-thin (5-25μm) fibres was only developed in 1932, when Games Slayter accidentally directed a jet of compressed air into a molten glass stream [21]. Modern glass fibres are produced via pultrusion, as it allows for greater control over fibre diameter [22]. The most common glass fibre in use today is E-Glass, made from alumino-borosilicate. Newly drawn glass fibre has exceptionally high tensile strain, due to the minimal amount of defects. The aspect ratio of a fibre leaves it susceptible to buckling however, as a fibre is often several metres in length, but only tens of microns in thickness. Unsupported, they are therefore poor in compression, as well as being poor in shear. With the development

of polyester resins in the 1940's it became possible to set the fibres in such a manner that their orientation could be controlled, maximising the benefit of their tensile strength, whilst the resin matrix provided improved compressive and shear strength. This combination also allowed glass fibre to be moulded into complex shapes, reducing or removing the requirement for a frame to which the material had to be fixed. An early application of the material was the manufacture of complete boat hulls, but the material was quickly adopted by both the aviation and automotive industry, although in the aviation industry it was never used for primary structural components in mass commercial production.

The development of carbon fibre in the 1960's resulted in a composite that was strong and light enough to completely replace metal structural components in aircraft, with new designs including progressively more carbon fibre by weight as manufacturing techniques advanced (Fig. 2-2).

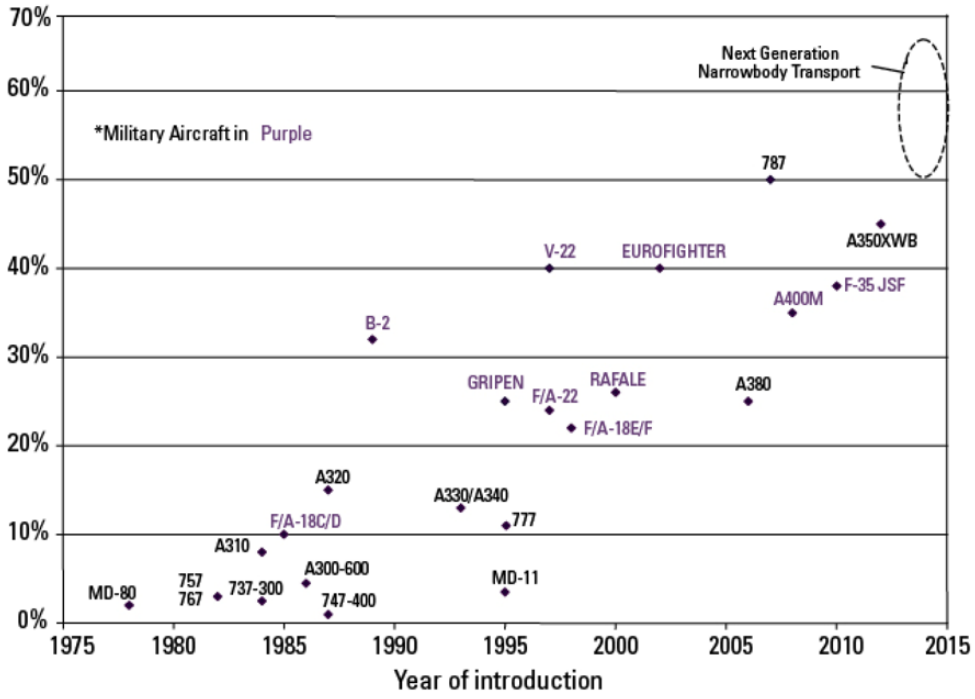

Figure 2-2: *Plot of composite by weight against time as new aircraft designs take advantage of the weight savings offered by CFRP [23]*

The first carbon fibres were made in 1879 when Thomas Edison carbonised cotton thread and small pieces of bamboo by subjecting them to extreme temperatures, with the resulting threads used for filaments in light bulbs [24]. The first high performance carbon fibres were not made until in 1958 by Roger Bacon from heated strands of rayon, a semi-synthetic cellulose fibre made from wood pulp [25]. This initial attempt was not

particularly effective, resulting in a fairly weak fibre with just 20% carbon content. A new process developed by Richard Millington in 1960 significantly improved on this, creating a very strong fibre with 99% carbon content [26]. The vast majority of modern carbon fibre is made from polyacrylonitrile (PAN), using a method first developed in Japan, then expanded and patented by the UK Ministry of Defence.

Carbon fibres are formed from sheets of carbon atoms arranged in a hexagonal pattern, similar to graphene sheets. The difference between carbon fibre and regular graphene sheets is the manner in which the layers physically interlock, greatly improving the strength of carbon fibre, as its structure is not purely held together by Van der Waals forces. The manner in which the sheets interlock depends on the precursor material, i.e. the material from which the fibre is made. Carbon fibre made from PAN is turbostratic, with a chaotic structure giving good tensile strength. Using mesopitch as a precursor material results in a graphitic structure, with a high Young's modulus but less tensile strength. Carbon fibre components are typically laminates made of multiple layers, or plies, of fibres. Early fibres, such as T300 or AS4, had a diameter of around 12 μm whilst modern fibres such as IM6 are as little as 6 μm in diameter [27]. Thinner fibres are typically stronger, as they contain far fewer defects, hence carbon fibres are stronger than those made of glass (Fig. 2-3).

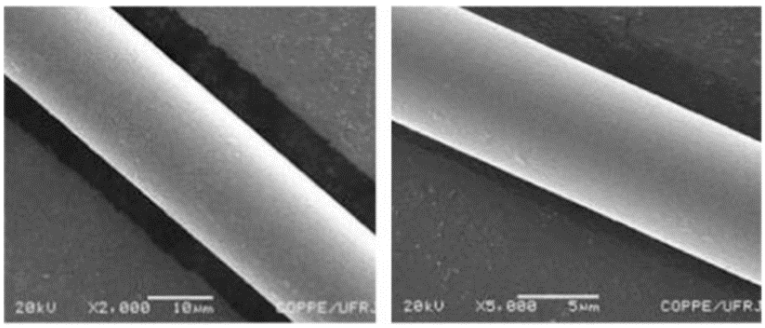

Figure 2-3: *Comparison of the diameters of a glass fibre, (Left), and a carbon fibre, (Right), which is around half the diameter. Figure from [47]*

The fibrous reinforcement in a laminate is aligned in such a manner as to be able to cope with the loading the component is expected to experience. For example, a component that is expected to undergo a lot of axial twist will have fibres aligned at $\pm 45°$, whilst a beam like structure which might experience a large bending moment would likely consist of a large number of $0°$ plies.

As mentioned, resin plays a vital role in a composite, providing the matrix structure capable of controlling the orientation and transferring load between the fibres, and preventing them from buckling under compressive loads. Modern resins can be

either thermosetting or thermoplastic, depending upon the desired properties and application. Thermosetting resins are typically stronger and stiffer, as well as being less energy intensive during manufacture. These resins are typically epoxy, and cure via a cross-linking process, which gives them their high strength and stiffness, but also prevents them from being reworked once the cross-linking begins during cure. Their chief drawback is their comparative brittleness, which can lead to problems with impact damage and delamination. Thermoplastic resins are much better under impact, but suffer reduced strength and stiffness as a result of their polymeric chains being formed from intermolecular forces rather than the chemical bonds found in thermoset resins. This does mean they are reworkable however, but require significantly higher processing temperatures than thermosets.

As a whole, composite components offer reduced weight whilst maintaining strength and stiffness, as well as improved fatigue resistance when compared to metal alloys. At present, these improvements however are offset by increased material costs, and the complexity of manufacturing the components. Modern automated processes in particular are prone to generating defective components, which are either scrapped or extensively reinforced, eliminating the benefits of the reduced weight. In order to understand how these defects are generated, we must first consider the forming regimes and the mechanisms they invoke in uncured prepreg laminates, in order that we might understand how to go about characterising the material. Due to the novelty of prepreg, most existing characterisation techniques have been adapted from those used for dry fibre reinforcement, with a varying degree of success. It will therefore be necessary to consider the behaviour of dry fibres if we are to understand the purpose of the characterisation techniques which have been developed.

2.1.2 Dry fibre manufacturing techniques

There are a variety of ways in which continuous fibre composite components can be manufactured. Dry fibre techniques all involve placing the fibres in the desired location, either in a mould or around a mandrel, and then adding the resin in some manner before curing it. The cure itself is typically dependent upon the type of resin used, and the level of part quality required. Low quality parts can be cured at room temperature, however higher performance resins typically require the application of heat, and if porosity is to be avoided, pressure. Resin transfer moulding (RTM) utilises a two part mould, into which a dry reinforcement preform is laid (Fig. 2-4).

Pre-mixed resin and catalyst with a very low viscosity are then pumped into the mould under low pressure, permeating the dry fabric and following a pre-determined path throughout the part, defined by channels built into the reinforcement architecture.

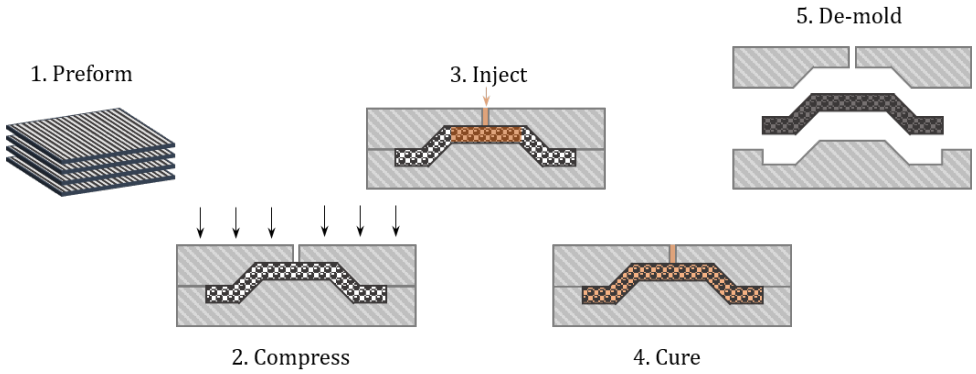

Figure 2-4: *Schematic of RTM process in which a dry preform is impregnated in a two part tool[45]*

The low viscosity is usually achieved by heating the tool. Due to the double sided mould RTM creates parts with a high quality surface finish that require little post-work, and the whole system can be readily integrated into an automated process. A slight deviation on the process, Vacuum Assisted RTM (VARTM) pulls resin into the dry preform with a vacuum drawn within the sealed mould, rather than forcing the resin in via pressure. The resin again flows in predetermined channels in the preform to ensure the part is fully wetted, and can result in high fibre volume fractions of up to 70%. Resin Film Infusion (RFI) attempts to address the problem with the uneven resin distribution which sometimes occurs in RTM by placing films of resin between each layer of reinforcement, rather than drawing resin in from an external source. When the part is heated and placed under pressure the viscosity of the resin lowers and it soaks evenly into the dry preform, first wetting the large regions of porosity which exist between the plies, before fully impregnating the dry core once pressure is applied [75, 76]. This also allows the use of much tougher, higher viscosity resins because of the significantly shorter flow path required to fully wet the fibres [78].

Filament winding is a highly automated dry fibre technique typically employed in the construction of continuous parts, such as pressure cylinders or boat hulls. Tows of dry fibre are pulled from a head, which moves along the length of a rotating mandrel. The tows are typically drawn through a resin bath just prior to their reaching the mandrel, impregnating them with resin, which in turn helps keep the tow in place.

Controlling fibre position and orientation is one of the most problematic facets of dry fibre lay-up. Because the fibres are stiff and loose, it can be hard to get them to conform to a geometry and remain in the correct position whilst the resin is added. A common way of combating this is to stitch several layers of fibres together at once,

however this necessitates that some volume of the final material is arranged in a non-load carrying manner, reducing the efficiency of the material.

2.1.3 Pre-impregnated fibres

Preimpregnated fibre (prepreg) was developed in an effort to overcome some of the drawbacks encountered when creating composite components using the previously mentioned dry fibre techniques, the chief issues being porosity, which must be below 1% for aeronautical applications, fibre volume fraction and fibre orientation. Developed initially to assist hand-layup processes, prepreg essentially consists of a layer of fibre sandwiched between two films of resin (Fig. 2-5), with the whole structure being referred to as a ply [74]. For automated processes these sheets are then cut into thin tows in order to aid formability.

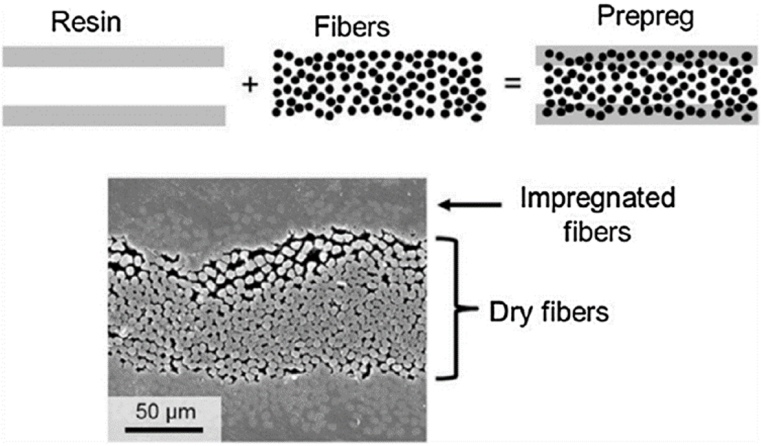

Figure 2-5: *Preimpregnated carbon fibre is made by rolling two sheets of resin onto each face of a bundle of fibres. This typically results in an impregnation gradient from pure resin at the surface to a fully impregnated fibre/resin zone, with a dry fibre region in the middle of the tow (see for example Fig. 1-1) Image from [74].*

The resin is designed to be tacky, or sticky, at room temperature, but with a sufficiently high viscosity to prevent the resin from flowing from the fibres, meaning that when the material is applied to a mould, it remains fixed in position and orientation. Similarities with RFI are apparent, with the short flow path allowing for the use of even fully thermoplastic resins with high viscosity. Mixed resin systems are also possible, with prepregs used in aviation being divided into 'generations'. The first generation refers to a prepreg with only thermoset resin. Second generation prepregs include a dissolved thermoplastic toughener, with a similar processing temperature to the main thermoset resin. This toughener acts by causing crazing prior to brittle fracture, hindering the formation of cracks and delaminations within the laminate. Crazing is the

formation of fine filaments called fibrils connecting the two surfaces of what would otherwise be a brittle fracture plane. In order for fracture to occur, these fibrils must themselves be broken, requiring further load. This behaviour is particularly prevalent in thermoplastic polymers due to their structure being formed of weak Van der Waals forces and stronger covalent bonds. when the former is overcome, the crack surface initiates, however the strong covalent bonds result in the formation of the aforementioned fibrils [90]. Third generation prepregs go a step further, including particulate thermoplastic reinforcement (Fig. 2-6), again as a craze stopper and also as a flow restrictor. These particles remain solid throughout the cure, promoting a uniform distribution of resin throughout the part by limiting resin flow. This also allows for the use of tougher and more viscous thermoplastics, improving resistance to interlamina fracture. A side effect of using this preimpregnated system is that the only path by which air can leave the part is via the dry fibre core, unless the material is laid in such a way as to allow for regular gaps between the tows from which air can be drawn. [79, 80].

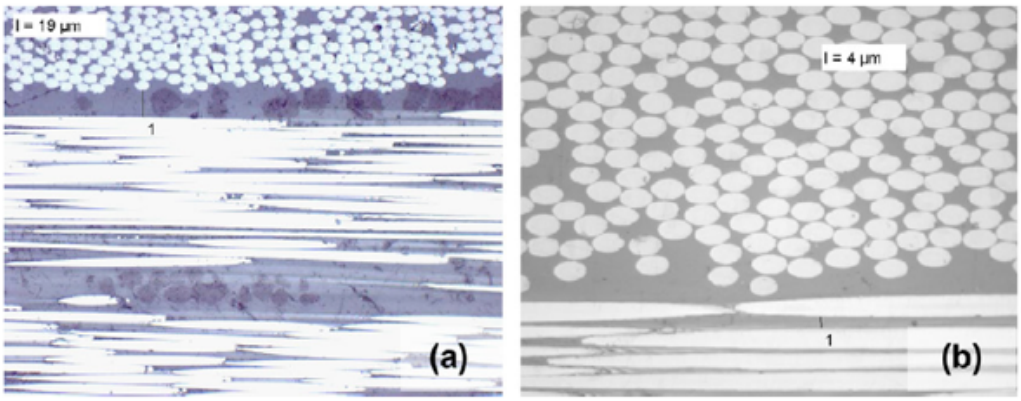

Figure 2-6: *(Left) S.E.M. imagery of a third generation prepreg, in this instance M21/T700. The particulate thermoplastic reinforcement is clearly visible in the resin interface in the form of the darker particles. (Right) Image of a second generation prepreg, 977-2/HTS with a clear resin interface. Image from [10]*

2.1.4 Woven and unidirectional reinforcement

When used for hand layup prepreg is typically woven into sheets, in which bundles (or 'tows') of fibres are interlocked in two orthogonal angles, i.e. 0/90°. The type of weave patterns can have a significant influence on the properties of the sheet, changing its drapeability - a vital characteristic when considering formability as discussed in the next section, or even resulting in a bias in its mechanical properties. An advantage of woven plies is that two angles are laid at once, speeding the manufacturing process,

and assisting in ensuring that the relative orientation of these plies is perfect. The plies themselves are also completely uncoupled in terms of thermal expansion, reducing issues with warping and thermal stresses accumulated during cure. A major disadvantage however is the inherent 'crimp' that must exist if the fibres are to weave together, that is to say, the fibres are not perfectly straight (Fig. 2-7). As fibrous reinforcement is at its strongest when loaded perfectly in-plane, the wave like structure in a woven prepreg results in a loss in mechanical performance and a slight reduction in fibre volume fraction.

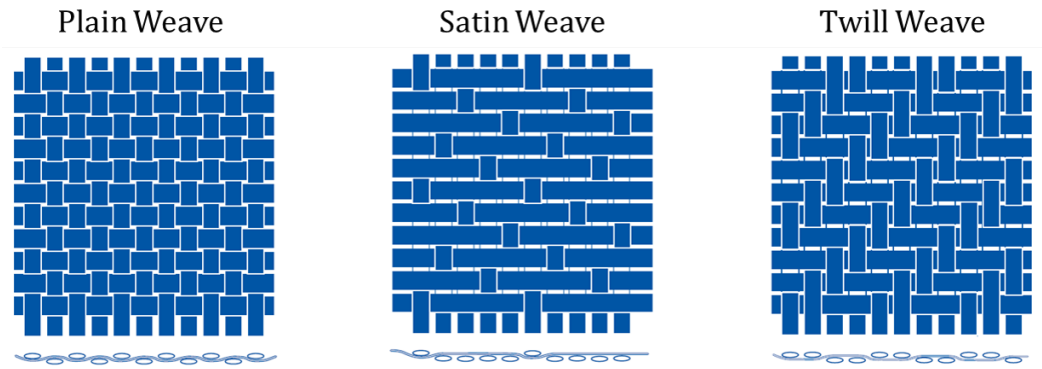

Figure 2-7: *Different types of weave offer differing degrees of drapeability and fibre crimp, impacting how easy they are to use and their final mechanical properties.*

Uni-directional prepreg, in which the fibres in each ply are all aligned in the same direction, is therefore the strongest form of fibrous reinforcement in tension. This performance comes with significant drawbacks in terms of ease of use and formability however. Woven prepreg has much more structure to it, preventing it from pulling apart when it is being formed to a shape and making it perfect for hand layup. The dividing of the fibres into small tows also allows the material to shear fairly readily, making it significantly easier to form sheets of woven material to a doubly curved surface when compared to a single large sheet of UD prepreg. The chief advantage of UD comes when we move away from traditional hand layup techniques and begin to consider the modern automated methods for which it was developed, chiefly Automated Fibre Placement and Automatic Tape Laying, discussed in the next section.

2.1.5 Automatic manufacture

With the increasing commercial interest in carbon fibre composites, two key automated processes have emerged in an effort to improve repeatability and precision whilst reducing material wastage and production time. Automated tape laying (ATL) involves rapidly depositing large strips of uni-directional material to form a laminate. Due to

the width of these strips it is only possible to form very simple, non-severe geometries straight from the machine head, such as blades for wind turbines.

Laminates laid by ATL can however be used in Double Diaphragm, or Hot Drape Forming (DDF and HDF respectively). In this case, the laminate is laid flat, then formed as a whole over a complex mould, using heat and pressure.

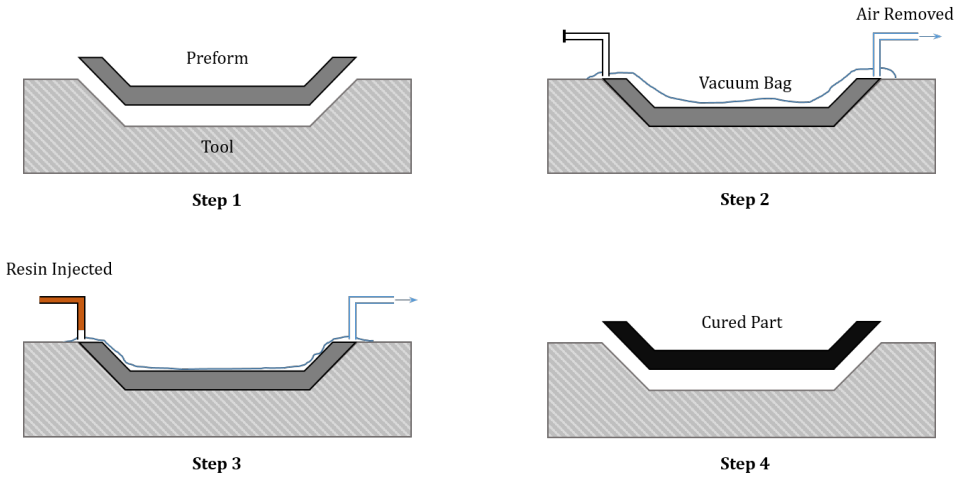

Figure 2-8: *Schematic of vacuum forming process in which resin is drawn into a dry preform using a vacuum[45]*

This process can be very quick, however typically runs into problems when forming components with double curvature, due to the large deformations the laminate must undergo to reach the final desired geometry. The mechanisms involved in this process are discussed in Section 2.3.

Automated fibre placement (AFP) was developed from filament winding specifically to allow for the manufacture of complex geometries. In AFP, multiple thin tows (3-12mm wide) of prepreg are laid at once directly onto the tool whilst under tension, using a head that allows individual tows to be drawn out at different rates, and capable of cutting and starting individual tows on the fly. This allows the head to steer through tight geometries and reduces material wastage to a minimum. It is not as fast as ATL however, with rate of production reducing as component complexity increases.

Both of these processes have been adopted on a large scale by the aeronautical industry, allowing for the mass production of components ranging from wing skins to primary structural components such as spars. A number of challenges still exist however, primarily with the generation of performance hindering defects within the final components, which can have major implications on the strength of the part.

2.2 Process modelling

The development phase of composite components, especially those made via automated processes, is often long and expensive. This is in part due to the various complexities already discussed, however it is further compounded by the difficulty of applying predictive modelling techniques to the actual forming of the component. Modelling the final component itself is not overly complex, and is used extensively in developing the geometry and specifications of the part. Modelling the behaviour of the flowing uncured resin and loose fibres as they are subjected to heat, pressure and the chemical changes which occur during the cure is far more complex however, resulting in extreme computational cost when considering current modelling techniques, often making it impractical. What models do exist typically focus on the manner in which woven materials will drape when conforming to a geometry, in order that phenomena such as shear locking (explained in the next section) might be avoided. As it stands, development of the manufacture of composite components made from UD tapes typically relies on extensive trial and error prototyping, which can be hugely expensive, in both time and financial cost. The advantages of a more efficient modelling approach are therefore clear.

2.2.1 Pin jointed net theory

Pin jointed net theory PJN was developed to investigate the drapeability of dry woven reinforcements as they conform to a geometry, and is the foundation from which many modelling techniques such as PAM-FORM have been developed. PJN is a kinematic model assuming inextensible, infinitely stiff fibres locked at crossover points [34], in which the fibres are infinitely thin vectors between the crossover points. All deformation therefore occurs in the form of rotation about the crossover points.

As the cross-over points restrict slippage, rotation of the fibres suggests the area between cross-over points will eventually reduce to 0, resulting in a compressive force upon the material. Assuming the fibres cannot cross over one another suggests a maximum deformation point. When considering a real system, with fibres of an actual thickness the maximum deformation point will be met sooner unless the fibres can be forced on top of each other in an out of plane deformation. In this way, PJN can determine a potential initiation point for defect formation in woven materials. This behaviour also gives rise to a phenomenon known as the shear locking angle, in which the restriction of rotation leads to the fibres being loaded in tension, resulting in a rapid stiffening of the system, drastically limiting further deformation of the material [35].

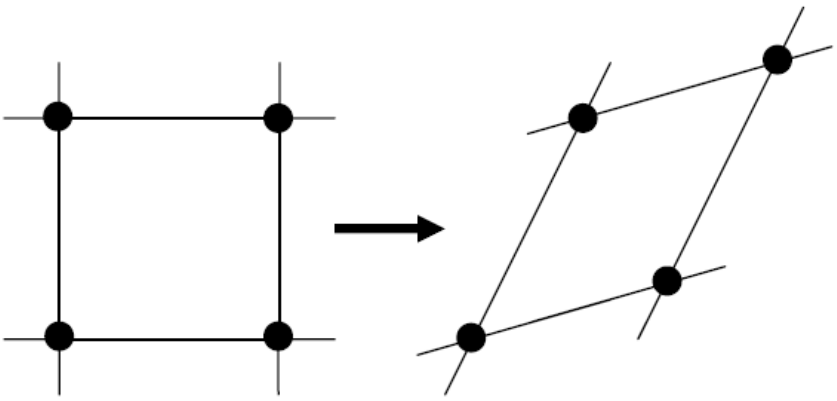

Figure 2-9: *Net deformation around crossover points in PJN theory [46]*

Almost all draping simulation software is based on the PJN assumptions, however only recent additions begin to consider the possibility of fibre slippage at the crossover points. Wang et al. [37] performed drape trials based on PJN assumptions looking at the adherence of various materials to the predicted fibre angles and rotations. Glass fibres showed good correlation, whilst carbon fibres showed signs of slippage despite being rougher. Wang et al. suggest this behaviour is due to the stiffness of the carbon fibres resulting in fewer contact points, and therefore less potential crossover points. Lai and Young [38] created a model which took into account slippage, and works well with complex geometries. This system is constitutive, with the base model prediction being altered by separate additional slippage values and step angles for each crossover point, creating a progressive deformation as displayed by Fig. 2-10.

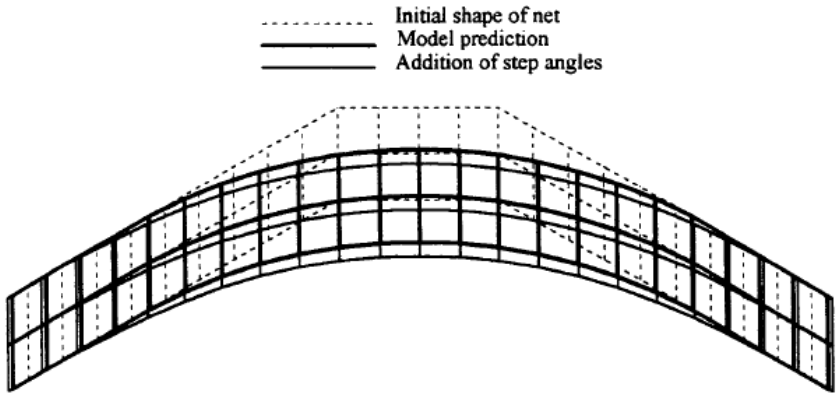

Figure 2-10: *Constitutive fibre slippage model showing initial rigid net prediction followed by net prediction assuming flexible fibres followed by final shape modelling slippage at the crossover points with the use of step-angles [38]*

2.2.2 Finite element modelling

Finite Element (FE) modelling aims to provide approximate numerical solutions to a global, physical problem. Most FE approaches are built from kinematic models, considering the motion of elements relative to one another in a mesh. The accuracy of the FE approach is therefore dependent on these elements and the kinematic models governing them. For isotropic materials undergoing fairly simple deformations FE can be an extremely powerful and rapid tool, as the elements can be quite large without losing accuracy. However, even considering a heterogeneous material such as uncured prepreg greatly reduces the efficiency of the process, particularly for large components. This is due to FE having to model each material, i.e. the resin and the fibres, individually. The elements therefore must be of the order of microns in size, then pieced together to make a component that is often metres in size creating a huge number of elements which must be analysed relative to one another, resulting in an infeasible computational cost. This is before even considering the complex mechanics involved, (see Section 2.2). Whilst modern FE packages often have all the required models the sheer number which must be employed, combining these with the fidelity required in the mesh means that conventional modelling techniques are unsuitable for predicting the behaviour of uncured composite components during forming.

PAM-FORM is a good example of a commercially available FE code, developed to represent thermoforming of fibre reinforced thermoplastic composites (Fig. 2-11). This code is capable of capturing all the key mechanisms experienced within a laminate during forming, such as inter and intraply shear and the stretching of a ply, allowing for the deformation of a stack of plies within a laminate to be considered [42]. In order to be able to achieve this however, each ply must be individually discretised, resulting in huge computational costs for larger components.

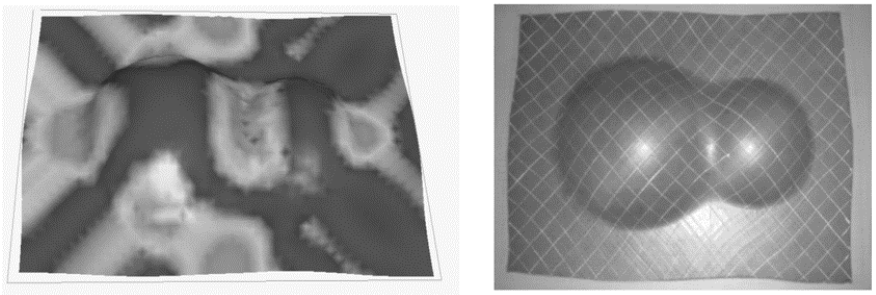

Figure 2-11: *(Left) Predicted and (Right) experimental forming of a stack of* $\pm 45^{\circ}$ *non-crimp fabric, the prediction carried out using PAM-FORM [42]*

The limitations of existing modelling techniques are clear when considering defect

formation. Models based on PJN are not designed to model defect initiation as a result of stresses generated by complex mechanisms during forming, rather they consider the geometric constraints imposed by the architecture of the reinforcement fabric. Modelling based on an F.E. approach could feasibly model defect initiation as a result of forming induced mechanisms, however it is limited by computational cost, due to the complexity of the problem, and also by the lack of understanding surrounding the mechanisms generated during forming processes. The key component missing from all modelling techniques when predicting the behaviour of preimpregnated fibres, in particular the UD fibres used for automated processes, is an accurate characterisation regime and method of capturing the complex behaviour of a ply of uncured prepreg under shear. In order to assess which characteristics are vital during the forming of a laminate, we must consider the defects and the mechanisms which generate them.

2.2.3 Modelling out of plane ply wrinkling

Work by Dodwell et al. [3] aims to predict the formation of wrinkle defects (described in Section 2.3 in a C-section laminate which is being debulked over a male tool. Debulking is a commonly used term describing the process in which a vacuum bag is used to draw air from and consolidate a laminate prior to cure, redistributing resin and moving the part closer to its final cure part thickness (CPT). This process is typically employed at several intervals during the lay-up of a part. The work introduces a one dimensional model which considers the elastic buckling of plies as they are consolidated over a male radius whilst being constrained axially. The axial constraint can be varied in order to determine a critical limb length, representing material either side of the corner feature, such as might exist in a primary structural component such as a wing spar.

This model considers interply shear and the bending characteristics of uncured prepreg as the primary mechanisms behind wrinkling in a debulk scenario, however the paucity of accurate input parameters representing the material characteristics is explicitly stated. Clearly the mechanisms which cause the defect of interest are key when looking to model its formation.

2.3 Defect formation

Defects in composite components typically involve some localised loss of desired fibre orientation or fibre volume fraction. The implications of these defects can range from severe performance reductions with regards to part strength, to uneven surface topology complicating the final assembly of the structure. Performance reduction is naturally the most problematic, as it often results in either scrapping the entire part - costly in time

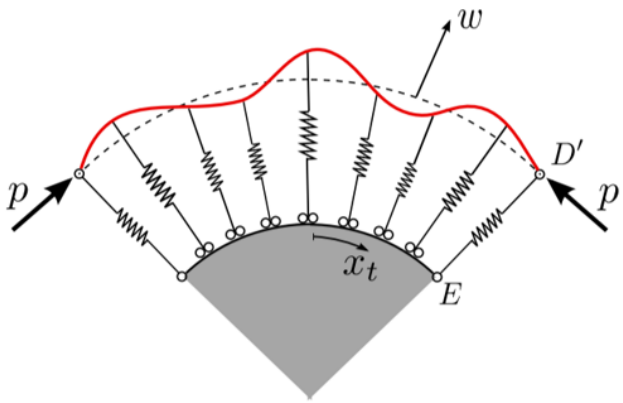

Figure 2-12: *Schematic showing the principles of the model presented by Dodwell et al. [3], in which the buckling response of the laminate is simplified to the bending stiffness of a single layer laid upon a Winkler foundation. Rigid loads, p, applied as boundary conditions, prevent the laminate from forming bookends as shown in Fig. 2-15, forcing the laminate to buckle.*

and materials as carbon fibre is extremely difficult to recycle - or having to substantially reinforce the part thereby resulting in a weight increase, negating the benefit of using carbon fibre in the first place. Defects resulting in abnormal surface finishing are often easier to rectify, using post cured pad ups which can be machined back to provide an even surface without compromising the strength of the part. A detailed taxonomy of the wide array of defects encountered in composite parts is provided by Potter [20] (Fig. 2-13).

From the sheer volume of potential defects presented we can assume that the forming of an immaculate component is by no means simple, however some defects are more important than others. Of these defects, those induced by geometry and resulting in fibre misalignment are of particular interest, not just because of their implications for the final part, which are often severe, but also because of how they come about. Lay-up, cure and handling related defects are typically the result of some unintentional processing error, and as such are simply avoided by enacting a more rigorous process. Voiding has been extensively researched, and was part of the driver behind the development of preimpregnated fibres and processes like RFI. Geometry induced defects are however the result of the mechanics involved in attempting to create complex, high performance components. As such, their occurrence is not so much the result of a fault in process as it is a result of a lack of understanding of the mechanisms involved.

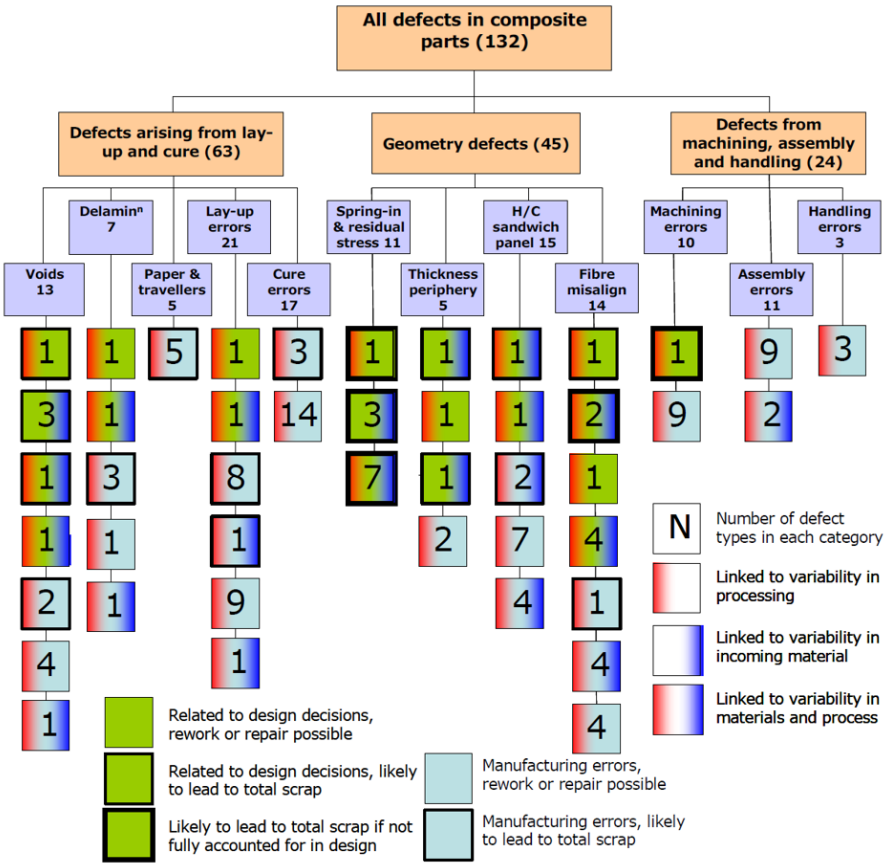

Figure 2-13: *Overall taxonomy of defect types in RTM and autoclave mouldings [20]*

2.3.1 Types of defect

Of the various defects encountered in composite components, wrinkling, which falls under the category of fibre misalignment in Fig. 2-13, is one of the most problematic. A wrinkle is a severe, localised out of plane deviation in ply orientation that can lead to a drastic reduction in strength - up to 60% for a wrinkle with an amplitude of just 2mm [3].

Wrinkling can be sufficiently severe that it produces visible surface undulations as in Fig. 2-14, however it can also be contained internally with no obvious signifier, requiring that parts be subjected to rigorous non-destructive testing methods prior to certification such as ultrasound imaging. A similar wrinkling defect called marcelling occurs in-plane rather than out of plane, however usually to a lesser degree and without such severe ramifications, as the amplitude of the change in fibre orientation is contained by the comparatively large volume of surrounding material.

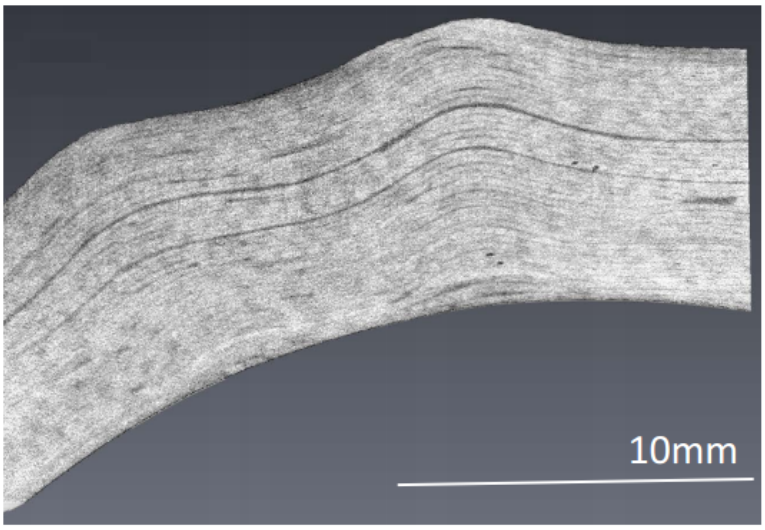

Figure 2-14: *A wrinkle defect in a corner radius. This type of defect often occurs during a process known as debulking (see Section 2.3.2), in which a vacuum bag is used to consolidate plies to a tool surface [3]*

A common defect in drape formed components is bridging, which occurs when the laminate is not pushed adequately into female tool corners, and thus does not represent the intended geometry post cure. This is not simply a geometric issue however, as the component is designed to carry the load through a specific path, and the deviation of the final shape from this path can lead to strength reductions. The void between the laminate and the tool often leads to issues with fibre volume fraction and uniformity of resin content at the tool face, as the resin is not constrained in any way, and therefore free to flow from the prepreg.

A group of defects more common to dry forming methods is porosity and resin starvation. Porosity in particular must remain below 1% in aerospace components due to the negative impact on part strength [94], and was one of the driving factors behind the development of pre-impregnated carbon fibre. Porosity refers to air bubbles trapped within the laminate resulting in a loss of strength, but also acting as initiation points for cracks and delaminations. This typically occurs when high viscosity resins are required to flow a great deal [77], or when adequate air channels are not provided, as described in Section 2.1.2. Resin starvation occurs when resin is allowed to flow too much, or is distributed away from a region under abnormally high pressure during the forming or the cure, often caused by irregular geometry. This defect is largely solved with the use of third generation materials however, which restrict resin flow in order to maintain the desired fibre volume fraction, and frequent debulking which, whilst vital in combating porosity, presents a number of challenges when considering the formation

of wrinkles.

2.3.2 Forming processes

During the debulking process, a part will usually be reduced by up to 20% of its original thickness from layup to final cure, with approximately 12% [7] of this thickness being lost during the debulk cycle. In flat plates, this in rarely problematic, as every ply moves equally towards the tool surface. Parts with some curved geometry are more complex however. When curvature is introduced, the reduction in part thickness results in a change of radius in the corner, requiring the plies to effectively either gain length in a female corner, or lose length in a male corner. Considering first the female scenario, the extremely high stiffness in the fibre direction means this increase in length cannot be accommodated by the stretching of the fibres. They must instead be able to slip in from the ends of the component, leading to a 'bookend' effect, with a tapered edge. If this slip does not occur, the plies will act to hold off pressure, leading to bridging and poor consolidation. For the male scenario to consolidate correctly, the excess material generated from the reducing radius must somehow be moved to the edge of the part, again leading to a tapered bookend (Fig. 1-3) for a female tool, and the inverse of this behaviour for a male tool (Fig. 2-15). If the plies are prevented from moving, they become subjected to axial loading. Due to the uncured resin matrix being unable to offer any support in compression, this leaves the plies vulnerable to buckling, as each ply acts individually [3].

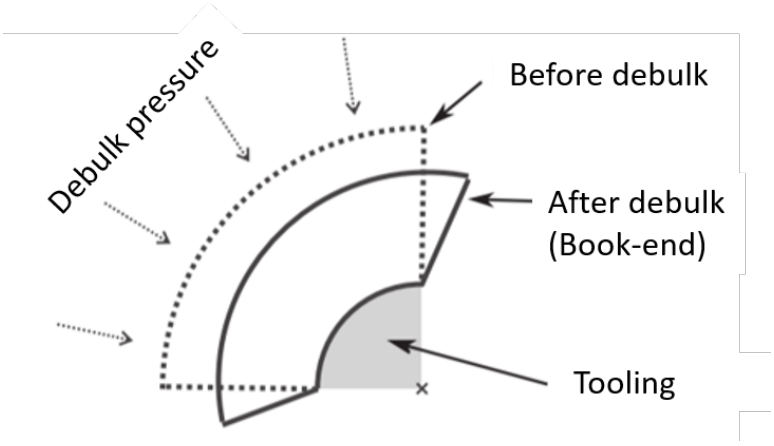

Figure 2-15: *Debulk over a male tool generates excess material. If this material cannot move outside of the original boundaries at either end, wrinkles will form as a result of plies buckling [3]*

This is the mechanism described by the model discussed in Section 2.2.3, which considers the formation of wrinkles in a consolidation scenario. The requirement for

plies to slip is even more pronounced in drape forming of pre-laid laminates to curved tooling, although the general mechanism is the same. The behaviour is similar to that of a beam subjected to a bending moment, wherein as the laminate conforms to a curved feature, one side is subjected to compression, whilst the other is put under tension. As discussed regarding consolidation, the only way in which these stresses can be accommodated is by allowing the plies the mobility required for them to reposition successfully. Drape forming also has particular problems when attempting to conform UD prepreg to double curvature [2], often generating wrinkles termed as 'smiley faces' (see Fig. 2-16) as the plies must essentially rotate, or scissor if they are to form correctly.

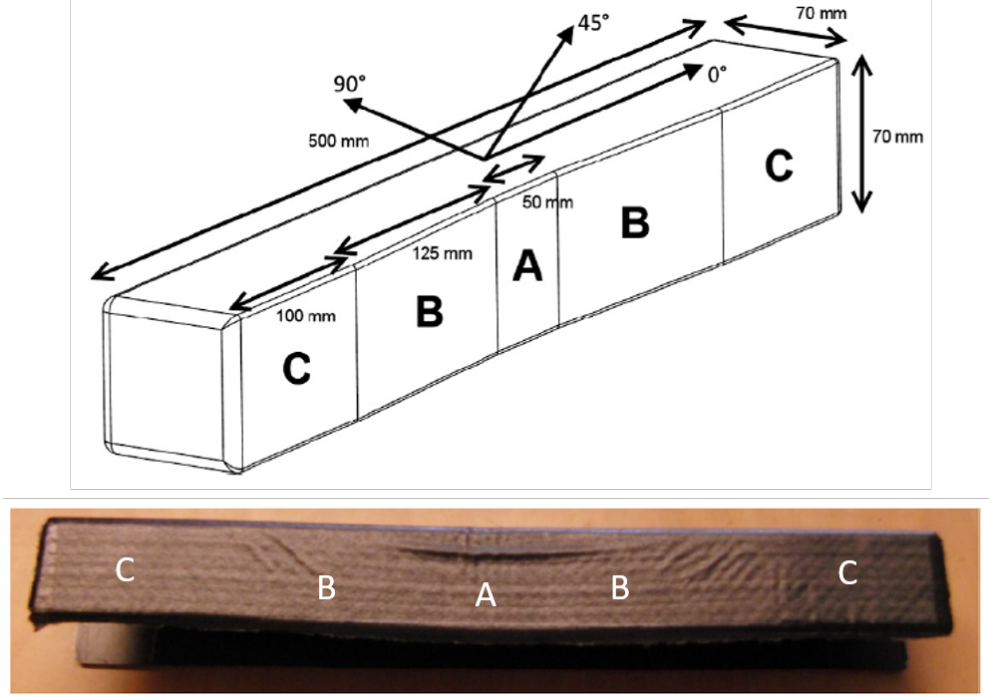

Figure 2-16: *(Top) Tool with a ramp feature on one face where section A is indented from but parallel to sections C, and section B connects these regions in a straight line. (Bottom) 'Smiley face' wrinkles typically form in this type of feature due to the requirement of some rotational deformation between the plies as they are draped on the tool. Images from [93]*

As mentioned briefly in Section 2.1.4, this is to do with the difficulty of shearing wide sheets of UD material along the fibre axis, which must happen if the plies are to rotate. This problem is less pronounced in AFP manufactured components, as the plies are placed much closer to their final geometry, and are not required to deform as much.

A surprising potential source of wrinkle defects in a component is the tension imparted in the material from the machine head whilst it is being laid. The tension

imparted in the tows is required to ensure that the correct fibre orientation is achieved, and relies on the high stiffness of the fibres to prevent excessive deformation of the fibres themselves. Over short components this is rarely problematic, however, for components with significant length this can result in deformations of mm's in length. This in turn translates into a significant shear stress over the interface of two plies, maximising at the end at which the tow was terminated.

Wrinkling and bridging seem therefore to be influenced by the same factor; the mobility of the plies in the laminate whilst they are subjected to various forming induced loads. If the plies are not able to shear past one another, there is no way of dispersing the stresses built up during forming, often resulting in severe defects.

2.4 Mechanics in forming

Current understanding of the mechanics involved in the forming of carbon fibre prepreg focuses mostly around woven materials, stemming from the vast knowledge base of the textiles industry. The behaviour of dry weaves is only of limited use however, as the resin must play a significant part in the system, even in its uncured state. The understanding of the behaviour of UD prepreg is even more sparse, due in part to the relative novelty of the material.

2.4.1 Inter and intraply shear

Intraply shear as defined in [30] involves the movement of fibres past one another within a ply. This differs from interply shear, which is the relative movement of one ply to the next within a laminate (Fig. 2-17). The extent to which intraply shear can occur in woven materials is limited by the cross points in the weave itself, as excessive deformation will result in fibre compaction as the material rotates in a scissor-like manner. Interply shear response is closely linked to the weave type, with weaves which induce a large degree of crimp in the tows having a higher frictional resistance than low crimp weaves [30].

2.4.2 Ply bending

If wrinkling is effectively the bucking of a ply, being able to determine the bending stiffness of the material becomes hugely important. Work to date has determined that bending resistance is heavily influenced by intraply shear properties, rather than just the stiffness of the fibres, as a single ply is in essence a bundle of individual elastic beams with viscoelastic interfaces. As such, plane sections do not remain plane in

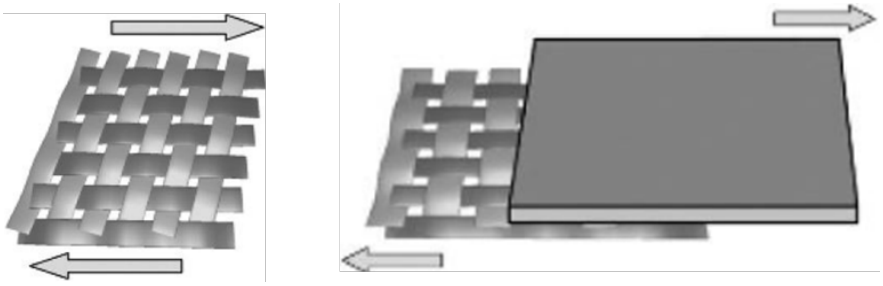

Figure 2-17: *(Left) Intraply shear in woven material results in a rotational scissor-like effect. Excessive rotation can lead to wrinkle defects. (Right) Interply shear involves two separate plies moving relative to one another in a laminate. Figures from [30]*

bending, ruling out the application of engineers bending theory and requiring instead consideration of either a Timoshenko or Benham and Crawford-esque element (see Chapter 5).

2.5 Material characterisation

The majority of existing characterisation methods were originally developed for dry, woven fibre. These techniques have their roots in the textiles industry, building on the Kawabata Evaluation System for Fabrics (KES-F). This system provides methods by which tensile strength, shear strength, bending stiffness, compressibility and frictional behaviour of a fabric might be assessed, however, they are not widely used for reinforcement fabrics, work by Lomov et al. [41] being a rare example. This is largely due to the tests working of single point data due to the lengthy and contrived methodologies, at fairly low levels of deformation, as well as the cost of the testing equipment [30]. This framework has allowed for the development of a number of purpose built rigs for woven prepreg however, in particular the Bias Extension and Picture Frame tests, which primarily focus on intraply shear and twist.

There are very few characterisation techniques for UD material, in part due to it being such a recent development. Several attempts have been made at adapting methods used for woven materials, with varying degrees of success. In general, the problem with characterisation techniques for prepregs is the difficulty in determining what part of the prepreg is responsible for the observed characteristic, i.e. is the response resin dominated and therefore viscoelastic, or fibre dominated and therefore purely elastic. The is exacerbated by current techniques often involving several modes of deformation at once.

2.5.1 Standard shear characterisation methods for woven materials

A number of characterisation tests evolved alongside the development of modelling techniques such as PAM-FORM, in particular the adaptation of techniques such as the picture frame test and the bias extension test for use with preimpregnated fabrics. These tests were used both to provide input parameters, and to validate the predictions of the modelling technique [42].

Picture Frame

The picture frame test is a method by which intraply shear and twisting behaviour might be investigated for woven material. The test rig is a hinged diamond frame which fully clamps a single ply around the edges, before the top and bottom corners are drawn apart in an Instron at a set rate, measuring the required load to reach a certain degree of deformation (Fig. 2-18).

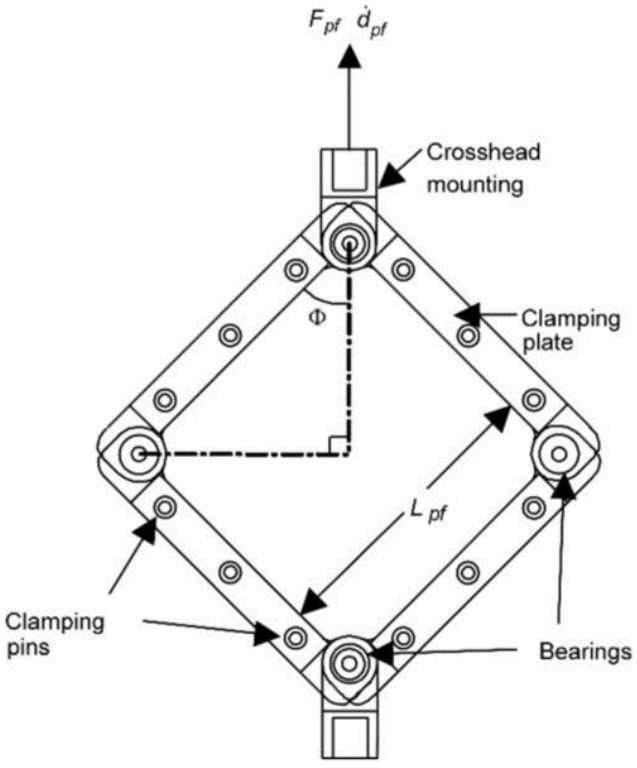

Figure 2-18: *Picture frame test rig, in which the sample of woven prepreg is clamped within the frame, such that the orthogonal fibres run parallel to the limbs of the frame. The application of a tensile load to the uppermost edge elongates the diamond whilst pulling in the sides, forcing the sheet of material to deform.*

The method of clamping employed depends on the material being investigated. For dry preforms, it is possible to push pins through the material, minimising the impact of the clamping on the test area as the material is free to rotate [28]. Prepreg must be clamped with direct pressure from the frame however, meaning the sample is not in pure shear at the boundaries [29]. Whilst the methodology is fairly simple, the accuracy and repeatability of the test is very sensitive to the sample preparation, with small fibre misalignments resulting in a large amount of variation between samples ($\pm 20\%$). The test is able to generate wrinkling defects via the shear locking mechanism described in section 2.2 at a shear angle of around $50 - 70^{\circ}$ depending on the material and type of weave [30].

Bias extension

The bias extension test is another technique for investigating intraply shear and shear locking in woven material. In this test setup the top and bottom edges of a rectangular sample are clamped with tows aligned at $\pm 45^{\circ}$ to the direction of the applied tensile force. The test requires that the sample be of an aspect ratio $\lambda = L_0/w_0 = 2$, where width w_0 >100mm. When loaded in tension this leads to several distinct regions of deformation in the sample, the most important being the large region of pure shear in the middle, section A in Fig. 2-19.

This test therefore has the benefit of being able to invoke pure shear in the sample without the influence of the rigid tool boundaries present in the picture frame test. This also improves repeatability as the sample is less sensitive to the initial orientation of the fibres. It is harder to determine the shear resistance however, as the behaviour of the pure shear region must be decoupled from the contributions of the adjacent regions which also contribute to the reading taken from the Instron, and the pure shear region itself is less clearly defined. One particular counter for this is the use of Digital Image Correlation (DIC) to perfectly image the shear strain in the sample. Work by Harrison et al. [28] has developed a normalisation technique which allows the investigation of alternative sample aspect ratios, and more critically allows for the correlation of data with that from picture frame tests as well. This allows data from the bias extension test to be translated into shear stresses and strains, and therefore used to provide variables for process modelling. The data analysis required is noted as being extremely complex however, making the picture frame test preferable but less representative due to the boundary conditions.

The applicability of PJN to unidirectional laminates has been investigated by Larberg et al. [46] using the Bias Extension technique described in section 2.5.1. The fibre rotation in the shear zone was predicted using PJN theory in order that it might be

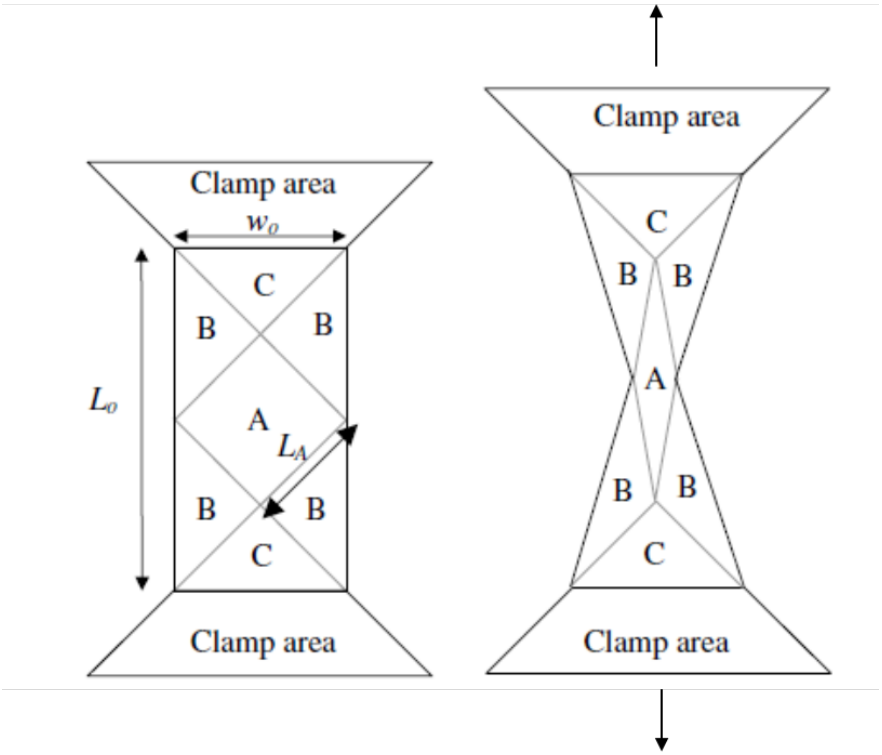

Figure 2-19: *(Left) Bi-axial extension test setup investigating intraply shear in a ±45° coupon. (Right) Clamping scenario ensures a region of pure shear in zone A. Using a speckled surface deformation can be observed with Digital Image Correlation [8]*

compared to experimental results, with the deformation being monitored using DIC. The experimental results showed that adherence to the PJN theory varied with prepreg type, with 977-2, a second generation material showing very little adherence to PJN fibre angle predictions whilst M21, a third generation material, showed perfect agreement for the first 40mm of deformation, after which the coupon began to split (Fig. 2-20) It is suggested that this occurs at the point at which the force required to further rotate the fibres is greater than the friction between layers.

In the early stages of loading the deformation was constant across the coupons, however as deformation progressed, bands of moving material began to form. No deformation was recorded within these bands; rather they sheared past one another as solid blocks. It is suggested that the initial uniform behaviour was governed by intraply shear, and that as deformation progressed the force required to achieve continued intraply deformation exceeded that required to provoke interply friction, whereupon this mechanism dominated as the individual plies moved over one another. Although this test could not quantify intraply deformations it could still be observed that the onset

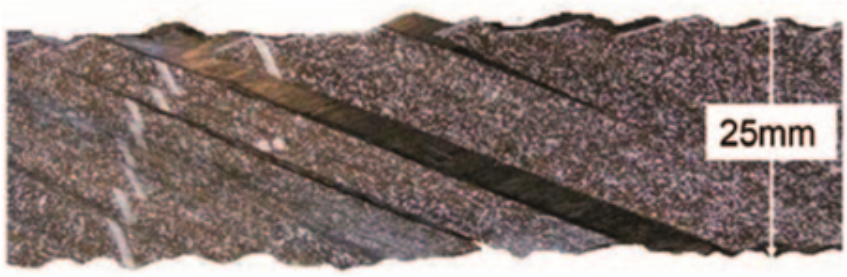

Figure 2-20: *Deformation of a sample of M21 prepreg using the bias extension technique resulting in the splitting of the upper, speckled ply and the observation of the ply below it [46]*

of banding was dependent upon load rates [36], suggesting that this reaction is also governed by the resin component of the prepreg. Although this experiment shows the importance of intraply shear in UD composites it does not help with the characterisation of shear in bending.

The chief drawback of these methods, as mentioned, is that each test invokes a number of mechanisms at once, making it impossible to identify the dominate mechanism in the forming process and the dominant material response. The tests themselves are also not particularly representative of the forming conditions present when considering consolidation or drape, especially when considering the influence of pressure applied by a vacuum bag or autoclave. In the mentioned tests, the only lateral pressure which occurs arises as a result of the Poisson's ratio of the material, which is magnitudes smaller than the processing pressures we are looking to mimic.

2.5.2 Interply shear

A common method of investigating interply shear is the fibre pullout test, in which a single ply is drawn from a small laminate whilst under some degree of pressure (Fig. 2-21). This test evolved from the single fibre pullout test developed for cured composite materials, which investigates a failure mechanism whereby the interface around the fibre cracks, allowing the loaded fibre to pull free of the matrix. For an uncured material the problem is slightly more complex, as the behaviour is heavily influenced by the uncured resin, which results in some viscoelastic yield, rather than a comparatively simple frictional behaviour.

There is also a problem with continuity of the sample. As the ply is drawn from the laminate, the sample area is effectively reducing, which in turn lessens the resistance to movement. In the original form of the test this is not problematic, as it accurately represents the failure mechanism. When considering forming however, movement of the ply in one area of the laminate will result in it drawing material in from elsewhere,

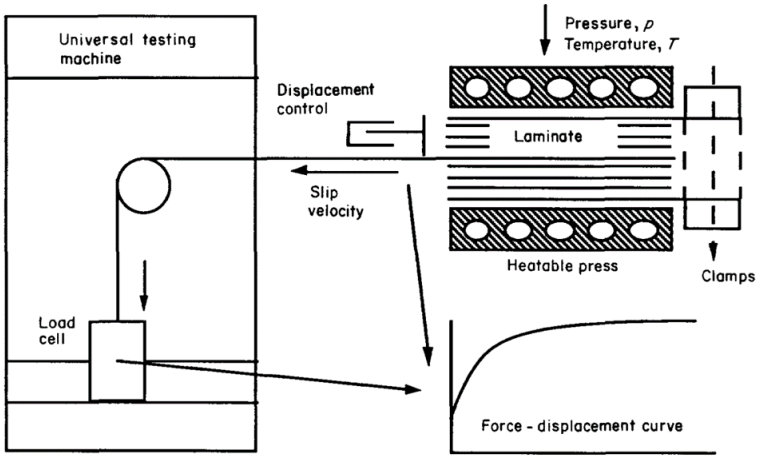

Figure 2-21: *Fibre pull out test setup employed by Scherer et al. [33] in which a ply is drawn from a small laminate under some pressure.*

i.e. no void will form. Therefore for this test to be representative of forming processes, the sample area must be preserved in some way.

This issue is addressed with the rigs developed by Murtagh [31], Wilks [32] and Larberg et al. [10], in which two small fibre clad plates are drawn into contact with a larger, central plate (also fibre clad), with the use of a pressure cylinder. The small side plates can then be drawn across the central plate and the resistance measured, whilst the testing area remains constant. The difference in apparent behaviour when comparing load traces from interply shear testing and fibre pullout is clear to see.

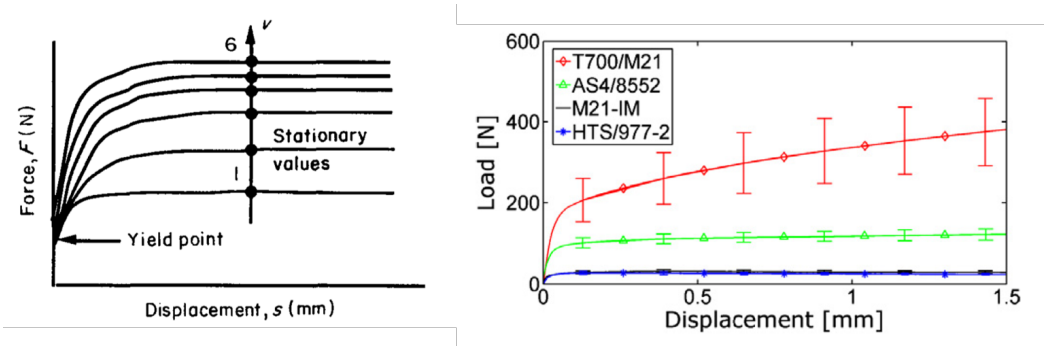

Figure 2-22: *(Left) Load vs. extension for a fibre pullout test [33] (Right) Load vs. extension for an interply shear test [10]. Note that the difference in load is due to sample size.*

In the results gathered by Scherer et al [33] the yield point is taken to be the y-intersect, however the load clearly has a two stage response, with a transition from an initial gradient to an apparently frictional behaviour. In the interply shear test we

get a similar initial response but with some residual post yield stiffness, assuming the yield point to be at the transition of the two gradients. This has major implications for forming processes which involve large amounts of shear strain, such as DDF. Initial modelling of this behaviour has typically been to represent the yield point with a simple coulomb friction model [10], however it is noted that the system is clearly much more complex. Wilks [32] suggests a constitutive model that begins to consider the viscoelastic nature of the resin, such that shear stress:

$$\tau = \eta\dot{\gamma} + \mu\sigma_n \tag{2.1}$$

where η is viscosity, $\dot{\gamma}$ is shear strain rate, μ is frictional coefficient and σ_n is pressure.

2.5.3 Peirce cantilever

The Peirce cantilever test is another method by which bending stiffness might be gauged, this time by observing the shape and deflection of a cantilevered beam of material as it sags under its own self weight [43]. This test was originally designed for dry fabric reinforcement, and a particular limitation exists in which the accuracy of the results degrades with increasing self weight, potentially limiting applicability to preimpregnated fibres. In the Peirce cantilever test, a rectangular sample is held as a single cantilever, with the resulting deflection allowing the measurement of the bending stiffness of the sample (Fig. 2-23). The limitations of this technique are discussed in more detail in Chapter 5.

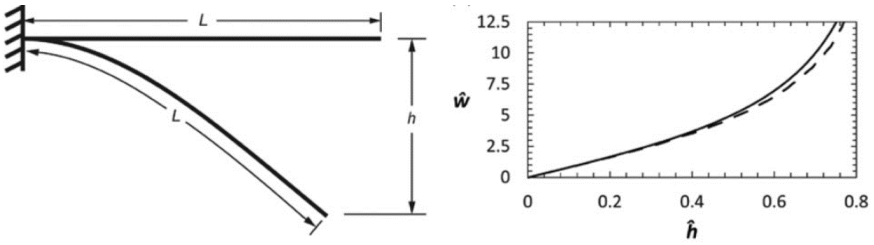

Figure 2-23: *(Left) Schematic of the Peirce cantilever test in which one end of a sample is clamped, with the deformation from self weight being measured. (Right) Non-dimensional weight, $\hat{w}$, against non-dimensional height, $\hat{h}$. The solid line represents a polynomial approximation [44], and the dashed line is drawn from Peirce's own formula presented in [57]*

2.6 Multi-scale

As discussed in section 2.2.3 work by Dodwell et al. [17] investigates modelling methods for predicting wrinkling around corner radii, showing that unless interply slip is allowed during bending, localised buckling instabilities will arise, resulting in wrinkling similar to that seen in physical components. This work has been superseded by a multi-scale model now in development [17] based on Cosserat principles. This novel technique is a form of finite element modelling which captures fine scale behaviour without using a prohibitively large number of elements, drastically reducing the time taken to run a simulation. The key to this technique is the new type of elements employed. These elements are representative volume elements or RVE's, and rather than portraying a homogeneous area of a material, they convey the behaviour of a small heterogeneous section consisting of several plies.

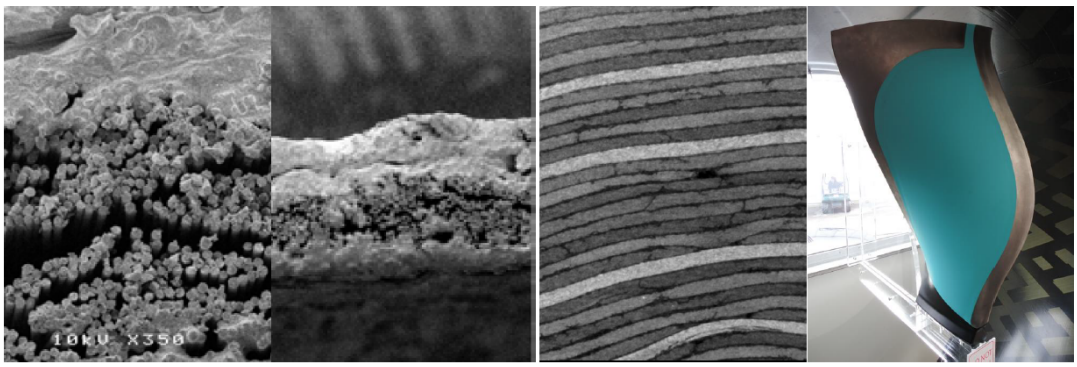

Figure 2-24: *Multiple scale in a composite make up. From Left to Right: fibre/resin scale (5μ m), ply scale (0.25mm), laminate scale (5-30mm) to the large-scale composite structure (>1m)*

Figure 2-24 shows the physical equivalent of what the multiscale approach must achieve. On the micro scale, the model must be able to account for the structure of a single ply of prepreg, including the flow and cure characteristics of the resin, and the permeability and frictional behaviour of the fibres. This must then be upscaled to consider the impact of these parameters on mechanisms controlling the deformation of a small stack or package of plies, with this package then being scaled to the full laminate thickness, and then finally the full scale component with its geometry. The underlying principle of the Cosserat approach is that the response of the fine, micro scale RVE is generalised using new rotational degrees of freedom, which are then applied to the elements of the coarse, macro-scale element, replicating the general behaviour of the more computationally expensive RVE in a much less expensive element. The accuracy of the Cosserat approach is typically less than that provided by conventional FE approaches due to this scaling, however it is still quite capable of capturing the

buckling of individual plies due to process induced loads. As with all models, one of the key limitations when considering accuracy is the validity of the input parameters, hence the necessity for extensive and reliable characterisation techniques.

2.7 Concluding remarks

The benefits of composite materials are clear. Tailoring a structure to meet specific load paths allows for increased efficiency when matching strength against weight. Minimising weight is a key driver in the civil aeronautical industry as it has a huge impact on fuel efficiency and running costs. The increasing demand from industry has led to the introduction of sophisticated, high rate, automated processes capable of laying composite components rapidly and repeatedly, however this development has not been entirely smooth, as the pace of material development has outstripped the understanding of the material in its uncured form. This, combined with the less sympathetic nature of automated production regarding reworking of material and the understandably high standards required of components for aviation, has led to significant problems with manufacture induced defects in final parts. This is exacerbated by the tailored nature of the components, which do away with the redundancies offered by isotropy in order to reduce component weight as much as possible, amplifying the impact of defects in load paths.

The defects encountered in manufacture are not unavoidable, however, counteracting them often requires an extensive development phase, relying on a trial and error based approach due to the difficulties of process modelling such a complex material. Novel modelling techniques are being developed in response to this but, much like their predecessors, they will still require a deeper understanding of the mechanics at work during forming and consolidation in order that the material characteristics might be properly represented. Several bodies of work have begun on the path towards characterising uncured carbon fibre prepreg, drawing on techniques developed for dry, woven preforms. These works note the difficulty of portraying the nature of the uncured material, often simplifying the material response.

The intent of this work is to therefore focus on two key behaviours exhibited during forming, and critical to the avoidance of wrinkle defects. The first of these is interply shear, a vital mechanism in the realignment of plies within a laminate as they dissipate the stresses built during forming. Intraply shear also helps in this regard, but is most important when considered with respect to bending stiffness, as this shear behaviour will dominate the bending response of the material. In order to analyse interply shear, the shear test method developed by Larberg et al. [10] shall be employed using a cus-

tom built rig. The key focus shall be the accurate modelling of the material response, allowing insight into the individual contributions of the fibre and resin to the overall behaviour of the system. This in itself will allow the suggestion of optimum forming parameters when looking to avoid wrinkling and bridging, and will provide modelling inputs for advanced techniques in development. By deepening the understanding of one single mode of deformation, interply shear, it will be possible to better understand the results presented in characterisation techniques which invoke multiple modes of deformation simultaneously. With that in mind, a technique called Dynamic Mechanical Analysis (DMA) shall be adapted to investigate intraply shear in bending by considering a Timoshenko beam and recalculating the gathered data.

Chapter 3 shall build upon the literature discussed in order to investigate the interply shearing of two sheets of 0° unidirectional prepreg in greater detail, presenting a heuristic model which captures the essence of the load traces obtained using a rig developed from that presented by Larberg et al. [10]. Chapter 4 shall expand this area of research by considering the influence of interface angle on interply shear, allowing the results to be applied to industry standard laminates. In Chapter 5 the results gathered in the previous chapters will be used alongside data gathered from DMA to unpick the influence of intraply shear and interply shear in the bending response of both a single ply and a small laminate of uncured prepreg. Chapter 6 then brings all the gathered characteristics together in a laminate scale demonstrator, and compares experimental data against a simple energy minimisation model. Chapter 7 finally draws some concluding remarks, and details plans for future work.

CHAPTER 3

INTERPLY SHEAR IN UNIDIRECTIONAL CARBON FIBRE PREPREG

Summary

Understanding the interply shear behaviour of uncured carbon fibre prepreg is fundamental to avoiding process-induced defects during manufacturing of large-scale components. Shear tests for 8552/AS4 and a derivative of M21 resin with an IM7 fibre are compared to a one-dimensional viscoelastic-plastic model for interply shear. A methodology capable of determining the parameters of temperature, rate and pressure required for minimum resistance to movement of a prepreg is presented. Investigating the new resin dominated parameter of joint strength and fibre dominated coefficient of friction values individually shows that friction increases with temperature, contrary to previous work, and that the new value of joint strength is predominant at lower temperatures. Rate dependent variables are strongly linked to the resin behaviour, confirming the need for a viscoelastic model. Simple application to industrial scenarios is discussed along with more complex process modelling.

3.1 Introduction

A number of studies [9, 10, 11] have investigated interply slip properties of uncured carbon fibre pre-preg. In each case the shear rheology is characterised by a temperature dependent coefficient of friction. Using an interply slip-rig similar to that used in this work (Section 3.5), the studies showed significant variability between different generations of carbon fibre prepreg [10]. In each case, interply friction displayed a convex dependence on temperature, attaining a minimum at an intermediate manufacturing temperature (see Fig. 3-1).

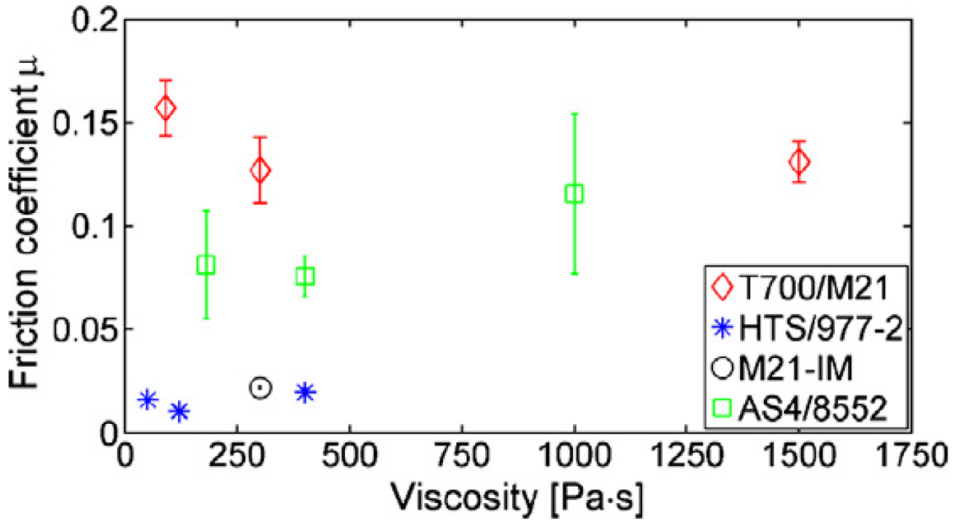

Figure 3-1: *Plots of coefficient of friction against viscosity for several materials, showing a tendency towards some minimum value. Resin viscosity typically reduces with increasing temperature. Image taken from [10]*

The work attributed the initial decrease in friction to hydrodynamic lubrication of the interply region as the resin viscosity decreases with temperature, whilst the subsequent increase was due to intensified intermingling of fibres at higher temperatures. Further experimental work focused on determining surface roughness measures [10] and understanding matrix distribution at different stages of the various processes, whilst using Stribeck theory [9, 11, 12] to determine different regimes of hydrodynamic frictional behaviour.

Although a reasonable initial approximation, the use of a frictional model suggests that the layered structure is infinitely stiff in shear, and that any deformation occurs in the form of slip at the interface above a critical value of stress. Stress/strain traces from the work of Larberg et al. [10] (Fig. 2-22 (Right)) suggest this to be a simplification, noting the presence of some pre-yield stiffness before a post-yield response

after a gradual yield. For forming processes in which shear strains are relatively small (e.g. consolidation over a corner radius, Section 3.2.) the purely frictional model can significantly overestimate the associated shear stresses, whilst underestimating large shear strain behaviour. The intention of this chapter is to extend the characterisation of interply shear behaviour developed in [10] to account for a number of key dependencies not previously investigated; primarily the fact that the small initial shear strain and subsequent large strain slip both exhibit a strong rate dependency, arising from the viscoelastic contribution of the resin. A heuristic model will then be developed to help decompose the observed behaviour into the separate contributions of the resin and fibre.

The first step is to consider the interply shear strain required in two different manufacturing scenarios, forming and consolidation over a corner radius (Section 3.2), in order that we might determine the level of fidelity required in the modelling of the load traces gathered from characterisation tests. Some classic material models and previous work on modelling these load traces is then presented in Section 3.3. In Section 3.4 a one-dimensional viscoelastic-plastic model is derived which captures the behaviour observed in the literature, with Section 3.5 describing the experimental method developed to validate it. This model, parametrised by the experimental data (Section 3.6), provides simple metrics by which to compare through-thickness shear properties (Section 3.7) for different materials and manufacturing conditions (e.g. temperature, pressure or rate), providing insight into the mechanics governing the material response. The parametrised model presented here suggests process dependent conditions (temperature and rate) for optimal manufacturability. The chapter concludes with a summary of the key findings, and possible future avenues of research.

3.2 Interply shear strain in consolidation and forming

A laminate of uncured carbon fibre prepreg can be simply represented as a stack of thick, stiff, fibrous layers separated by thin, weak, resin layers. Applying a shear load parallel to these layers will result in a localised shear deformation in the weak resin layers, whilst the fibrous layers move relative to one another without themselves shearing to any appreciable degree (see Fig. 1-2). The deformed shape suggests the shear deformation is carried almost exclusively by the weak interface layers between the plies. The stiffness of this interface region therefore appears the governing factor when determining resistance to interply shear, requiring us to consider the more complex viscoelastic properties of the resin.

By understanding the geometry of the part and forming process employed it is

possible to calculate the shear strain required for the part to conform to the required geometry (see for example the out-of-plane wrinkles shown in Fig. 2-14), allowing shear strain to be determined from a combination of the tool angles and percentage consolidation, rather than having to manually measure to slip between each layer. These shear strains typically become fairly significant due to the very thin plies, and as such the shear strain, γ is modified as per Hencky strain such that $\gamma_{large} = \ln(1+\gamma)$. This is discussed in more detail in Section 3.7.6. If we consider two different forming approaches we can understand the difference in shear strain required. First we consider a debulk scenario (Fig. 3-2 (Left)), such as might occur after deposition of plies around a radius using AFP.

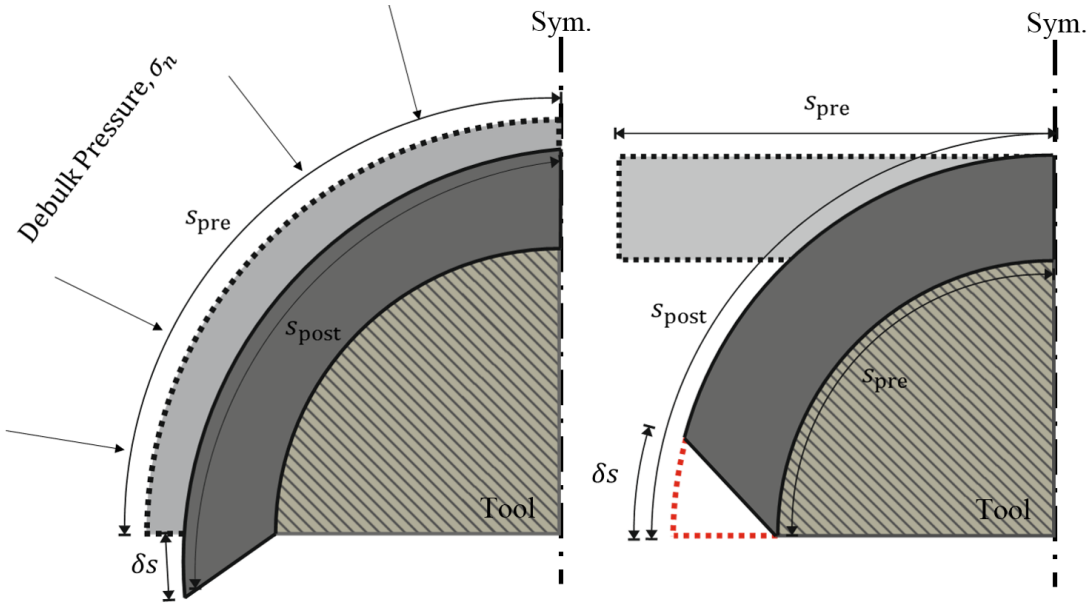

Figure 3-2: *(Left) Consolidation of a composite laminate over one half of a symmetrical semi-circular tool. (Right) Drape forming of a composite laminate over the same tool. δs is the total slip. Due to symmetry the right hand edge of the laminate is effectively fixed horizontally.*

For this example the total slip at the free edge can be calculated as the difference between the outer arc length before and after debulk. The pre-debulk arclength $s_{\text{pre}} = (r + \frac{1}{2}(Nh))\theta$, where r is tool radius, N is number of plies, θ is tool angle and $h/2$ is ply thickness. The post-debulk arc length $s_{\text{post}} = \theta(r - \frac{1}{2}((1-\alpha)Nh))$, where α is the percentage consolidation. Therefore for the consolidation scenario, the required shear strain is

$$\gamma_{\text{cons.}} = \ln\left(1 + \frac{s_{\text{pre}} - s_{\text{post}}}{\frac{1}{2}(Nh)}\right) = \ln\left(1 + \alpha\theta\right). \tag{3.1}$$

Figure 3-2 (Right) relates to a drape forming scenario in which a laminate is laid flat then formed to a geometric tool. For this example the interply slip is the difference in length between the arc length at the outer radius $s_{\text{post}} = \theta(r + \frac{1}{2}(Nh))$ and the length of the laminate $s_{\text{pre}} = \theta r$. Thus

$$\gamma_{\text{form}} = \ln\left(1 + \frac{s_{\text{post}} - s_{\text{pre}}}{\frac{1}{2}(Nh)}\right) = \ln(1 + \theta) \tag{3.2}$$

Interestingly, the shear strain generated is primarily dependent on the angle of the corner radius θ, and for the consolidation case the level of consolidation. In both cases the shear strain increases incrementally as we move away from the axis of symmetry, reaching a maximum at the free edge. If we consider $\theta = \pi/2$ and the level of consolidation is $\alpha = 12\%$ [7, 3], we see that the corner consolidation example generates a maximum shear strain of $\gamma_{\text{cons.}} = 0.17$, whilst the drape forming scenario requires a much greater maximum shear strain of $\gamma_{\text{form}} = 0.94$.

3.3 Modelling interply shear

The load traces obtained from both fibre pull-out and interply shear testing do not readily lend themselves to existing material models. Figure 2-22 (Right) shows a transition from some initial stiffness to a hardening response, following a fairly gradual yield. The importance of capturing this initial response depends upon the shear strain at which yield occurs compared to the shear strain required for the part to form. For example, if the critical shear strain is very low, and the shear strain required to form is very high, there is no need to accurately model the initial response, rather a simple frictional model fitted to the post yield response will suffice (Fig. 3-3 (Left)). In practice, results in section 3.6 show the opposite to be the case, particularly for the consolidation scenario presented earlier, thus requiring the initial behaviour to be considered. Just as importantly, the post yield stiffness has significant implications for large strain scenarios. A simple improvement on the frictional response is to instead consider two gradients taken to fit the initial gradient, K and the post yield gradient K_t (Fig. 3-3 (Right)).

There are two key considerations when looking to model the shear response of uncured carbon fibre prepreg. Firstly, the assumed localisation of the deformation to the resin interface dictates that we take the resin response to be dominant so long as the interfacial layer exists in any thickness, requiring some representation of viscoelasticity. Secondly, the post yield behaviour cannot be simply represented as plastic, but must instead consider some form of work hardening.

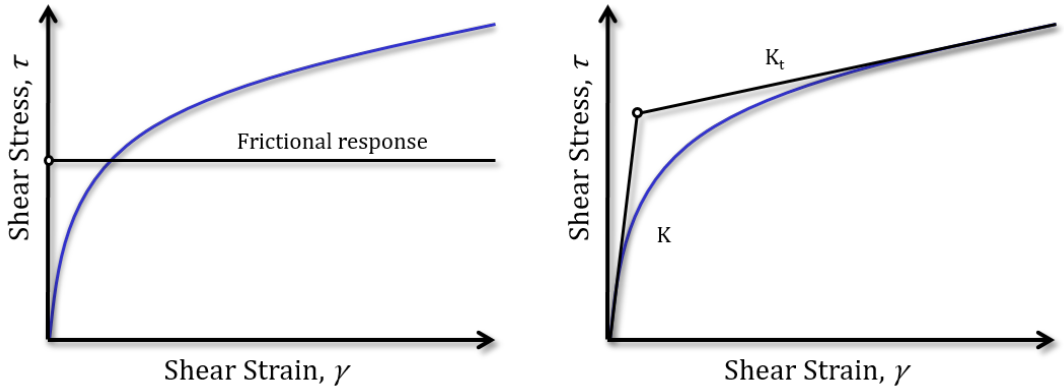

Figure 3-3: *(Left) A Coulomb friction approximation of a typically stress/strain trace significantly overestimates the initial material response, whilst underestimating the post yield behaviour. (Right) Constructing a bilinear response greatly improves the accuracy of any attempt of modelling the behaviour, although the gradual yield is still not captured well.*

3.3.1 Viscoelasticity

As discussed in Chapter 2, the resin matrix of a carbon fibre laminate is designed both to transfer tensile load to the fibres, and to carry compressive loads which would otherwise cause the fibres to buckle. It can only perform these functions when cured however. Whilst a cured thermoset resin is fairly elastic in its response, uncured resin is a viscoelastic liquid lending very different properties to the overall characteristics of the prepreg.

Viscoelastic materials display characteristics common to both pure elastic and viscous materials when undergoing deformation. Of particular importance is their dependency on strain rate [49], which could potentially limit the rate at which parts are formed.

Classic viscoelastic models

Two base models for viscoelastic materials exist, representing a viscoelastic material as a Hookean spring and Newtonian dashpot connected either in series or in parallel (Fig. 3-4). These are the Maxwell Model and Kelvin-Voigt Model respectively. Due to the manner in which the components are combined, one is better suited to modelling creep, whilst the other is suited to relaxation.

The connection of a spring and dashpot in series as found in a Maxwell Model is displayed in Fig. 3-4 (Left). In this model the stress on each component is equal to the total imposed stress and the sum of the strain is each component gives the total system strain [50]. An equation relating stress to strain in a Maxwell material is therefore a

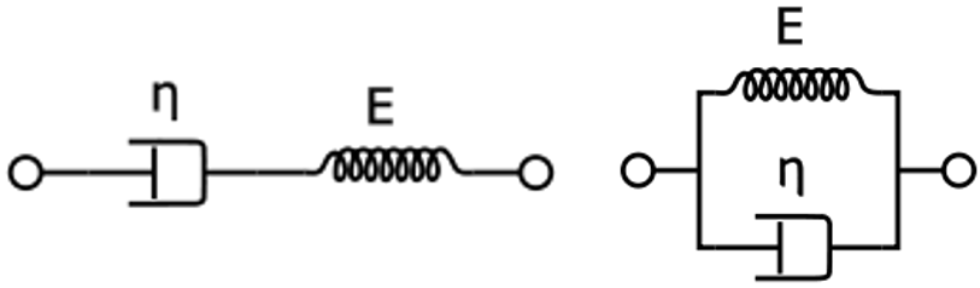

Figure 3-4: *Hookean spring and dashpot aligned in (Left) series, as per the Maxwell model and (Right) parallel, as per the Kelvin-Voight model.*

constitutive equation combining the relationship of a Hookean spring:

$$\sigma = E\epsilon \tag{3.3}$$

where σ is stress, E is Young's modulus and ϵ is strain, and a Newtonian dashpot, presented as:

$$\sigma = \eta\dot{\epsilon} \tag{3.4}$$

where η is the viscous coefficient, and $\dot{\epsilon}$ is strain differentiated with respect to time. The time dependent strain in the material can be presented as:

$$\dot{\epsilon} = \dot{\epsilon}_s + \dot{\epsilon}_d = \frac{\dot{\sigma}}{E} + \frac{\sigma}{\eta} \tag{3.5}$$

where $\dot{\epsilon}_s$ relates to the strain in the spring and $\dot{\epsilon}_d$ relates to the strain in the dashpot. As the Maxwell model portrays strain as a linear function of time it cannot be used to predict creep, as the dashpot will extend indefinitely once the spring has stopped extending. It can be used to predict relaxation by prescribing a constant strain ϵ_0 however.

A Kelvin Voigt model with a spring and dashpot in parallel is displayed in Fig. 3-4 (Right). As the components are in parallel the strains in each component are equal to the overall strain. The overall stress is therefore equal to the sum of the stress in each component [51]. Combining the component stress equations for the spring and dashpot we can determine the stress within the material to be:

$$\sigma = \sigma_s + \sigma_d = E\epsilon + \eta\dot{\epsilon} \tag{3.6}$$

As such we are able to investigate the change in rate of deformation and model creep for a constant stress. The stress or strain in the material can therefore be determined

by applying a constant load or rate of deformation. This allows the calculation of the constitutive Young's Modulus for each particular mechanical action which should indicate the contribution of each component of the prepreg. The successful application of these models requires that the viscosity, controlled by temperature, be constant throughout each test.

In practice, initial testing has shown that the complexity of uncured prepreg as a material prevents the simple application of one of these material behaviours however, requiring that a more tailored solution be considered.

Time series decomposition

The Kelvin-Voight and Maxwell models are both examples of time series decomposition. Time series decomposition separates a time series into distinct components, a time independent component, T_t, and a time dependent component, S_t. These components are typically combined in one of two common forms. Firstly, additive decomposition, in which

$$y_t = T_t + S_t \tag{3.7}$$

is used when there exists some residual material response independent of rate, i.e. at $du/dt = 0$. The Kelvin-Voigt model is a good example of additive decomposition, with the spring in parallel to the dashpot meaning that even infinitely slow deformation must account for the stiffness of the spring. By contrast, multiplicative decomposition, of the form

$$y_t = T_t S_t \tag{3.8}$$

is used when there is no material response at zero rate, with the Maxwell model demonstrating this. The arrangement of the spring and dashpot in series means that infinitely slow deformation will simply result in the extension of the dashpot component with zero stiffness and no deformation of the spring.

If we let our time independent component:

$$T_t = E\epsilon \tag{3.9}$$

and our time dependent component:

$$S_t = \eta\dot{\epsilon} \tag{3.10}$$

as per the Hookean spring and Newtonian dashpot presented in the previous section,

we can plot stress against strain for each series (Fig. 3-5).

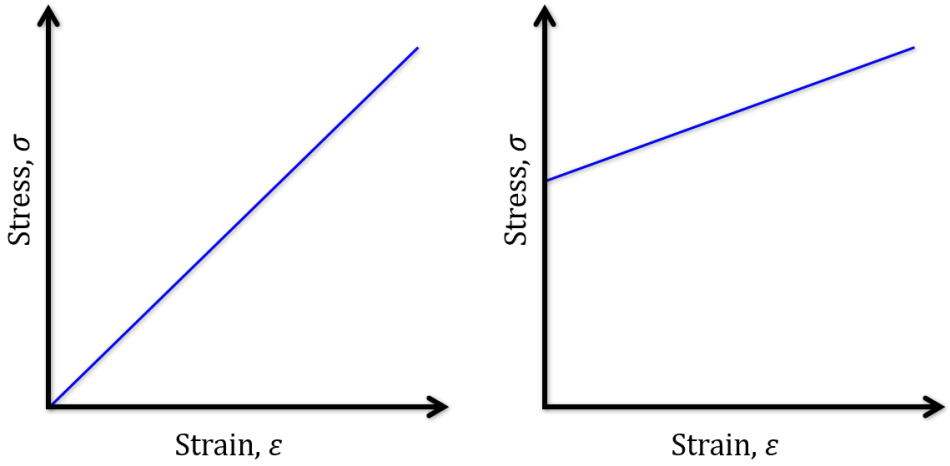

Figure 3-5: *Stress vs. strain response for a multiplicative (Left) and an additive (Right) series respectively*

Of these two behaviours multiplicative decomposition initially appears to be best suited, as it starts at (0,0), as per the traces presented by Larberg et al. [10]. This is problematic however, as the findings in Section 3.4 suggest the existence of some rate independent elastic component, which is not captured in this model. The solution is to consider a combined series of the form:

$$\sigma = m\epsilon \tag{3.11}$$

where

$$m = E + \eta\dot{\epsilon} \tag{3.12}$$

The additive behaviour required to capture the rate independent elastic component is therefore provided by Eqn. 3.12, which is then substituted into Eqn. 3.11 to provide the overall behaviour observed in the tests.

Although this might seem contrary to the classical viscoelastic models discussed in the previous Section, considering the manner in which strain is generated during an interply shear experiment this begins to make sense. Due to the manner in which the carbon fibre is clamped into the test rig, deformation is achieved by applying load directly to the fibres in the prepreg (see Section 3.5 for detailed methodology). Although deformation localises at the resin interface, the direct application of stress from the test rig to the elastic fibrous region means that the initial response must be

purely elastic.

The strain rate at the interface is dependent upon there being some strain in the fibres, hence the rate independent elastic component. The deviation from classical viscoelasticity is therefore necessary in order to capture the behaviour of the structure as it is loaded, rather than generalise the response based on just one of the constituent materials.

3.3.2 The limitations of Coulomb friction

With a model in place for the initial gradient, the next aspect to consider is the yield event seen in Fig. 2-22. Work by Larberg et al. [10] shows this yield to be both temperature and pressure dependent. This points towards some frictional contact between the fibrous region of the two plies at their interface, as well as the resin contribution. Due to the fairly non uniform distribution of resin, and that fact that it will inevitably redistribute when subjected to pressure (particularly at higher temperatures when the viscosity is low), the frictional component does not come as surprise. Attempting to model this as a simple Coulomb yield event however does not seem reasonable, due to the adhesive nature of uncured resin. Considering the equation for Coulomb friction, in which our critical shear stress, τ_c is calculated as:

$$\tau_c = \mu\sigma_n \tag{3.13}$$

where μ is coefficient of friction and σ_n is normal stress, or pressure, we would have a system in which resistance to shear would reduce to 0 as σ_n reduced to 0. The presence of the resin will however presumably result in some resistance to deformation at $\sigma_n = 0$.

Mohr-Coulomb yield criterion

For a system in which there exists some adhesive material behaviour, a Mohr-Coulomb model is immediately better suited to representing the yield stress, such that:

$$\tau_c = \tan\phi_\mu\sigma_n + j \tag{3.14}$$

in which j represents the joint strength, in this case the adhesion of the resin, and ϕ_μ is the angle of internal friction calculated from the angle of the failure envelope on a plot of critical shear stress against normal pressure (Fig. 3-6).

The coefficient of friction thus equates to μ =tanϕ, such that

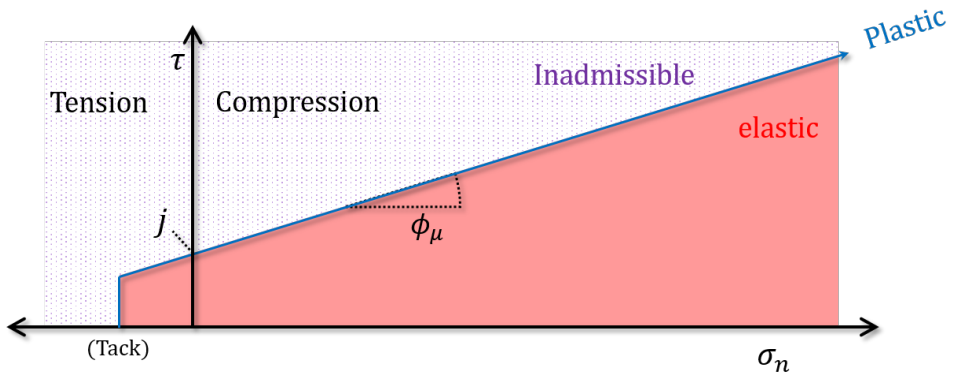

Figure 3-6: *Calculating joint strength, j, and internal friction angle, ϕ_μ, from a plot of critical shear stress vs. normal pressure.*

$$\tau_c = \mu\sigma_n + j \tag{3.15}$$

This model therefore considers the contributions of both the fibres and the resin matrix to the yield behaviour using the parameters μ and j respectively. Observing the relationship between these parameters over varying test conditions will allow the determination of the changing dominance of the individual materials in governing the yield behaviour during a cure cycle.

3.3.3 Post yield hardening

The final behavioural aspect to consider is the post yield stiffness. The assumption of purely frictional behaviour results in a post yield response with zero stiffness, which clearly does not match the load traces gathered by Larberg et al. [10]. One way in which to capture this behaviour is to model it as plastic flow, which is a common cause of material non-linearity. Nonlinearity occurs when stress and strain are linked via a strain dependent matrix, rather than a matrix constructed of constants. This poses the problem of deriving equations in which the material properties are dependent upon the strain, without knowing the strain in advance.

Suppose that yield has occurred (i.e. $\tau \geq \tau_c$) then an additional shear strain increment is applied $\Delta\gamma$. This strain increment can be decomposed into elastic ($\Delta\gamma_e$) and plastic ($\Delta\gamma_p$) contributions, such that $\Delta\gamma = \Delta\gamma_e + \Delta\gamma_p$. This results in the unloading cycle shown in Fig. 3-7.

From the decomposition it follows that

$$\Delta\tau = K\Delta\gamma_e = K(\Delta\gamma - \Delta\gamma_p) \tag{3.16}$$

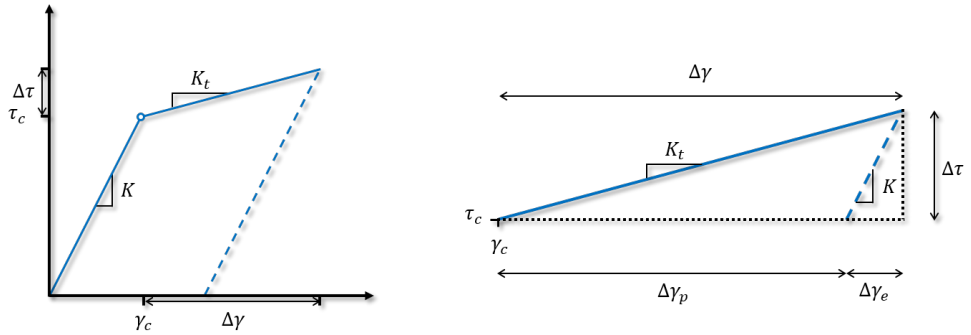

Figure 3-7: *(placeholder) Stress-strain plot in uni-axial stress, idealised as two straight lines where τ_c is the stress at yield*

The hardening rule, which will account for the post yield stiffness, is then defined by

$$\Delta\tau = H\Delta\gamma_p \tag{3.17}$$

where H is the strain-hardening parameter. Equating Eqs. (3.16) and (3.17) it follows:

$$H\Delta\gamma_p = K(\Delta\gamma - \Delta\gamma_p) \text{ therefore } \Delta\gamma_p = \frac{K}{H+K}\Delta\gamma \tag{3.18}$$

The post yield response is therefore given by

$$\Delta\tau = K_t\Delta\gamma = K\left(1 - \frac{K}{K+H}\right)\Delta\gamma \tag{3.19}$$

where K_t is termed the consistent tangent stiffness. Rearranging Eqn. 3.18 for the hardening parameter gives the expression

$$H = \frac{KK_t}{K - K_t} \tag{3.20}$$

The hardening parameter H can therefore by determined from the two gradients, K and K_t.

3.4 One dimensional viscoelasto-plastic model for inter-ply shear

Drawing together the various models discussed in Sections 3.3.1 and 3.3.2 we can create a heuristic model capable of representing the key aspects of the stress/strain traces

plotted from experimental data. Firstly, adapting Eqn. 3.6 for shear stress, τ, gives the relationship:

$$\tau = \left(S + \eta \frac{d\gamma}{dt} \right) \gamma = K\gamma \tag{3.21}$$

where S is the rate independent elastic shear stiffness, η the coefficient of viscosity and $d\gamma/dt$ the strain rate. The parameter K denotes the overall initial rate dependent shear stiffness. To determine S and η, the pre-yield gradient K is plotted against increasing strain rates R. It follows from Eq. (3.21), that the rate independent parameter S is given by the y-intercept, whilst η can be fitted in the least square sense, in this instance using `MATLAB`'s inbuilt function `cftool` [81].

The shear strains encountered in both industrial forming processes and the experimental setup can be large (i.e. $\gamma > 0.5$), therefore 'true' strain measures must be considered. If $u(t) = Rt$ is the displacement for some constant displacement rate R, h is the through thickness dimension (where for the material used, individual ply thickness $h/2 = 0.25$mm) it follows that

$$\gamma = \ln\left(1 + \frac{Rt}{h}\right) \quad \text{and} \quad \frac{d\gamma}{dt} = \frac{R}{h + Rt} \tag{3.22}$$

For small shear strains such as those seen in the initial response, i.e. γ <0.15, t is small and it can be assumed that $d\gamma/dt \simeq R/h$.

Selecting the correct thickness from which to determine shear strains is in itself an interesting problem. If we consider the structure of a laminate as being a series of thick stiff fibrous layers and thin weak resin layers, it seems logical to assume that deformation will localise to the resin layer. Observing the formation of the model however, we can see that changing the thickness will result in a simple ratio change, so long as the same thickness is used throughout. We should therefore consider the scale we are most interested in investigating; the micro-scale process or the macro-scale deformation. For the purposes of this work, in which tests are conducted for two plies and one deformable interface, we take h to be twice the ply thickness so that the results can be more readily scaled to laminate deformation. This approximation is discussed in more detail in Section 3.7.

The onset of interply slip is defined by a Mohr-Coulomb yield criterion as presented in Eqn. 3.15, such that μ is the coefficient of friction, σ_n is the normal stress and j a measure of joint strength. Joint strength initially appears similar in concept to tack, however the parameter presented here specifically describes the shear joint strength, whereas tack relates to the tensile joint strength. The coefficient of friction μ and joint strength j are determined by calculating τ_c over a range of confining pressures σ_n.

Knowing that the two straight lines intersect at the critical shear stress τ_c the equation of the second straight line can be constructed

$$\tau = K_t\gamma + c \tag{3.23}$$

where c is the y-intersect, derived from the following steps

$$\tau_c = K_t\gamma_c + c = K\gamma_c \tag{3.24}$$

where critical shear strain $\gamma_c = \tau_c/K$. Substituting this into Eqn. 3.24 gives

$$\tau_c = \frac{K_t\tau_c}{K} + c \tag{3.25}$$

Rearranging for c and substituting back into Eqn. 3.23 finally shows shear stress to be

$$\tau = K_t\gamma + \tau_c\left(1 - \frac{K_t}{K}\right) \tag{3.26}$$

This model therefore gives an idealised bi-linear response, as shown in the stress-strain plot Fig. 3-8. The modelling parameters can be approximated from the experimental stress-strain data by first constructing two lines of best fit from the pre and post yield load paths, the gradients of which are approximations to K and K_t (Fig. 3-8), whilst their intercept gives the critical shear stress τ_c.

This simplified heuristic model is used to condense the set of complex experimental results into a small set of key parameters, whilst retaining the fundamental mechanics observed. This model and the set of parameters provide simple metrics by which to compare through thickness shear properties for different materials and manufacturing conditions (e.g. temperature, pressure or rate, see Section 3.6). Furthermore, such data provides vital input for process models, see for example [3, 4] (Section 3.7.7).

3.5 Experimental procedure, material and sample preparation

3.5.1 Methodology

Figure 3-9 (Left), shows a schematic of the test rig used to generate the stress/strain traces, which consisted of two independent components. Firstly, a lock-able hinged array connected to an Instron load cell at (i), consisted of a pneumatic cylinder (ii) which pulled together two plates (area, A = 50×50 mm^2) wrapped in a single layer of

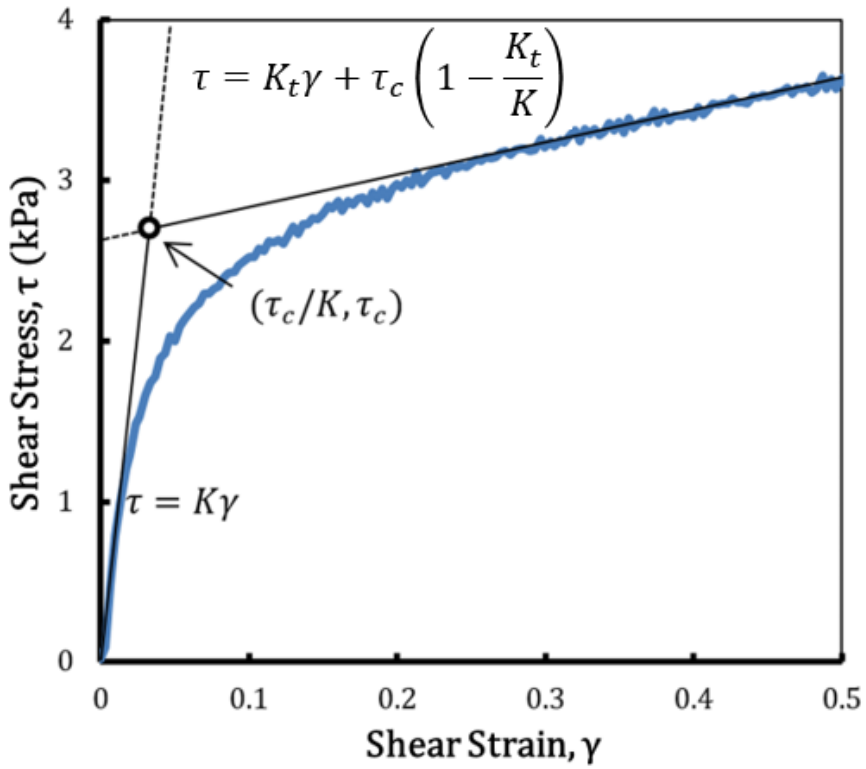

Figure 3-8: *The bi-linear stress-strain response for the viscoelasto-plastic model overlays a typical experimental stress/strain trace for fixed temperature of* $70°C$*, normal pressure* $\sigma_n = 75kPa$ *and strain rate* $d\gamma/dt = 3.33e\text{-}3s^{-1}$*. The plot is characterised by two lines, which describe the shear response pre and post-yield* ($\tau > \tau_c$)*.*

carbon fibre prepreg (iii). These plates clamped either side of a central plate (area, A = 100×150 mm^2)(iv), also wrapped in a layer of carbon fibre prepreg, which was fixed to the bottom mounting of an Instron testing machine (v). The carbon fibre was wrapped and clamped in such a way as to prevent movement of the ply relative to the plate surface. The rig was mounted within an environmental chamber, allowing the temperature of test to be controlled. The test procedure was as follows: (1) test temperature was achieved in the environment chamber (2) the pressure in the pneumatic cylinder was controlled to generate a normal clamping stress σ_n between the side and central plates (3) the Instron pulled the upper part of the rig at a constant rate $R = du/dt$, whilst the load cell recorded the force F. The rig itself is constructed from 10mm thick mild steel, with the arms being made from two beams each to ensure adequate stiffness (see Fig. 3-10) The use of threaded collars removed slack between the rig and the test fixture, as well as the risk of any lateral movement.

All experiments were carried out using AS4/8552, wrapped around each plate so that the fibres were oriented vertically (i.e in the direction of loading, referred to as

0°). This material was chosen as it is effectively the genesis material for a series of prepregs commonly used in the aerospace industry. Tests were conducted at a range of rates R, temperatures and confining pressures σ_n. Each test was conducted three times to ensure repeatability of results. The set of tests carried out are summarised in the test matrix, Table 3.1.

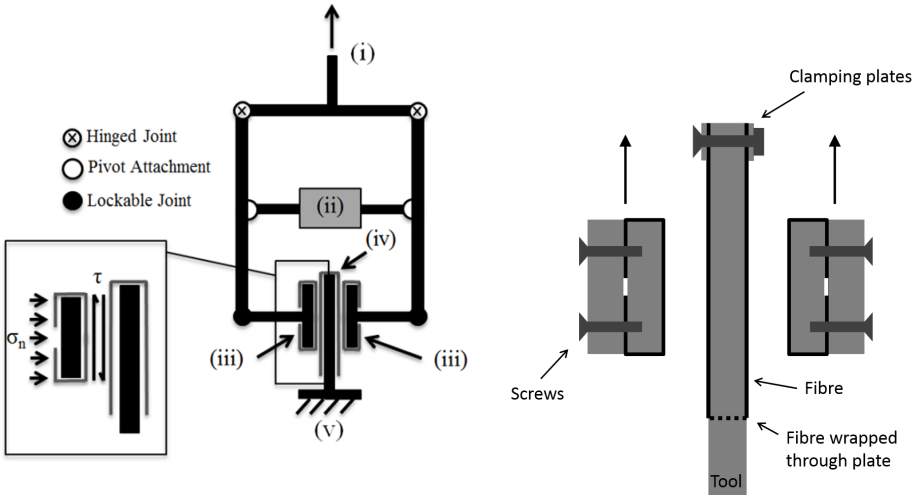

Figure 3-9: *(Left) Schematic of interply test rig in which the two individual parts move apart at constant rate du/dt and the required force is recorded. (Right) Detail of the fibre-plate clamping, with arrows denoting the direction of travel of the side plates. The dashed line on the centre plate indicates where the ply is passed through a gap in the tool so that it is effectively clamping itself.*

Figure 3-10: *Photograph of the interply shear test rig mounted in an environmental chamber. Note the threaded collars connecting the lower plate to the test bed.*

Rate R **(mm min^{-1})**	**Pressure** σ_n **(kPa)**	**Temperature** $(^{\circ}C)$						
		40	**50**	**60**	**70**	**80**	**90**	**100**
0.01	**75**	-	×	×	×	-	×	-
0.05	**75**	-	×	×	×	-	×	-
0.1	**25**	×	-	×	-	×	×	-
0.1	**50**	×	-	×	-	×	×	-
0.1	**75**	×	×	×	×	×	×	×
0.1	**100**	×	-	×	-	×	×	-
0.15	**75**	-	×	×	×	-	×	-

Table 3.1: *Experimental matrix for AS4/8552. Each* × *represents a set of at least* 3 *repeated experiments*

3.5.2 Rig calibration and measures to minimises sources of variability

Before carrying out these tests it was necessary to calibrate the rig for a material with a known coefficient of friction. A number of tests were carried out using PTFE instead

of CFRP; giving an average value of $\mu = 0.096$, which was within the documented range of 0.05-0.10 [13]. The following operational caveats were noted:

Side plates: As the side plates were mounted on a cross beam it was necessary to ensure that each plate moved at the same rate. By rigging extensometers between the side and main plates it was possible to monitor any potential discrepancies between the crosshead displacement and that of each plate. Over the course of several experiments it was proven that differential movement did not occur to any noticeable extent. A similar technique was also employed to ensure that the side plates did not rotate upon being loaded.

Controlling constant confining pressure: Another potential source of error was the continuity of the clamping pressure during testing, as this could not be measured directly. It was reasoned that the load applied by the pressure cylinder could be monitored by observing the pressure gauge on the air feed. Any fluctuations in this pressure would indicated a change in lateral loading. Due to the relatively low loads required to slip the interfaces it was also necessary to use a sufficiently accurate load cell with a maximum capacity of 1kN.

Controlling temperature: Temperature was measured by means of a thermocouple attached to the edge of one of the side plates. As the plates themselves are small and made of mild steel they have a fairly high coefficient of thermal conductivity, therefore it was safe to assume that the temperature at the middle of the plate would not differ significantly from that at the edge, and was well within the $\pm 5°C$ tolerance expected by industry in the manufacturing stages. It should be noted however that at low temperatures this error can lead to significant changes in resin viscosity. This was especially apparent in initial testing at room temperature, and was part of the motivation behind setting the lower temperature limit to 40°C.

Consistency of sample: As we were interested in the uncured properties it was also vital to ensure that the tests are conducted prior to the material going out of tack life, as this can have a significant effect on the behaviour of the material [73]. To ensure minimal out time from the freezer, each sample was defrosted for 20 minutes and prepared immediately before testing from larger pre-cut sheets to avoid repeatedly defrosting the entire role of material. During the test regime the target temperature was reached and held for 5 minutes before pressure was applied to ensure the samples were fully heated. In this way all samples could be tested from the same level of starting consolidation, although it was expected that some would consolidate more than others by the end of the test. Unfortunately, it was not possible to measure the change in ply thickness during the test. As such, the thickness value used in Section 3.4 was assumed to remain constant.

3.6 Results

Figures 3-11, 3-13 and 3-13 display a number of stress/strain traces for tests conducted at a variety of temperatures, pressures and rates. The traces show the same general behaviour, with an initial stiff response changing to a less stiff response after a gradual yield.

The variation of critical shear stress τ_c against temperature is plotted in Fig. 3-14 with associated error bars, reaching a minimum at 90°C. Figure 3-15 shows the plot used to derive parameters from Eqn. 3.15, fitting a straight line to the data, the y-intercept giving the joint strength j, whilst the gradient is the coefficient of friction μ. Figure 3-16 shows how the joint strength j and coefficient of friction μ change with increasing temperature. Joint strength (Fig. 3-16) decreases with increasing temperature. However, the coefficient of friction increases with temperature, Fig. 3-17.

The derivation of the parameters in Eqn. 3.21 is shown in Fig. 3-18, plotting initial stiffness against rate of deformation The intersect provides the rate independent shear modulus whilst the gradient gives the viscosity. The rate dependent data provides parameters for the viscoelastic model, see Table 3.3. The plots of S and η, shown in Fig. 3-19, show that both values decrease with temperature. However, strain hardening parameter H against temperature displays a peaked response, reaching an apparent maximum at approximately 60°C (Fig. 3-21).

Due to the manner in which modelling parameters are derived, there is a mix between error bars and regression coefficients. Values which were drawn directly from the stress/strain traces, i.e. K and τ_c, are shown with error bars generated from repeat tests. In Table 3.2 all values of j and μ with associated regression coefficients are given. The remaining modelling parameters are gathered in Table 3.3 from fitting data to these parameters, as such they are displayed with regression coefficients as they were not repeated. Typically, the error bars were relatively small, with an average error of 4-6% for K values and slightly more error (10-12%) for τ_c values as a result of τ_c being dependent upon two testing variables. The coefficients of regression are particularly good, in part due to the values being derived from plots of mean data.

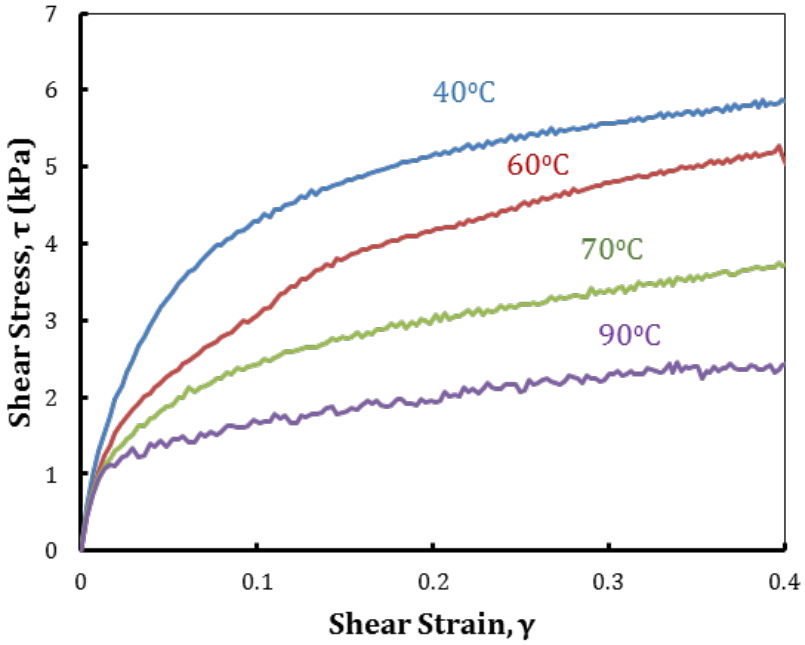

Figure 3-11: *Shear stress τ against shear strain γ for varying temperature. The data was generated at a fixed rate $d\gamma/dt = 3.33e^{-3}s^{-1}$ and pressure $\sigma_n = 75kPa$. The data was generated at a fixed rate $d\gamma/dt = 3.33e^{-3}s^{-1}$ and a temperature of $90° C$.*

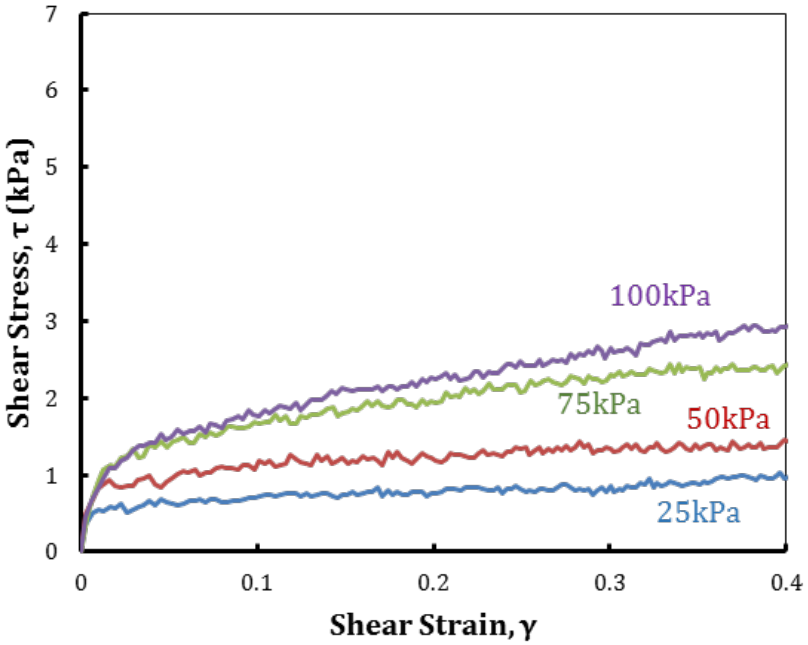

Figure 3-12: *Shear stress τ against shear strain γ for varying pressure, σ_n. The data was generated at a fixed rate $d\gamma/dt = 3.33e^{-3}s^{-1}$ and a temperature of $90° C$.*

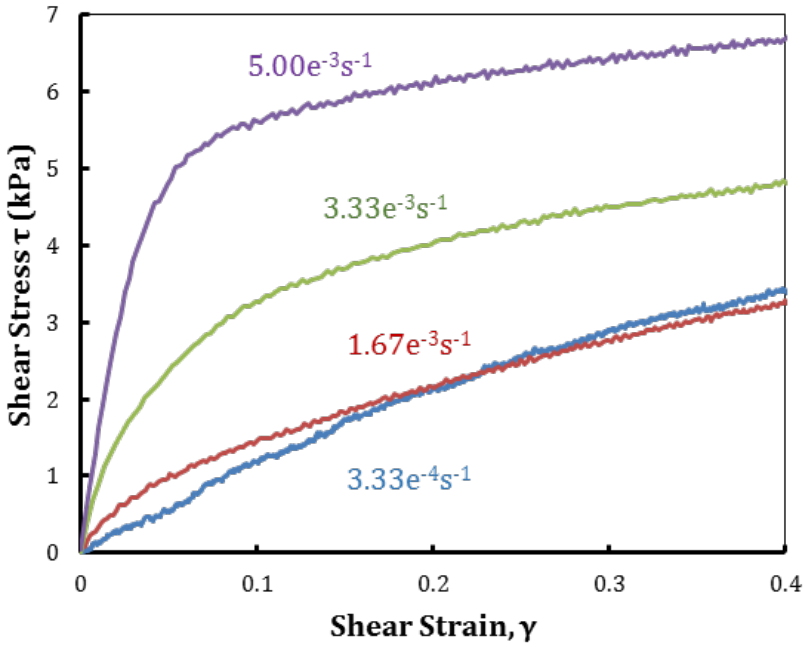

Figure 3-13: *Shear stress τ against shear strain γ for varying strain rate, $d\gamma/dt$. The data was generated at a fixed temperature of $70°C$ and pressure $\sigma_n = 75kPa$.*

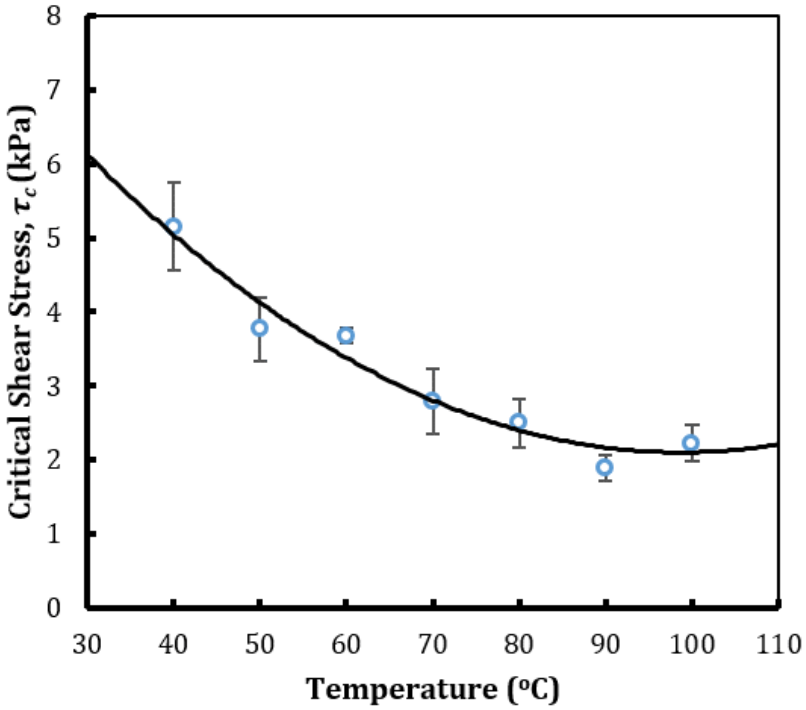

Figure 3-14: *Critical shear stress τ_c against temperature, for a strain rate $d\gamma/dt$=$3.33e^{-3}s^{-1}$.*

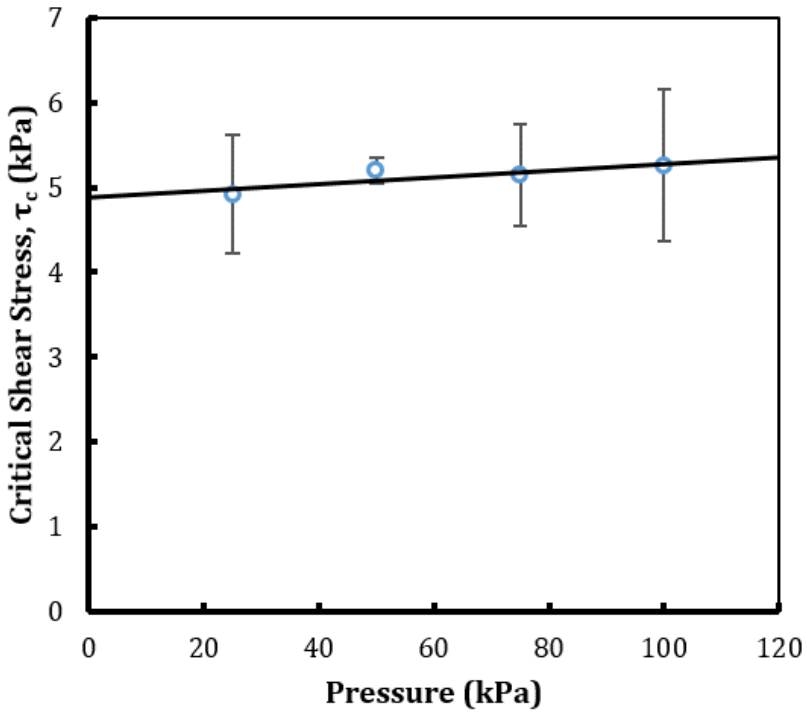

Figure 3-15: *Plot of critical yield stress τ_c against normal stress σ_n for a fixed temperature of $40^\circ C$ and strain rate $d\gamma/dt = 3.33 \times 10^{-3} s^{-1}$.*

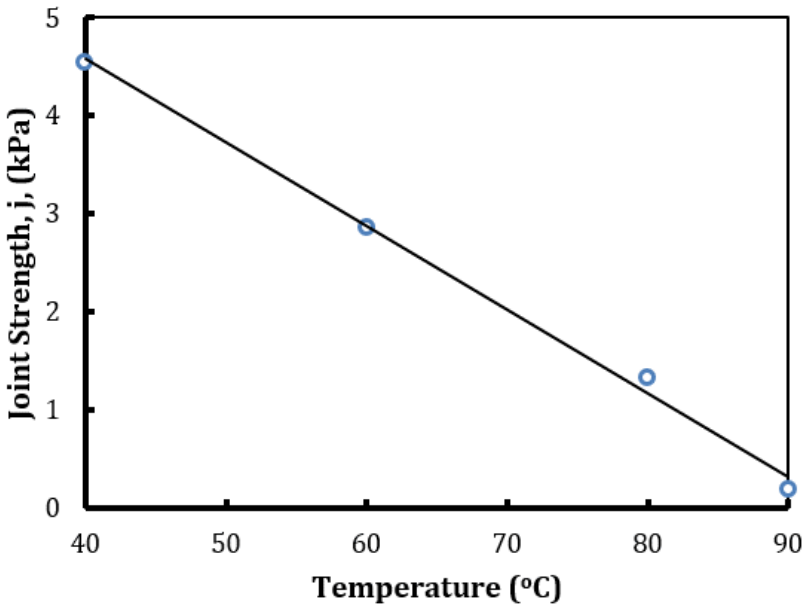

Figure 3-16: *Joint strength j against temperature. The data was generated at a fixed rate $d\gamma/dt = 3.33e^{-3} s^{-1}$.*

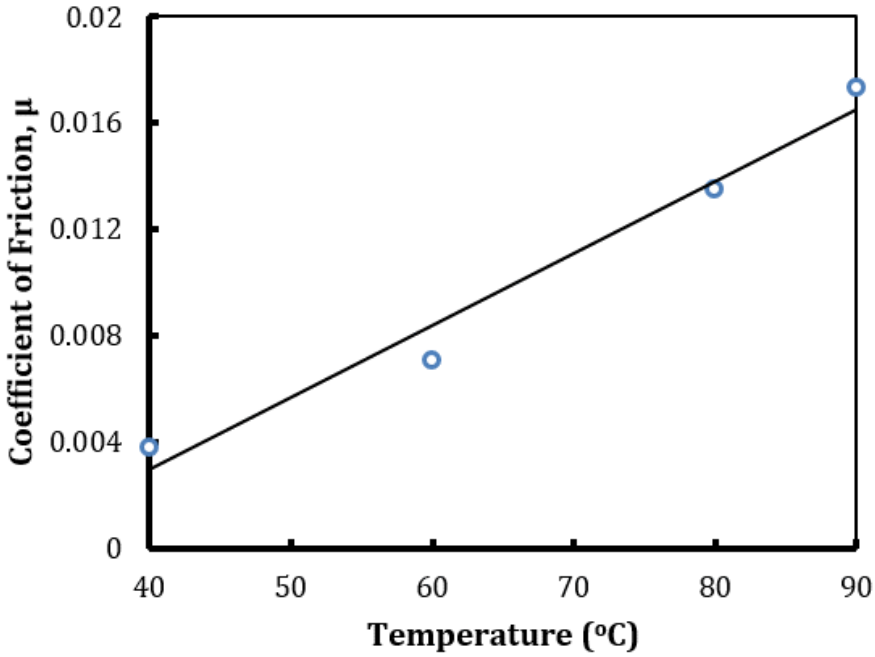

Figure 3-17: *Coefficient of friction μ against temperature. The data was generated at a fixed rate $d\gamma/dt = 3.33e^{-3}s^{-1}$.*

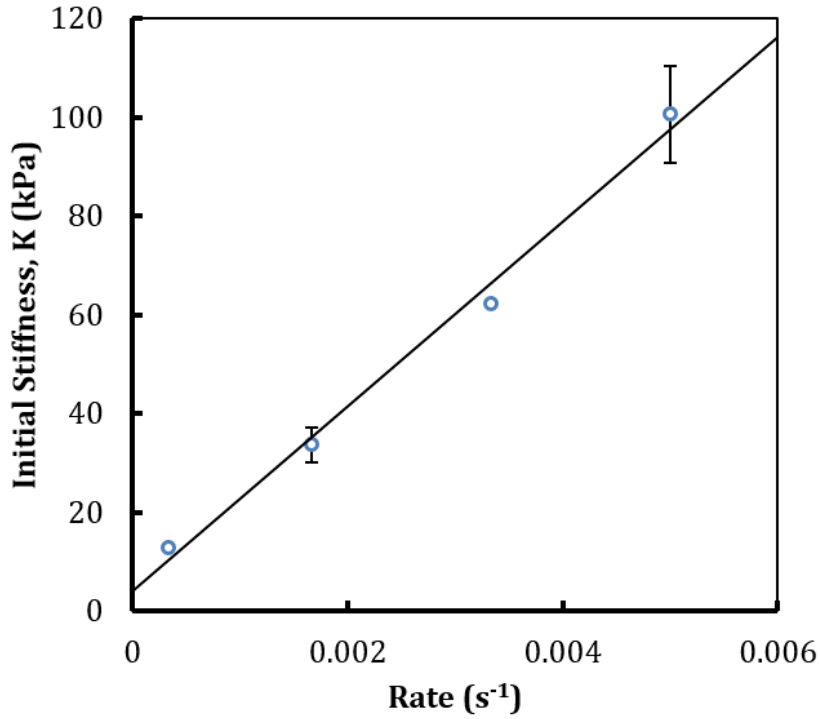

Figure 3-18: *Plot of K against $d\gamma/dt$ for a fixed temperature of 70° at a fixed pressure σ_n = 75kPa. Error bars for points 1 and 3 are obscured by the data points.*

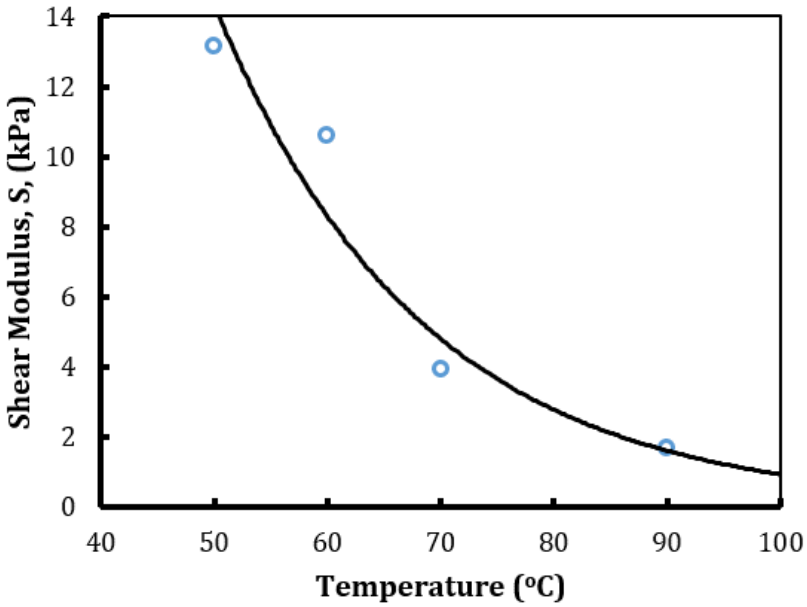

Figure 3-19: *Rate independent shear modulus S against temperature. All tests conducted at a pressure $\sigma_n = 75kPa$.*

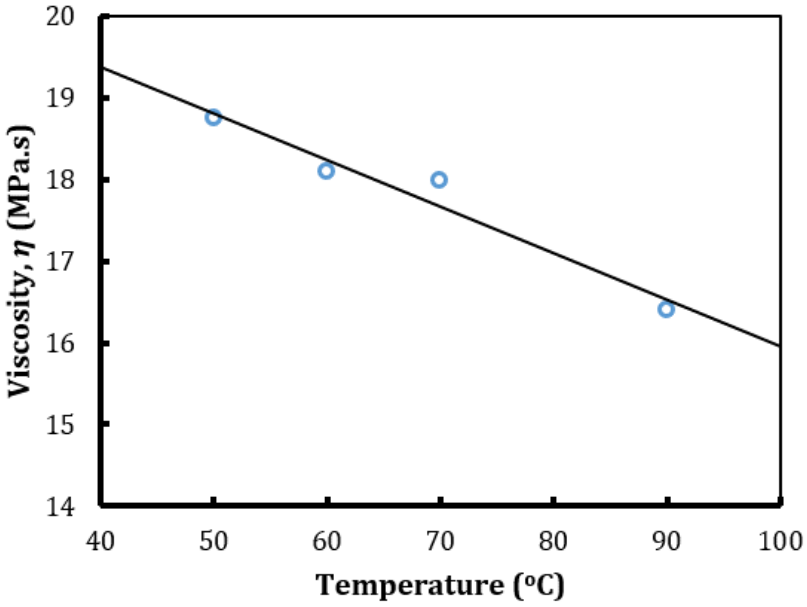

Figure 3-20: *Coefficient of viscosity η against temperature. All tests conducted at a pressure $\sigma_n = 75kPa$.*

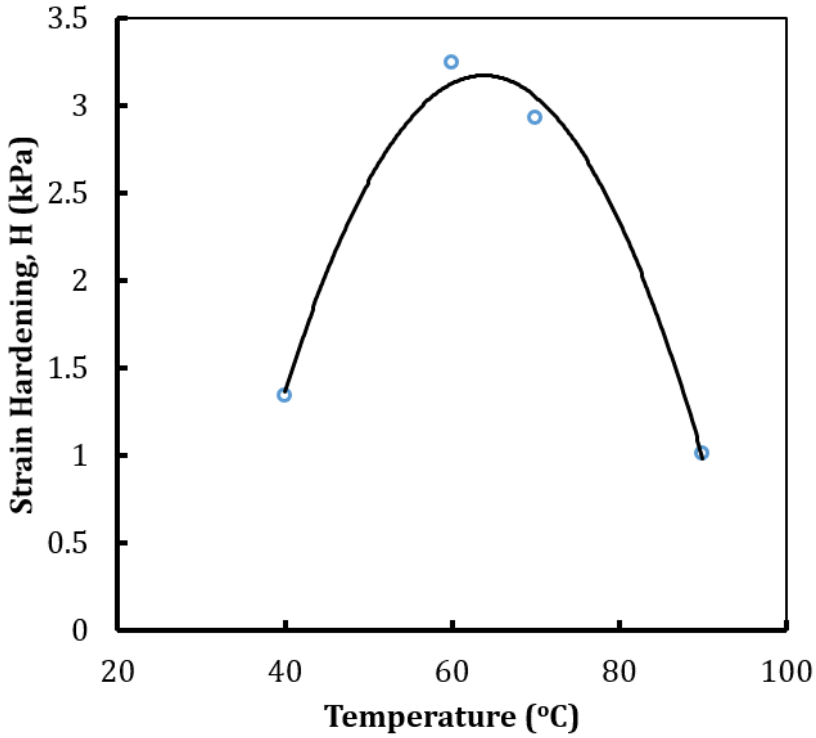

Figure 3-21: *(Left) Strain hardening parameter H against temperature. Tests conducted at a pressure σ_n=75kPa and a fixed rate $d\gamma/dt = 3.33e^{-3}s^{-1}$.*

	40°C		**60°C**		**80°C**		**90°C**	
	Value	R^2	Value	R^2	Value	R^2	Value	R^2
j **(kPa)**	4.55	0.960	2.86	0.915	1.33	0.978	0.180	0.979
μ	0.00381		0.00709		0.0135		0.0173	

Table 3.2: *Experimentally derived regression coefficients for j and μ at a fixed rate $d\gamma/dt = 3.33e^{-3}s^{-1}$.*

	50°C		**60°C**		**70°C**		**90°C**	
	Value	R^2	Value	R^2	Value	R^2	Value	R^2
S **(kPa)**	13.2	0.981	10.6	0.986	3.93	0.992	1.66	0.973
η **(MPa.s)**	18.7	0.985	18.1	0.986	18.0	0.998	16.4	0.956
H **(kPa)**	1.34	0.962	3.25	0.954	2.93	0.936	1.01	0.959

Table 3.3: *Experimentally derived vales and regression coefficients for S, η and H respectively. Each regression coefficient was drawn from nine data points conducted at a pressure σ_n=75kPa, with H values from tests at a fixed rate $d\gamma/dt = 3.33e^{-3}s^{-1}$.*

3.7 Discussion

3.7.1 Stress/strain traces

The stress/strain traces of Figs. 3-11, 3-12 and 3-13 obtained for variable temperature, pressure and rate show a similar response to those displayed by Larberg et al. [10], whereby each plot has two distinct regions. The first region, characterized by an initial stiffness, can be attributed to the shear behaviour of the two plies at small strains, before the interface yields. This is followed by a second region once the interface yields, at a reduced stiffness. Figure 3-11 shows the influence of temperature on these stress/strain traces. Increasing the temperature clearly reduces the initial stiffness and the yield point of the material, confirming the influence of the uncured resin on this initial response. Figure 3-12 shows the pressure dependency of the yield point, confirming the presence of some frictional behaviour. Interestingly, the initial stiffness is not affected whereas the post yield response clearly becomes stiffer with increased pressure. This suggests that the initial response is governed by the viscous uncured resin, whereas the yield and the post yield response are more frictional. The final trace, Fig. 3-13, further confirms this, showing a considerable rate dependency in the initial load response, thereby confirming the viscoelastic contribution of the resin. In order to better investigate the influence of temperature, pressure and rate we can now consider the new parameters derived in Section 3.4.

3.7.2 Interply yield

Plotting critical shear stress τ_c vs. temperature in Figure 3-14 shows a similar trend to results presented by Larberg et al. [10] and Dodwell et al. [3], who both plotted coefficient of friction at yield against temperature. Figure 3-14 differs in that τ_c is a combination of the effects of friction, μ, and the new parameter, joint strength j. The plot shows an initial decrease in τ_c as temperature increases, reaching a minimum at 90°C, after which τ_c increases with temperature. Dividing the shear into two separate mechanisms, as shown in Fig. 3-16, gives a better insight into the combined mechanics which contribute to τ_c. Comparing the values of j in Fig. 3-16 with the values of τ_c in Fig. 3-14 we see that the parameter j dominates at lower temperatures. This suggests that pre-yield behaviour plays a more significant role at low temperatures. From Fig. 3-14 the minimum reached at 90°C marks the point at which slip becomes the dominant mechanism. The behaviour of μ is particularly important. Previous work presented μ as a value with behaviour similar to the value of τ_c in this work, suggesting that μ is initially high at low temperature then falls to a minimum value before increasing again with temperature. This new model shows μ to be minimal at low temperatures then

increasing as temperature increases.

A possible explanation is that at low temperatures the fibres within each ply are separated by a thick layer of resin, formed from the resin rich zones present on the surface of each ply. This reduces the interply friction between fibres and the response is dominated by the shearing of the resin rich region. As temperature increases the resin layer is initially maintained, with the softened response being due to the lower shear modulus of the material at elevated temperature. As the temperature rises further the resin flows into the dry core of the plies [15], increasing fibre-fibre contact between adjacent plies. At this stage the increased level of fibre-fibre contact means that the results are almost purely frictional. This is illustrated by Fig. 3-22 (Left), which shows a cross section of unconsolidated AS4/8552 prepreg and Fig. 3-22 (Right) showing a cross-section of the same material after it has been heated to 80°C and had a normal stress of 100kPa applied.

Figure 3-22 (Left) shows a large amount of resin towards the surface of the ply, with a very noticeable dry core. By contrast, in Fig. 3-22 (Right) the resin appears to be distributed fairly uniformly following consolidation at temperature, with more fibres on the outer edge. There is also a considerable reduction in ply thickness as the resin has redistributed. This supports the hypothesis that low temperature interaction will be dominated by the resin layer, whereas high temperature interactions will be increasingly influenced by fibre-fibre contact.

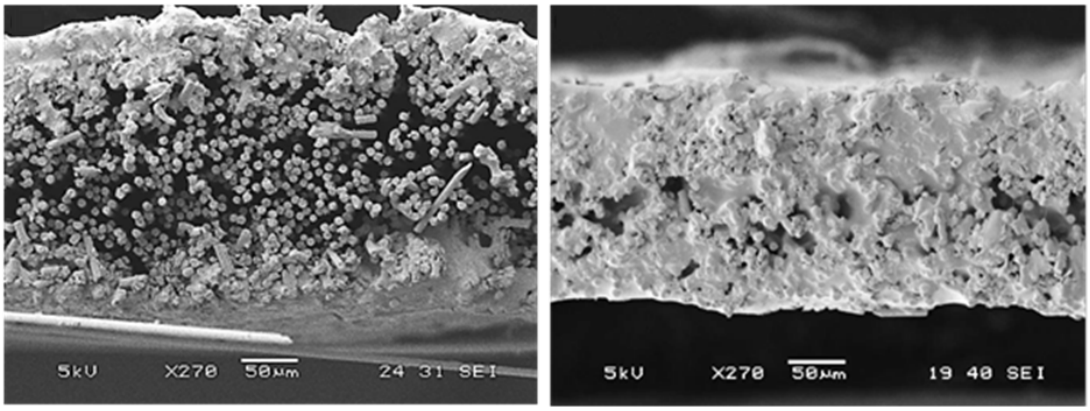

Figure 3-22: *(Left) Cross-section of a single ply of uncured, unconsolidated AS4/8552 prepreg (magnification ×270). (Right) Cross-section of AS4/8552 prepreg post consolidation at a temperature of* $80^{\circ}C$ *(magnification ×270).*

3.7.3 Viscoelastic parameters

By plotting K against $d\gamma/dt$ (Fig. 3-18) we can determine the rate independent elastic modulus S from the y-intersect. From Fig. 3-19 it is immediately apparent that this value is very small when compared to the material response at even the slowest rate of deformation, confirming the importance of modelling the initial response as a combined visco-elastic material.

Figure 3-19 shows the variation of the rate independent part of K with temperature. Figure 3-20 displays η values calculated via Eqn. (3.21) and how this value is also clearly influenced by temperature. Compared against Hexcel data sheets η is significantly higher than viscosity values quoted for pure 8552 resin at similar temperatures [16]. This is thought to be due to the resin being mixed with fibres. Whilst there is a layer of pure resin in the middle of the laminate, it can be seen in Fig. 1-1 that this layer is not uniform in any sense. As such, the fibres will contribute to the shear modulus of this region, and the viscosity. The stiffer the resin, be it due to rate or temperature, the more stress will be transferred to the fibres.

3.7.4 Post yield hardening

The phenomenon of post yield stiffness or hardness observed in the presented results can also be observed in the stress/strain traces presented by Larberg et al. [10]. Confidence in the rig function has been obtained by conducting a test whereby PTFE was wrapped around the plates rather than CFRP, resulting in a zero stiffness post yield response as expected of a frictional material, with a coefficient of friction of 0.096 which falls within the expected range for this material. This confirms that the post yield hardening is due to the material and not the test setup. Figure 3-21 shows the hardening parameter H peaks at 60°C before falling rapidly as temperature increases. It is thought that this hardening effect is due to the relatively slow rate at which the tests are conducted. This could result in the liquid resin reforming the joint once it has failed, progressively increasing the resistance to load as the reformed joint must be continuously yielded. At low temperatures the resin is too viscous to allow the joint to reform as the deformation progresses, however as the temperature increases the resin becomes sufficiently fluid to allow reforming of the joint. As suggested earlier, by 90°C the resin has become so fluid that it has almost fully flowed into the fibre core. As such, little resin lies at the ply-ply interface and we instead see an almost frictional response, with very little hardening. Fibre pullout tests conducted by Dodwell et al. [3] employed a much higher rate R of 1mm/min, and the stress/strain traces obtained showed little or no evidence of post yield hardening, suggesting the increased rate was sufficient to prevent reforming of the

interface, either through the effective stiffening of the resin due to rate, or simply due to the speed of deformation. This appears to be confirmed when applying Eq. (3.20) upon which it can be seen that the post yield modulus, K_t decreases as rate increases.

3.7.5 Interply slip versus laminate shear

Up to this point the discussion and results presented appear to suggest that both the pre-yield shear and post-yield slip behaviour are the result of localised mechanisms at the ply interface. However, the shear strains and strain rates presented are all calculated relative to ply thicknesses, rather than to the thickness of the interface. The principal reasoning behind this is that the characterisation has been designed with laminate behaviour in mind (see Section 3.7.7). Laminate shear parallel to the layering can be modelled as a set of two shear springs in series; a soft spring for the interface and a stiffer spring for the fibrous ply. Shear modulus here is denoted as G, where G is equivalent to K and K_t of Eqs. (1)and (7). Work by Dodwell et al. [17] shows that that $t_{ply} \simeq 16 t_{int.}$ and $G_{ply} \simeq 1000 G_{int.}$, thus

$$\frac{\bar{t}}{G} = \frac{t_{int.}}{G_{int.}} + \frac{t_{ply}}{G_{ply}} \simeq \frac{t_{int.}}{G_{int.}} \left(1 + \frac{16}{1000}\right) \simeq \frac{t_{int}}{G_{int}}. \tag{3.27}$$

where $\bar{t} = t_{int.} + t_{ply}$. From this we see that the shear stiffness of a laminate parallel to the layering is dominated by the weak interface whilst the contribution to laminate shear from the fibrous region is negligible. As such

$$G = \frac{G_{int.}\bar{t}}{t_{int.}}. \tag{3.28}$$

The laminate shear stiffness G is therefore an approximation of the shear behaviour of the ply as a result of localised shear or slip at the interface between the constituent layers. Considering shear behaviour on a ply level, the strain can be simply changed based on the t ratio, changing the strain axis on the results without affecting the behavioural pattern. For this work laminate shear stiffnesses are considered since these are most relevant for the laminate-scale consolidation and forming applications considered in Section 3.7.7

3.7.6 Discussion of potential errors and model limitations

With the careful application of certain caveats as discussed in Section 2, it was possible to achieve a very high level of repeatability during testing. There are however some limitations with this test rig. As the experimental set-up was contrived to investigate a specific material function, i.e. interply slip, certain inconsistencies in mechanism exist

when compared to a real application. One of these is that rate of deformation in a real part is not constant as debulk/forming progresses. With the rate dependent results it is now possible to account for this in process modelling. A particular limitation with the model is that it is one dimensional with shear occurring on a single plane. In reality the shear is also through thickness, and as discussed is influenced by the irregular geometry of the interface, making it two dimensional. As such accuracy suffers and certain behavioural aspects are overlooked. The model also assumes an initial elastic behaviour, suggesting that at small strains the deformation will reduce to zero when load is removed, which does not seem feasible due to the viscous nature of the resin being dominant at these strain levels [18]. Whilst this model is a good starting point it is clear that further investigation is needed into these areas.

Large Deformations and Shear Strain

As mentioned at the start of this Chapter layerwise deformation induced particularly during drape forming processes significantly exceed that which can be considered 'small' in terms of calculating shear strain. The technique presented in Section 3.2 calculates shear strain for large deformations by considering the shear strain to be $\tan\phi$ then calculating the value for large strain as the Hencky or logarithmic strain.

In hindsight, this value may be misleading, as it is best suited for large tensile deformations rather than shear deformation. A more appropriate method is to consider Green strain. In order to calculate the Green strain the deformation gradient, $\mathbf{F}$, a matrix, must be calculated. This can be achieved by observing the displacement $\mathbf{u} = [\mathrm{u,v}]^T$ of a point to be:

$$\mathbf{u} = \mathbf{x} - \mathbf{X} \tag{3.29}$$

where $\mathbf{x}$ is the deformed vector such that $\mathbf{x} = [\mathrm{x,y}]^T$ and $\mathbf{X}$ the reference vector, i.e. the original co-ordinates. The deformation gradient is therefore:

$$\mathbf{F} = \frac{\partial}{\partial \mathbf{X}}(\mathbf{X} + \mathbf{u}) = \frac{\partial \mathbf{X}}{\partial \mathbf{X}} + \frac{\partial \mathbf{u}}{\partial \mathbf{X}} = \mathbf{I} + \frac{\partial \mathbf{u}}{\partial \mathbf{X}} \tag{3.30}$$

which for a two dimensional system becomes

$$\mathbf{F} = \begin{bmatrix} 1 + \frac{\partial u_x}{\partial X_x} & \frac{\partial u_y}{\partial X_x} \\ \frac{\partial u_x}{\partial X_y} & 1 + \frac{\partial u_y}{\partial X_y} \end{bmatrix} \tag{3.31}$$

which for simple shear simplifies to

$$\mathbf{F} = \begin{bmatrix} 1 & 0 \\ \frac{u}{t} & 1 \end{bmatrix} \tag{3.32}$$

where u is the displacement in x (see Fig 3-23) and t is the original length in y (in this case ply thickness).

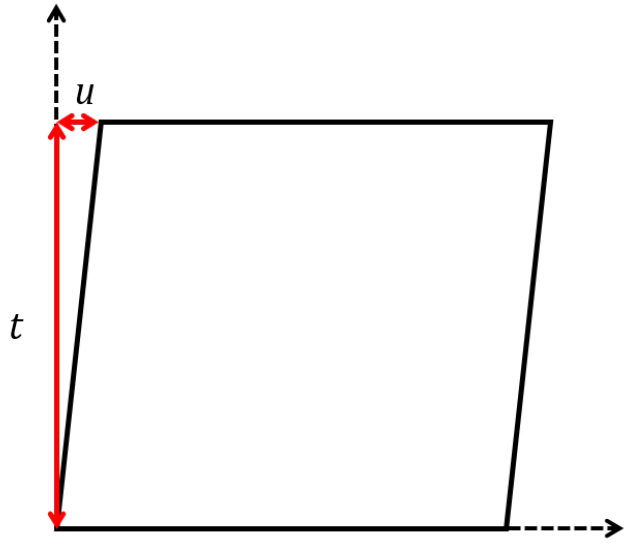

Figure 3-23: *Comparison of the progression of simple shear strain, Green strain and the value of strain calculated in Section 3.2*

The Green strain $\mathbf{E}$ is therefore:

$$\mathbf{E} = \frac{1}{2}\left(\mathbf{F}^T \cdot \mathbf{F} - \mathbf{I}\right) \tag{3.33}$$

In which $\mathbf{F}^T$ is the transpose of $\mathbf{F}$. Plotting Green strain along with the Hencky and simple strain for small deformations allows for an assessment of the inaccuracy in the presented data (Fig. 3-24).

This figure shows that Green strain and the value of strain calculated in Section 3.2 are reasonably similar at small deformations, however by the time Green Strain reaches a value of 0.4, i.e. the limit plotted in Section 3.6, the value of Hencky strain is approximately 7% smaller. Whilst this error is within the error boundaries expected in the test data at these values of strain, and therefore reasonably insignificant, it becomes significantly more important when considering the large strains (≈0.94) encountered during forming scenarios, and future work shall therefore account for this by using Green strain.

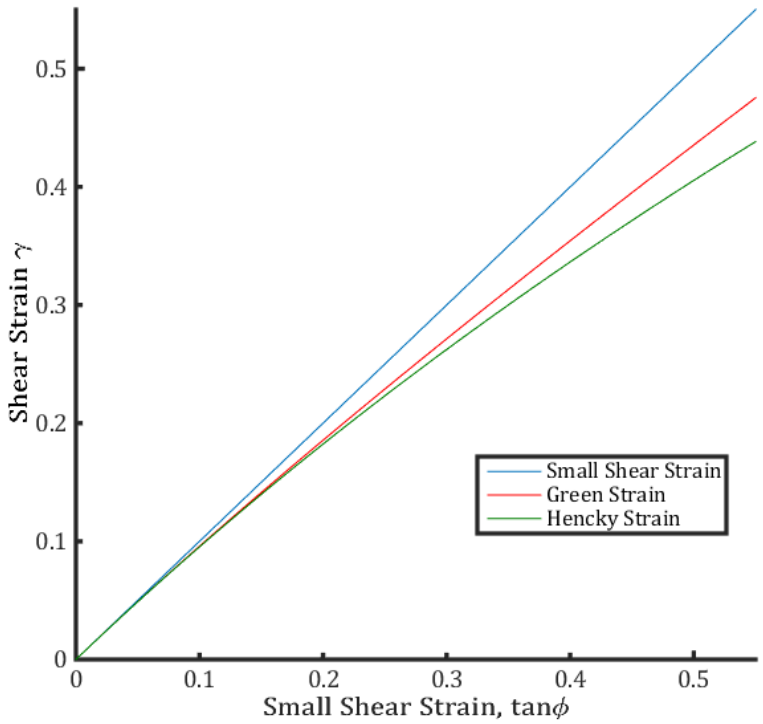

Figure 3-24: *Comparison of the progression of simple shear strain, Green strain and Hencky strain 3.2*

3.7.7 Optimum forming parameters for process induced shear strains

By consulting the material specific stress/strain traces it is possible to determine which combination of temperature, pressure and rate of deformation will result in the lowest shear stress to achieve that particular shear strain. In Fig. 3-2 (Left) the shear strain required to consolidate the part is 0.17. At strains this low the key variables are the initial stiffness, K, and the critical shear stress, τ_c. As the process of corner consolidation is dependent on the application of pressure, it is more pertinent to determine which variables give the lowest τ_c value, as this is a pressure dependent variable, unlike K. With this in mind we can see that the optimum forming temperature is 90°C at as slow a rate as possible to minimise K.

The scenario displayed in Fig. 3-2 (Right) induces a much higher shear strain of 0.94, meaning post yield behaviour has a much larger influence on the shear stress values of interest. In this instance we are looking to minimise both H and τ_c. As such, high temperature is still desirable but results suggest the forming process might be conducted at a high rate of deformation, contrary to both intuition, and results

presented in [18]. It is important to note that these suggestions are based on the notion that the ability for plies to slip or shear within a laminate is key to the reduction of wrinkle defects. However, this data is drawn from tests deliberately designed to isolate the shear behaviour on flat plates. Whilst reducing resistance to slip reduces the end load generated by shear, it also causes the plies to act individually, rather than as a laminate, increasing vulnerability to wrinkling via end load generated from other sources. This coupling is investigated in detail in Chapter 5.

3.7.8 Application to laminate modelling

The work presented works well when considering the movement of one ply relative to another. However, the ply-interface-ply package this forms is not immediately suitable for upscaling into a many-layered laminate, as it effectively consists of one resin interface layer between two full fibrous layers, as the resin at the ply to tool interface is disregarded due to the manner in which the sample is clamped. The optimum package for upscaling would consist of a single full resin interface between two fibrous layers of half thickness. However, if we were to use this value of h to determine the experimental shear strains, we would need to account for the reduction in stiffness due to the omitted fibrous region by reducing the measured deformation proportionately. This would require a much more comprehensive understanding of the individual contributions of the fibrous and resin layers to the overall stiffness. By adopting the two ply package used in this work we are able to propose a conservative estimate of the optimum forming parameters, as the test package is actually thicker than the repeatable package, resulting in a lower prediction of shear strain for a given value of applied stress than would actually occur.

3.8 Effects of particulate thermoplastic reinforcement

A similar test program has been conducted on a third generation material, in which additional particulate reinforcement is added to the interface region to aid with fracture toughness. The results and discussion for this material are included in Appendix A on account of the material being proprietary.

3.9 Concluding remarks and future work

The focused test program has allowed a thorough investigation of two materials, the second generation 8552/AS4 and a proprietary derivation of the third generation M21/IM7. The results give a clear insight into how the manipulation of temperature, pressure and

rate can influence the behaviour of uncured prepreg. The key characteristics of the stress/strain traces can be summarised as follows:

(1) The initial stiffness is dependent on both rate and temperature, but is independent of pressure.

(2) The point of yield, i.e. the transition between the two regions of behaviour is dependent on rate, temperature and pressure.

(3) The post yield stiffness (or hardening) is dependent on rate, temperature and pressure.

A new model has been presented that combines viscoelastic and plastic behaviour in order to characterise the through thickness shear response of uncured composite prepreg. This model avoids the overestimation of yield stress acquired from a purely frictional (plastic) model, and avoids the underestimation presented by a purely viscoelastic model. The combination of these two behaviours allows for increased accuracy when considering shear strain levels encountered during the forming of production parts. The model is a first step however as the yield point predicted and subsequent change in gradient of the stress/strain trace is instant, whereas experimental stress/strain traces show a more gradual transition. As a result, the model slightly overestimates the yield stress, however it is a significant improvement over the estimation from a purely frictional model. The logistic equation presented in Section 3.9.1 represents the next step in this modelling approach, capturing the gradual yield behaviour and allowing for the data to be automatically fitted, rather than manually fitting gradients.

The test methodology has proven itself capable of predicting the parameters required for minimum resistance to ply mobility, with temperature having the largest impact. For 8552/AS4 prepreg this minimum resistance is at a temperature of 90°C, with a similar minimising behaviour being observed for the material presented in Appendix 1. For other materials it is expected that a similar minimum resistance point will also be primarily temperature dependent due to the nature of uncured resin. Other parameters can be manipulated to further improve formability depending on the manufacturing process used. Certain applications require the use of pressure, such as the example discussed in Section 3.7.7, where the aim is to achieve maximum consolidation through the use of pressure. As such, the pressure effectively both drives and restricts the slip. It therefore becomes necessary to balance the pressure required to consolidate the part against the pressure required to allow plies to slip within the laminate. This coupling is the driving factor behind the work presented in Chapter 6 using a curved, laminate scale demonstrator.

Material parameters derived from this technique have already been used to accu-

rately predict wrinkle formation in a corner consolidation model derived by Dodwell et al [3], with results comparing favourably with data gathered from industry. This example used coefficients of friction gathered from early tests in a similar manner to Larberg et al [10]. However, more recently, the parameters from the methodology developed in this chapter have been applied to a complex modelling technique investigating the bending of a small laminate, and experimentally verified with good results [17].

3.9.1 Logistic equation

Whilst the model presented in Section 3.4 captures the general behaviour of the experimental stress strain traces, it is by no means perfect. Two key limitations exist; firstly, the gradual yield behaviour is not captured, as the model consists of two straight lines with an instantaneous yield point at their intersect, resulting in a discrete change in stiffness, whereas the actual plots show a gradual transition. The second limitation is that the lines must be manually fitted to the data by eye, an inaccurate and laborious process. Recent work has looked at adopting a logistic function of the form:

$$f(x) = \frac{L}{1 + e^{-k_1(x - x_0)}} \tag{3.34}$$

which produces the sigmosoidal plot shown in Fig. 3-25, where x_0 is the x value of the sigmoid's mid point, L is the curve's maximum value and k_1 is the steepness of the curve. This also greatly improves compatibility with process modelling applications, as numerical methods typically function better with smooth gradient transitions.

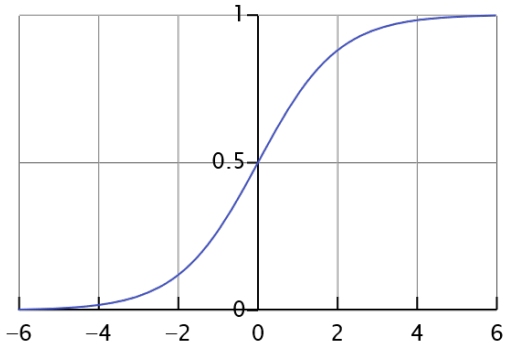

Figure 3-25: *Standard logistic sigmoid function*

To adapt this function to fit the test data x_0 must occur at the point (0,0) with the maximum y value $L = \tau_c$. Finally the function must tend towards some post yield gradient k_2. Substituting these requirements into Eqn. 3.34 we get:

$$f(x) = \frac{2\tau_c}{1 + e^{-k1(x)}} - \tau_c + k_2 x \tag{3.35}$$

The gradient of the curve at any point is therefore:

$$\frac{df}{dx} = \frac{2k_1\tau_c e^{k_1(x)}}{\left(1 + e^{k_1(x)}\right)^2} + k_2 \tag{3.36}$$

Taking the initial gradient of the curve df/dx at $x = 0$ to equal the initial stiffness, K, we see

$$K = k_1\tau_c + k_2 \tag{3.37}$$

and if the gradient df/dx at $x = \infty$ equals the post-yield gradient, K_t

$$k_2 = K_t \tag{3.38}$$

therefore

$$k_1 = \frac{K - K_t}{\tau_c} \tag{3.39}$$

Thus the shear strain, τ, at any point on the curve can be calculated as:

$$\tau = \frac{2\tau_c}{1 + e^{-\left(\frac{K-K_t}{\tau_c}\right)\gamma}} - \tau_c + K_t\gamma \tag{3.40}$$

This model can then be directly fitted to the stress/strain results gathered from experimentation (Fig. 3-26, providing values of K, K_t and τ_c which can be broken down into their constitutive equations respectively to provide the modelling parameters.

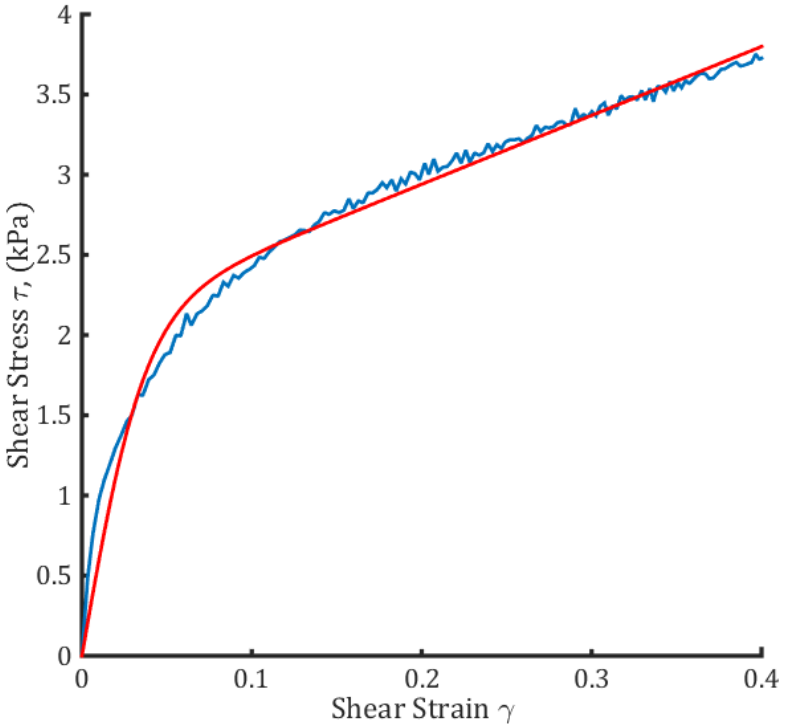

Figure 3-26: *Logistic function of the form presented in Eqn. 3.40 fitted to experimental data taken at 70° C, pressure σ_n = 75kPa and a strain rate of $3.33e^{-3}s^{-1}$*

The model does appear to slightly under predict the initial stiffness, K, however this is potentially due to the comparative sparsity of data points in the y axis as a result of the steep gradient. The general fit of the model is significantly better than that shown in Section 3.4 however, as it accounts for the gradual yield and is constructed from a single line, rather than two intersecting plots. The models used to deconstruct the values of K, K_t and τ_c remain entirely valid, allowing the extraction of vital modelling parameters. The aim of this new function is to provide a more accurate stress input for running models, such as that presented in Chapter 6. Re-evaluating the previous data and plotting them against the new logistic function (see Figs. 3-27, 3-28 and 3-29) gives confidence in the validity of the function over a wide range of variables.

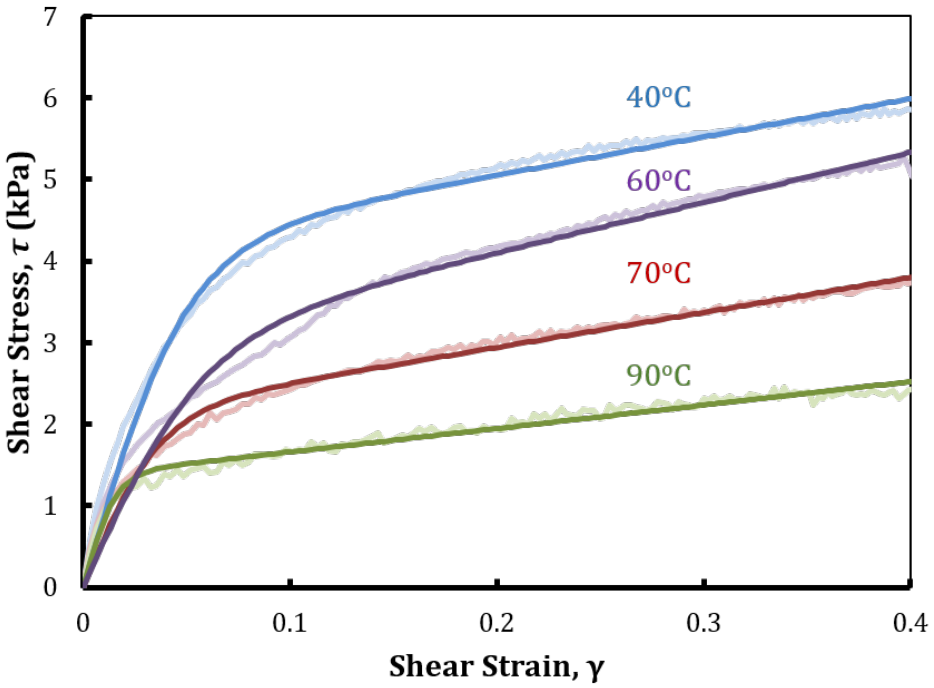

Figure 3-27: *Logistic function fitted to data from Fig. 3-11*

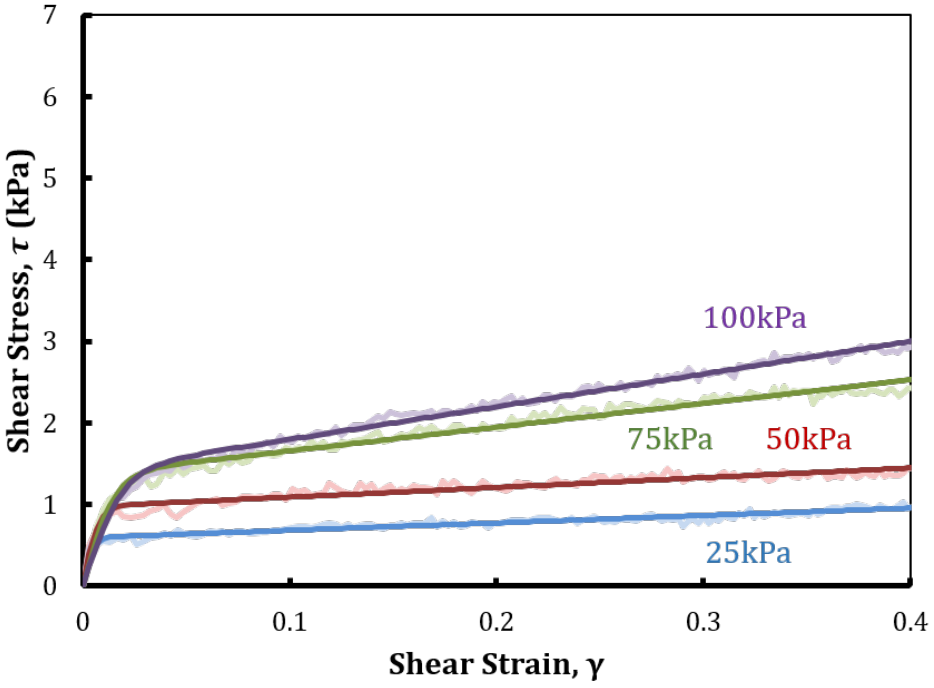

Figure 3-28: *Logistic function fitted to data from Fig. 3-12*

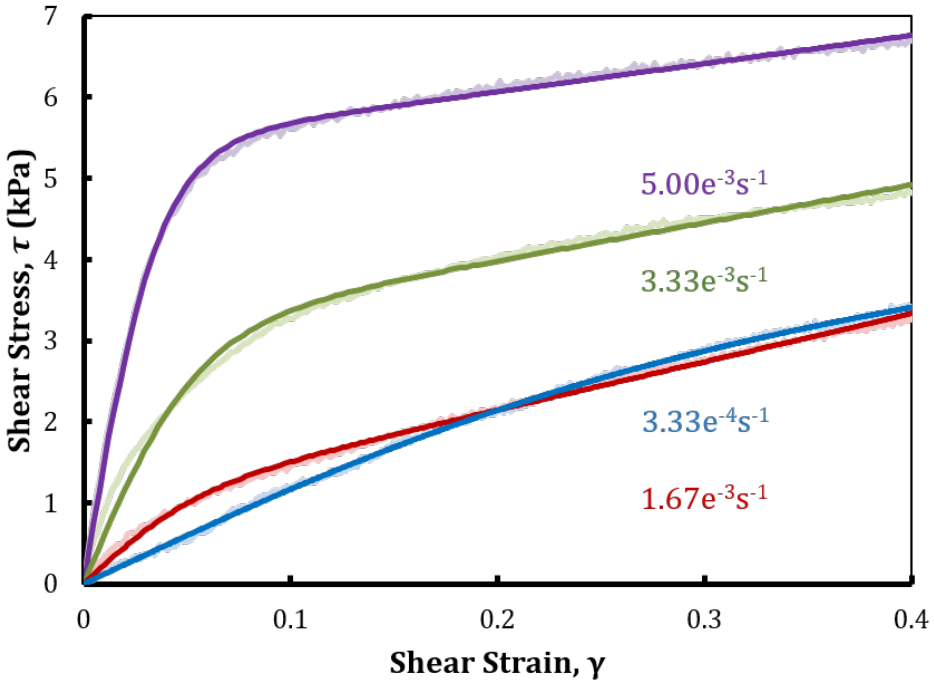

Figure 3-29: *Logistic function fitted to data from Fig. 3-13*

CHAPTER 4

THE INFLUENCE OF ANGLED INTERFACES ON INTERPLY SHEAR

Summary

Interply shear is a vital mechanism in the forming of uncured laminates to complex geometries. Previous work has focused on characterising this mechanism for $0° - 0°$ ply interfaces and comparing them to a viscoelasto plastic model consisting of both a pre-yield stiffness and some residual post yield stiffness, connected by a Mohr-Coulomb yield criterion. These results become invalid when considering industry standard laminates however, as work in the literature has observed ply orientation to have a significant impact on formability. To remedy this, shear tests are conducted for a range of interface angles and pressures. The results suggest that the geometric roughening with increasing interface angle of the fibrous region of the ply relative to the direction of movement or shear, is responsible for both the stiffening of the pre-yield response and the weakening of the post-yield response. In the former case, this is due to improved stress transfer to the resin, whilst in the latter it is due to the reduced fibre-fibre contact between plies. The likelihood of interply versus intraply deformation of angled plies is discussed in detail along with its implications to industry.

4.1 Introduction

The main limitation with the results presented in Chapter 3 is that interply shear is only characterised for $0° - 0°$ interfaces. In reality, most practical laminates comprise plies of different orientations, typically $0°$, $+45°$, $-45°$ and $90°$. Examination of the literature shows the orientation of the ply could have a significant effect on interply shear. Scherer and Friedrich [33] use fibre pull-out tests to investigate a yield shear stress which must be overcome to initiate slipping, similar to the value of critical shear stress, τ_c. This yield point is observed to decrease if the plies are laid orthogonally to one another. It is suggested that this behaviour is due to a reduction in the thickness of the resin interface when one ply is angled relative to the next (see Fig. 4-6, Section 4.5). Further forming tests on various laminates showed the expected interply slip, along with an increased tendency towards intraply shear in plies approaching $90°$ [33].

The effects of angled plies has also been investigated by Hallander et al. [2], who conducted a series of forming tests in which several laminates of varying stacking sequences were hot drape formed (HDF) into a C-section. The stacking sequence was observed to be critical in the forming of a defect free part, with sequences with orthotropic ply interfaces (i.e. $+45°$ to $-45°$) being able to shear to a greater degree in critical areas than those which were not orthotropic (e.g. $+45°$ to $0°$). Orthotropic plies appear to deform via a twisting interply shear mechanism, rather than the strictly load path aligned deformation investigated in Chapter 3.

To the applicability of the results gathered in Chapter 3, a range of interface angles are investigated using the characterisation method and model developed in Chapter 3 in order that the mechanics behind the behaviour observed in [33] and [2] might be better understood. Section 4.2 investigates three key forming mechanics observed by Hallander et al. [2] and how they might result in load path aligned interply shear. An adapted interply shear methodology is presented in Section 4.3, capable of investigating interfaces of a $0°$ ply and some ply of angle $\phi \leq 45°$, with results shown in Section 4.4. Section 4.5 presents a discussion on the impact of angled interfaces on both the pre and post yield behaviour, with the results from the surface roughness measurement technique used to support the findings, as well as a brief discussion on the impact of angled interfaces on formability. The chapter concludes with a summary of findings, along with planned future work.

4.2 Inter and intraply shear in standard laminates

Interply shear as defined in Chapter 3 is a transitional deformation from shearing of a two ply structure, to the relative movement of one ply to the next within a laminate. This differs from intraply shear, which occurs within a ply. The extent to which these mechanisms occur within a laminate made of UD material is dictated by the alignment of forming induced loading to the orientation of the fibres. For the sake of simplicity we shall consider the 0° fibres to be always be aligned with the forming induced load path in each discussed scenario. First we shall consider a laminate made of 0° plies with thin weak interfaces in bending (Fig. 4-1 (Left)). If the outer plies are to conform to the tool they must either stretch or slip relative to one another. As the load is aligned with the fibres the plies themselves are very stiff and are therefore unlikely to stretch under the low loads invoked by the forming process. This effect, combined with the stiffness mismatch between the fibrous layer and the interface, produces interply shear.

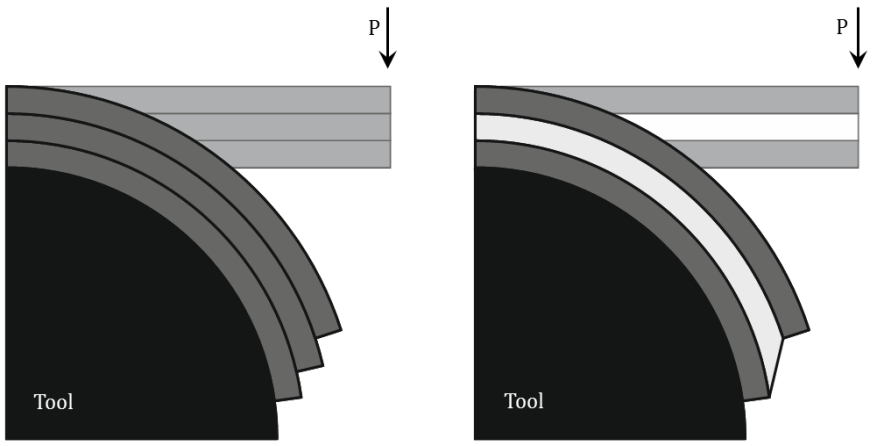

Figure 4-1: *(Left) Drape forming of a stack of* 0° *plies with a thin weak resin interface over a circular tool face. The plies must slip relative to one another in order to form correctly, resulting in the distinctive 'book-end' at the free edge. (Right) A* 90° *layer in the middle of the stack is weaker in the loading plane than the resin interface. The shearing of this ply alone can therefore accommodate the movement required for the two* 0° *plies to form correctly.*

In the second scenario the two 0° fibres are separated by a 90° ply, (Fig. 4-1 (Right)). In the 90° ply the load is orthogonal to the fibre direction, leaving the ply very flexible in shear and bending. In this instance, the deformation required for this laminate to form occurs as a result of intraply shear in the 90° ply. Interply shear is a stiffer response than orthogonal intraply shear as it requires shear to occur along the entire length of a fibre, rather than just across the diameter. Interply shear is in turn weaker than aligned intraply shear due to the thicker band of resin existing between plies than exists in-between individual fibres in a ply, creating a thick, weak layer in

which shear can occur through thickness.

Clearly the occurrence of interply shear at some $[0, \phi]$ interface depends on the magnitude of the angle. As the load path becomes more misaligned with increasing fibre orientation ϕ, the effective intraply stiffness weakens, until it becomes the dominant deformation mechanism.

The second mechanism to consider is that which occurs as two off-axis or angled plies are loaded. These interfaces can allow for some 'extension' of the plies through a rotational scissoring action [2]. This action is a form of interply shear, although this time the resulting movement does not strictly occur in the direction of the applied load and the angle of the plies changes constantly during the deformation (Fig. 4-2).

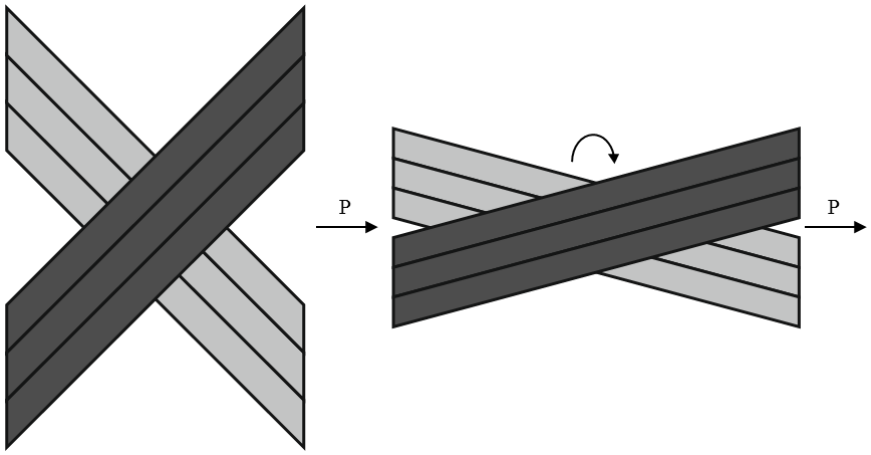

Figure 4-2: *The application of a tensile load to an angle-ply laminate* $(+\phi/-\phi)$ *will result in a rotational scissor-like interply shear response. This allows the effective extension of these layers without having to stretch the stiff fibres, although it does result in a significant Poisson's effect.*

Inherent in this rotational interply shear deformation is the need for some fibre aligned intraply shear. In woven composites this is a particularly critical mechanism, with excessive twist leading to a phenomenon known as the shear locking angle, after which wrinkle defects are increasingly likely to occur. This behaviour is investigated for unidirectional prepreg by Larberg et al. [10], who show that at small rotations intraply shear occurs uniformly across the plies. Once the deformation becomes very large, the increased packing of the fibres increases resistance to intraply shear, and the plies split into tow-like strips, which slip along the split as rigid bodies, effectively allowing further intraply shear to occur.

The methodology presented in Chapter 3 is suited to the investigation of interfaces consisting of a 0° ply and a second ply at any angle $\leq 45°$. Angles greater than this will most likely deform via intraply shear rather than the desired interply shear.

4.2.1 Interply shear when forming across a ramp or pad-up

When investigating a long spar-like demonstrator, Hallander et al. [2] describe a 'tensile' mechanism, which occurs in geometries requiring some extension of the plies during the forming of features like ramps and pad-ups, both of which constitute changes in laminate thickness as a result of the addition of discontinuous plies. The mechanism is also investigated in detail by Fletcher et al. [7], where it is shown that fibres running parallel to the load path (i.e. 0°) in a pad-up region can hold off consolidation (Fig. 4-3 (Left)), hindering forming and promoting defect growth. A constant percentage reduction across the part results in differential movement towards the tool face in continuous plies running from the thin to the thick region, requiring them to either strain or slip to prevent bridging. If the orientation of the ply is not aligned with this strain, the extension can be accommodated either through twist or via intraply shear, the latter of which would effectively involve ply thinning. In the 0° plies however interply shear must occur if the laminate is to form correctly to the tool geometry. The example presented by Fletcher et al. looks at an industry standard stacking sequence, showing a maximum required strain of 0.0003 (Fig. 4-3 (Right)). Whilst this strain is very small, it should be remembered that in order for it to be accommodated the entire 0° ply must slip along the length of a part up to 10m in length under a consolidation pressure.

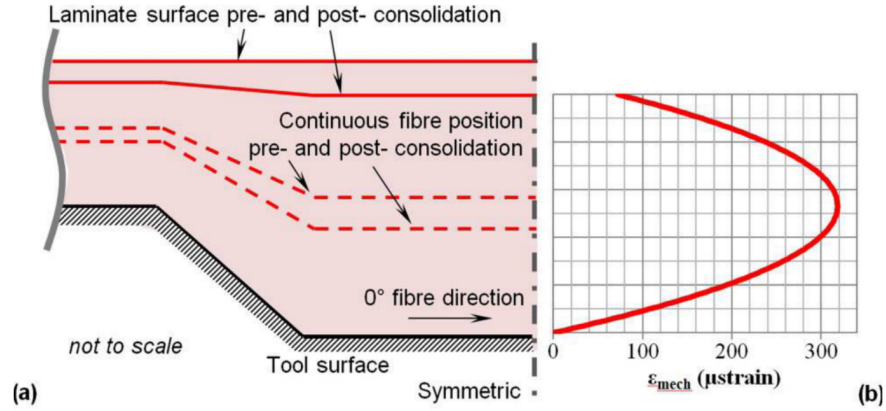

Figure 4-3: *(Left) Tensile strain in continuous plies running through a pad up occurs due to the difference in consolidation movement incurred by a constant percentage reduction across the part during debulk. Due to the thickness change material in the thicker region moves further towards the tool than in the thin region, requiring some length change in these fibres. The resulting tensile strain (Right) depends on the location of the ply drops in the laminate. Figure from [7]*

4.2.2 Application - Prediction of forming parameters

We can now consider the key forming parameters for different forming processes with respect to the shear strain they generate. Consider first the shear strain of 0.17 generated in the consolidation scenario presented in Chapter 3. At strains this low the key variables are the initial stiffness, K, and the critical shear stress, τ_c. For example, in Fig. 3-8 these two parameters account for 81% of the shear stress response at a shear strain of 0.17. The key forming parameters in this instance are a temperature of 90°C and low pressure, with a slow rate of deformation.

The drape scenario displayed in Fig. 3-2 (Right) induces a much higher shear strain of 0.94, meaning post yield behaviour has a much larger influence on the shear stress values of interest. In this instance we are looking to minimise both H and τ_c. From [10] the optimum conditions for reducing H would be to apply as high a temperature as possible, with as little pressure as possible, although it should be noted that temperatures in excess of 90°C have a negative impact on the value of τ_c.

The influence of an angled interface on formability can be determined from a direct comparison of K, H and τ_c values. By breaking these values down into their more complex constituent parameters (i.e. coefficients of viscosity/friction) we can better understand the mechanics behind each response.

4.3 Experimental procedure

The experimental methodology applied here is largely identical to that presented in Chapter 3, in order to facilitate a comparison of the results obtained. The only deviation in methodology was the rotation of the side plates, resulting in their resembling diamonds rather than squares. In order to ensure that this change in leading edge geometry did not influence the results a proofing experiment was run whereby the plates were kept in the square orientation, with the fibre wrapped at a 45° angle. Comparisons with the results from the rotated side plate at a similar angle showed an insignificant variation, within the standard error range. As the rotation of the side plates was significantly easier to set-up this was chosen for the final methodology.

An observation from Chapter 3 was the amount of time required to generate a reasonable array of data. Due to the large number of potential variables and lengthy test time it is necessary to focus on a key set of parameters lest the test program become too unwieldy. Tests were conducted at a single rate R = 0.1mm/min. A range of pressures are investigated (50-100kPa), as pressure is considered critical in the transition from resin dominated to fibre dominated response, as well as the post yield behaviour. Both of these aspects should be heavily influenced by the change in

interface angle. It has also been decided to limit the full pressure investigation to lower temperatures. This not only reduces the amount of time required to conduct the tests, but also allows a more detailed investigation of the post yield hardening response at the temperatures at which it is most noticeable and least understood. The set of tests carried out can be seen in Table 4.1, which each result having two to three repeats. In order to help better understand the interaction at the interface of two plies, a series of surface roughness measurements have been taken using a Talyscan 150 non-contact imaging machine, capable of providing a 3D image of the surface of a sample to a resolution of 1μm. Whilst this will not show a perfect image of the fibrous region, due to the resin layer, it should give some indication as to the structure at the fibre-resin interface.

4.4 Results

All values of initial stiffness, K, strain hardening parameter, H, and critical shear stress, τ_c gathered during the tests are shown in Table 4.1. Typically, K increases with angle, H reduces with angle and τ_c remains unaffected.

ϕ	σ_n (kPa)	**Temperature (°C)**											
		40			**60**			**70**			**90**		
		K	H	τ_c	K	H	τ_c	K	H	τ_c	K	H	τ_c
		(kPa)			(kPa)			(kPa)			(kPa)		
0	**50**	81.3	1.08	5.20	66.0	3.19	2.86	-	-	-	-	-	-
	75	81.2	1.47	5.15	64.6	4.10	3.09	62.2	4.14	2.85	54.8	1.30	2.89
	100	77.9	2.13	5.26	63.5	4.91	3.46	-	-	-	-	-	-
10	**50**	-	-	-	75.1	2.40	3.41	-	-	-	-	-	-
	75	90.0	1.32	5.29	71.9	2.92	3.61	69.2	2.93	2.79	59.1	1.01	1.83
	100	-	-	-	73.3	3.42	3.75	-	-	-	-	-	-
20	**50**	-	-	-	82.5	1.47	3.68	-	-	-	-	-	-
	75	93.9	1.24	5.49	84.3	2.66	3.85	-	-	-	62.4	0.85	1.82
	100	-	-	-	78.6	3.13	4.07	-	-	-	-	-	-
45	**50**	95.3	0.97	5.36	81.6	1.48	3.87	-	-	-	-	-	-
	75	95.6	1.46	5.34	82.5	2.33	4.14	80.6	2.20	2.92	65.6	0.57	1.96
	100	92.4	1.86	5.49	85.9	2.86	4.20	-	-	-	-	-	-

Table 4.1: *Experimentally derived values of K, H and τ_c for varying pressure, σ_n, temperature, and interface angle, ϕ. Tests were conducted at a strain rate $d\gamma/dt$ = 3.33e^{-}3s^{-}1.*

The change in joint strength j and coefficient of friction μ with increasing angle is shown in Table 4.2. μ strictly decreases with angle, whereas j increases. Regression coefficients are also displayed.

ϕ	Temperature (°C)					
	40			60		
	μ	j (kPa)	R^2	μ	j (kPa)	R^2
0	0.0038	4.95	0.960	0.0071	2.86	0.915
10	-	-	-	0.0082	3.01	0.885
20	-	-	-	0.0042	3.54	0.919
45	0.0027	5.2	0.669	0.0039	3.83	0.731

Table 4.2: *Experimentally derived regression coefficients for values of j and μ*

In Fig. 4-4 we see an increase in initial stiffness, K, with angle ϕ. The initial gradient is steep, before appearing to asymptote at 45°. Strain hardening parameter H is plotted against interface angle ϕ at 60°C and several pressures in Fig. 4-5. The test response shows an initially rapid decrease in H with changing ϕ with the response again plateauing as it approaches ±45° respectively.

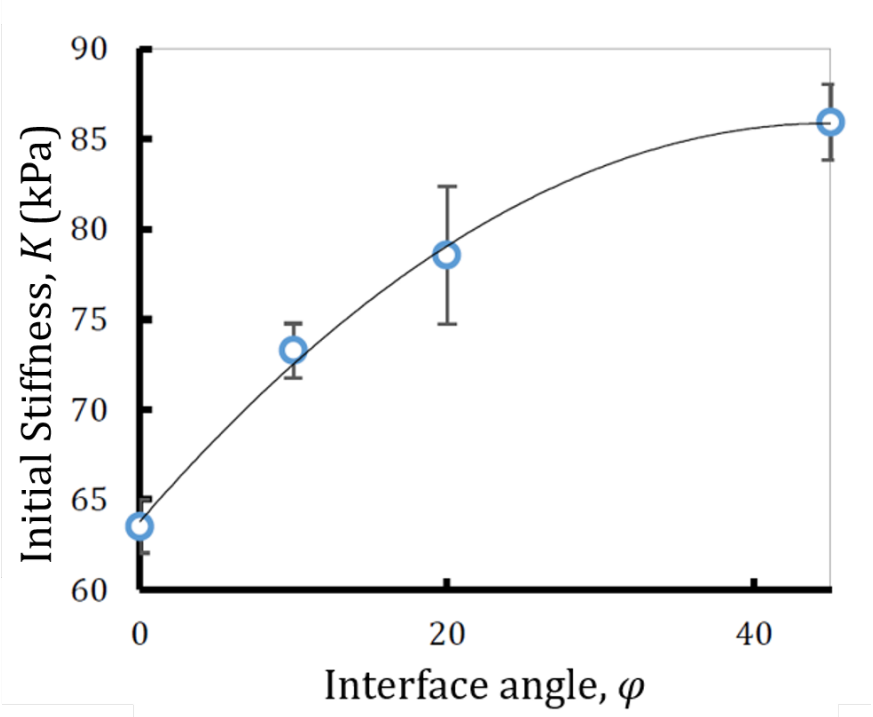

Figure 4-4: *Initial Stiffness, K, against interface angle ϕ. Tests were conducted at a temperature of 60°C and rate $R = 0.1mm/min$. Tests were conducted at a temperature of 60°C and rate $d\gamma/dt = 3.33e^{-}3s^{-}1$.*

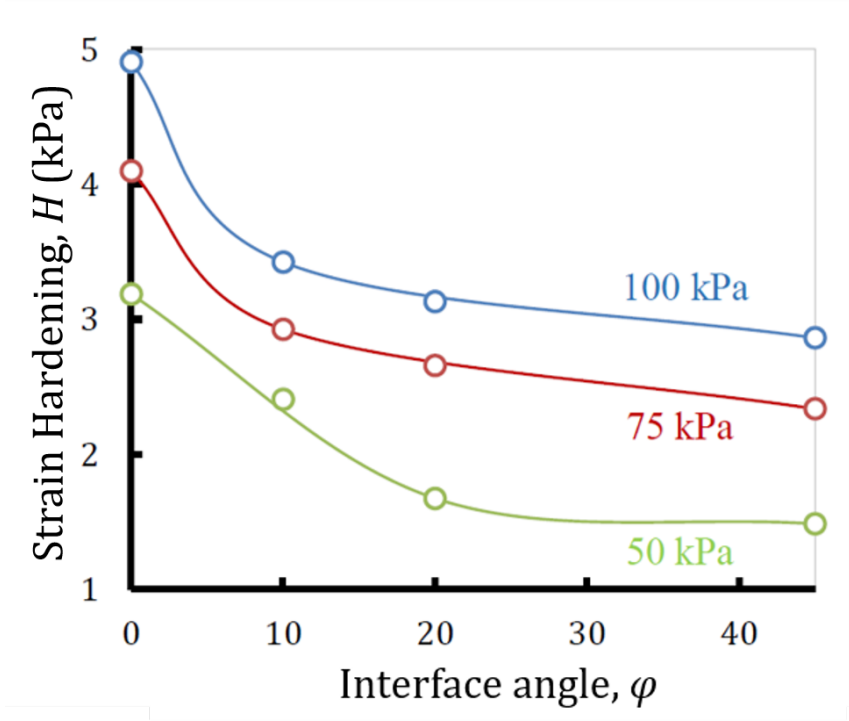

Figure 4-5: *Strain hardening parameter H against interface angle ϕ. Tests were conducted at a temperature of* $60°C$ *and rate* $d\gamma/dt = 3.33e^{-}3s^{-}1$.

4.5 Discussion

4.5.1 Initial stiffness and critical shear stress

The initial stiffness recorded is the shearing of the two ply structure prior to the yielding of the resin interface. In Chapter 3 it is observed that the initial response is resin dominated, being dependent upon rate of deformation and temperature. The observed increase in initial stiffness as ϕ increases from 0° to 45° Fig. 4-4 is a result of the manner in which the rigid fibre bed transfers load to the viscous resin interface. Shear stress in the resin is generated as the fibres are drawn through it. In the $0° - 0°$ configuration the applied load from the test rig is aligned with the fibre orientation, so the resulting movement occurs along the surface interface of the fibrous region. If we consider a cross-sectional view with the 0° fibre running from left to right this can be simply visualised as a smooth rigid body moving through a smooth viscous body (Fig. 4-6). In this instance stress transfer to the resin interface occurs purely as a result of the surface roughness of the fibres, and the sizing applied to it.

As ϕ approaches 90° the fibrous bed begins to move at an angle to the fibre orien-

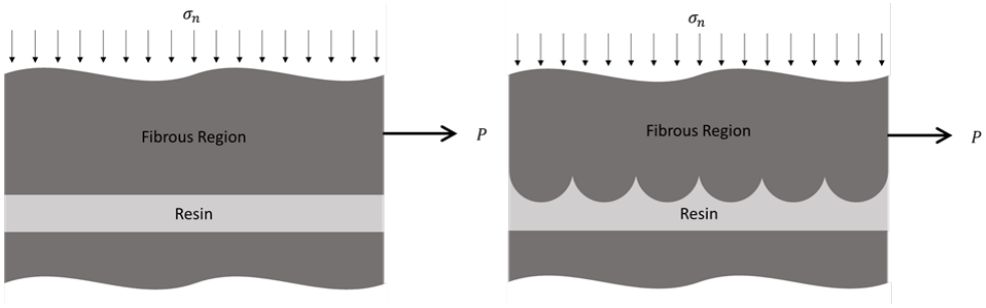

Figure 4-6: *(Left) Cross sectional view of fibre-resin interface for a* 0° *ply and (Right) a* 90° *ply. The geometry induced roughening of the surface of the fibrous region is of particular importance.*

tation. This results in a non-flat geometry at the interface, which becomes increasingly rough as ϕ increases. Stress transfer therefore becomes influenced not just by adhesion and fibre roughness, but the geometry of the fibre-resin interface in the plane of movement.

From Table 4.2 we can see that τ_c is not significantly influenced by interface angle. For some temperatures there appears to be a slight increase, whilst others show a slight decrease. The variation falls within the expected error range however, leading to the assumption that no change occurs. This supports the suggestion in Chapter 3 that this yield is a physical debond in the isotropic resin layer, and thus occurs at the same shear stress regardless of interface angle and the apparent stiffness of the resin. This is in contrast to the findings of Scherer et al. [33], however it should be noted that the yield value they report is from a comparatively simple model which does not consider both pre and post-yield response.

It is important to note that this behaviour assumes the fibres act together as a rigid body and do not pull apart as a result of the increasing tendency towards intraply shear as ϕ approaches 90° discussed in Section 4.2. For this test setup the rigid body assumption can be considered valid due to the manner in which the fibres are clamped and the fact that $\phi \leq 45°$ (see Section 4.3). Initial testing on angles >45° did show a tendency towards excessive intraply shear, rendering the methodology unsuitable and supporting the suggestions made in Section 4.2.

In an actual laminate the fibres will be less constrained. It is expected that this would result in orthogonal intraply shear becoming dominant at higher values of ϕ. This would further increase the formability of the part, although the undesirable side effect of ply thinning may occur. The τ_c values calculated in this paper are therefore higher than might be expected in an actual laminate, and are therefore a conservative estimate when considering formability.

4.5.2 Post-yield response

Plotting strain hardening parameter, H, against interface angle, ϕ, displays a reduction in hardening with increasing ϕ (Fig. 4-5). Work from Chapter 3 suggests that the post yield region is influenced by the level of fibre-fibre contact between plies during intermingling. The observed decrease in H seen in Fig. 4-5 is considered to be due to fibre packing at the interface. A $0 - 0°$ interface provides optimum packing density, and therefore the greatest degree of fibre-fibre contact. Even a slight misalignment between plies will drastically reduce the amount of fibre-fibre contact, resulting in the sharp decrease in observed hardening.

A tendency for increased hardening at around $60 - 70°$C was also noted in Chapter 3 and observed in Table 4.1 with the hypothesis being that if the resin is free to flow, it may allow some reforming of the interface post yield. If the flow of resin is hindered by angled interfaces, as suggested in the initial stiffness response, this could impede joint reformation, promoting the physical dislocation of ply interfaces which was considered to lower post-yield stiffness.

The values of coefficient of friction, μ, and joint strength, j, displayed in Table 4.2 appear to support the discussion. We can see that μ strictly decreases as ϕ approaches $45°$, supporting the hypothesis that increasing geometrically induced surface roughness leads to a reduced frictional contribution to the critical shear stress. Countering this we see a constant increase in j with ϕ, this time supporting the idea that the surface roughness aids in stress transfer from the fibrous region to the resin interface. It should be noted that the regression coefficients shown in Table 4.2 are significantly worse than those gathered for similar values in Chapter 3. This is in part due to being drawn from just three different pressures rather than the preferred four, but also due to the effect of investigating another variable, orientation, and the error related to the more complex sample preparation.

4.5.3 Surface roughness measurements

Surface roughness is identified by Larberg et al. [10] as an important factor in interply shear. In the work of Larberg the roughness off the fibres is used as justification for the difference in the frictional response of various generations of prepreg. For the work presented in this thesis, the changing geometric roughness of a ply interface as a line is drawn across a ply of some angle, is considered as a key driver in the manner in which stress is transferred from the fibrous region to the resin interface. This is investigated using a Talyscan 150 to generate a 3D data cloud which can be visualised as a grayscale image (Fig. 4-7 (Left)).

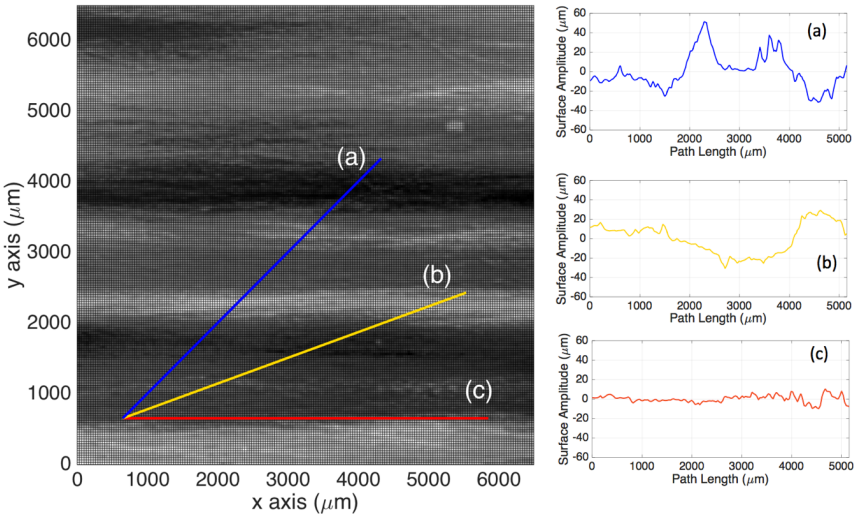

Figure 4-7: *(Left) Talyscan image of 8552/AS4 prepreg, with the fibre orientation running from left to right across the page. The plots on the right show the surface roughness at varying angles. Line (a) runs at* 45° *to the fibre orientation, line (b) at* 20° *and line (c) at* 0°

The image taken is of an unconsolidated ply of 8552/AS4, with the topology showing several peaks and troughs with a maximum amplitude of 60μm and a wavelength ranging from 500 to 1000μm. The almost periodic nature of these features appear to be the result of some form of 'combing' to orientate the fibres during the manufacture process, as the diameter of the individual fibres is only 8μm. By taking sections at various angles across the plot we can observe the change in roughness with fibre orientation (Fig. 4-7 (Right)). As the orientation of the slice approaches 90° we can see an increase in both the number and severity of features. The roughness increase with interface angle is therefore a result not just of the fibre cross-section, as suggested earlier, but also of the cross-section of the structure those fibres form at the interface, supporting the hypotheses presented earlier.

4.5.4 Implications for forming

By considering the statements made in Section 4.2, we can better determine the influence of angled interfaces on the formability of a part. The influence of the increasing initial stiffness with ϕ appears to have a negative impact, however this is tempered by the angle independent response of τ_c. This independence from angle means that so long as the required shear strain γ is greater than the critical shear strain γ_c, as it is in both examples in Fig. 3-2, the change in initial stiffness will have no bearing on the overall shear stress required to form. The reduction in post yield hardening with increasing angle ϕ is naturally beneficial to forming.

4.6 Conclusions and future work

The test methodology and modelling techniques developed in Chapter 3 have successfully been used to investigate a range of angled ply scenarios. The effects of angled interfaces are significant, with a change of 20% in values of K and H from a $0-0^\circ$ interface to a $0-45^\circ$. The results of these tests have given some insight into the effects of an angled interface within a laminate, suggesting that dissimilar angles are desirable at the interface for large strain situations, but detrimental to very small strain scenarios. Importantly for the former case, increasing the angle does not increase τ_c, making control of the interface angle very effective in combating post yield hardening. This could influence the degree to which ply blocking is utilised in the design of a laminate. Work on angle optimisation for structural efficiency has already shown that non-standard angles (such as 20° and 70° rather than 0°, 90° and 45°) might provide improved damage tolerance, [48], contrary to the perception in current design rules. A similar optimisation approach could potentially be employed to determine the optimal laminate stacking sequence and angles of plies for various forming scenarios such as those discussed above, as even a small mismatch in interface angle can noticeably improve formability. Whilst temperature remains the most influential parameter for forming, changing the stacking sequence of the part provides a benefit without the necessity of long periods of waiting for the part to reach temperature prior to forming.

The main impact of this research is its potential to influence laminate stacking sequence design. Prior to this work the output was predominantly focused on controlling the forming and manufacturing parameters, such as temperature and debulk pressure. This angled ply work now allows an insight into how the actual structure of the laminate can be manipulated in order to improve its formability.

An area of further interest is the investigation of combined load scenarios, in particular the bending and shearing of an uncured laminate. This process results in significant amounts of shear within a layered structure. Work on this process is presented in the next chapter, where a laminate beam of 0° plies is tested using a dynamic mechanical thermal analysis (DMA) rig. This work utilises parameters drawn from the model presented in Chapter 3, and with the new angled interface results it will be possible to investigate more realistic laminates.

As noted earlier, a key consideration in these tests is that the manner in which the angled plies are sheared might be considered to be unrealistic, as the angle remains constant and there is no 'scissoring' as would be expected on account of the Poisson's ratio effect when loading angled plies. Work has been planned to investigate this more complex process using a bi-axial test frame, however the simplified test presented in this

paper provides a valuable insight into not just the mechanics involved in the shearing of an angled interface, but also several of the parameters determined in Chapter 3, principally the strain hardening parameter, H.

CHAPTER 5

THE INTERACTIONS OF INTRA AND INTERPLY SHEAR IN UNCURED LAMINATE BENDING

Summary

If a wrinkle defect is effectively the buckling of a ply, its behaviour in bending must be considered. Existing methods for analysing bending behaviour such as the Peirce Cantilever technique require complex numerical analysis and can be fairly inaccurate on account of the difficulty of setting up samples and recording results. This chapter investigates the use of Dynamic Mechanical Analysis, which is an attractive option for a number of reasons, principally accuracy, repeatability and ease of use. In its current form it is limited by inbuilt assumptions in the analysis software which assume infinite shear stiffness. To combat this, the results obtained are recalculated using a Timoshenko shear modifier to investigate both the intraply shear stiffness, and the shear stiffness of the interply region. The latter result compares well with values calculated in Chapter 3, giving confidence in both test methods, whilst the intraply shear stiffness is an order of magnitude greater, as expected. The chapter concludes by suggesting how the technique for modifying the bending stiffness results might be applied to other deformation modes available to DMA, with a short example.

5.1 Introduction

In Chapter 3 it has been largely assumed that the shear behaviour of the laminate is dominated by the relatively weak inter-ply shear, however, the shear behaviour of uncured composite laminates is non-symmetric as shown by Dodwell et al.[17], and whilst the inter-ply shear behaviour determines the laminate shear parallel to the layering, intra-ply shear controls the laminate response in shear orthogonal to the layers, i.e in ply and laminate bending, see Fig. 5-1. The interaction between these two forms of shear underpins an understanding of forming and consolidation over complex geometric features.

Work in Chapter 3 has shown the interply shear response to be most influenced by temperature, whilst other parameters such as rate of deformation, pressure and stacking sequence (Chapter 4) also play a significant role. An observation in Chapter 3 is that minimising resistance to inter-ply shear theoretically improves formability by improving ply mobility and reducing the level of end loading a ply is subjected to when forming, reducing the risk of wrinkles. This is a coupled effect however, as reducing the stiffness of the resin interface in search of improved mobility will cause the plies to act as very thin, long, individual layers which are themselves more susceptible to buckling, despite the reduced loading. If we are to predict the formation of a wrinkle and accurately prescribe optimum forming parameters we must therefore consider the bending behaviour of uncured prepreg, both as a single ply and as a laminate.

5.1.1 Interply shear and the mechanics of ply bending

The bending behaviour of a single ply of uncured carbon fibre prepreg is complex on account of its highly heterogeneous nature. When analysing the bending stiffness of an isotropic material a number of assumptions can be made to allow the application of Engineers Bending Theory (EBT). Key among these is the assumption that plane sections remain plane, i.e. the material is assumed to be infinitely stiff in shear (Fig. 5-1 (Left)) [68].

This assumption is invalid for uncured prepreg however, due to the large contrast between the stiffness of the resin and the fibres. The high stiffness of the fibres prevents them from stretching or compressing under the bending induced stresses, instead they prefer to slip relative to one another, forcing the comparatively weak resin interface region to shear (Fig. 5-1 (Right)) and resulting in a shape commonly referred to as a ‘book-end’. Applying EBT to a material undergoing shear deformation will result in an artificially low value of bending stiffness being calculated. To remedy this, it is necessary to consider an additional shear term, such as that utilised in a Timoshenko

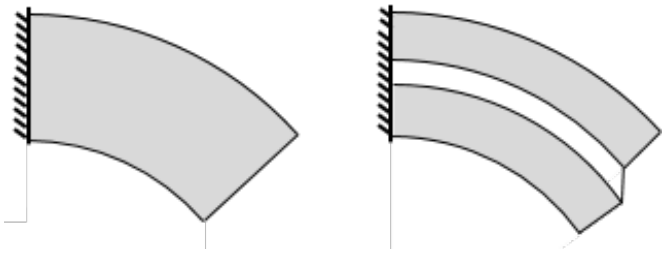

Figure 5-1: *(Left) Bending behaviour of a homogeneous isotropic material in which plane sections remain plane, and (Right) a heterogeneous anisotropic material made from two thick stiff outer layers with a thin weak central layer which is susceptible to shear deformation*

beam element (see Section 5.2).

5.1.2 Peirce cantilever

As noted in [19] and [58], there exists a lack of a mature system by which to determine the bending behaviour of preimpregnated carbon fibre. Liang et al. approach this by looking to adapt the Peirce cantilever test developed for dry fabrics in 1930 [57]. As described in Chapter 2, this test involves analysing the deformation of a singly clamped cantilever of a material as it deforms either under self weight, or under the effect of a small load mounted to the end of the sample. There are several issues with this test setup, the most obvious being that the measured deflection typically assumes the sample to be perfectly flat in the initial instance, which is not the case, although this could be considered a minor issue as it is fairly easily accounted for. The real complexity occurs in accurately converting the results such that the effective moment at any point on the beam might be considered. This is important due to the nature in which load is applied; being a self weight induced deformation the applied moment on any small segment $d\ell$ increases from the unclamped edge towards the clamped end, resulting in a non-uniform curvature, as can be observed in test results from [19] and work by [59] (Fig 5-2).

This behaviour therefore necessitates a fairly complex analysis process, and even then, is dependent upon the accuracy of the taken images. A further and perhaps more serious limitation exists when attempting to investigate the impact of viscoelasticity on the bending behaviour. As noted in Chapter 3, rate of deformation has a significant influence on the behaviour of the resin in shear. In a Peirce cantilever test there is no way of imposing a set rate of deformation, rather it is a function of the self weight and the degree to which the sample has deformed, initially starting at a high rate and then reducing as the resistance to further shear strain increases. For this reason and the complexity of the data analysis the a different test method is considered; Dynamic

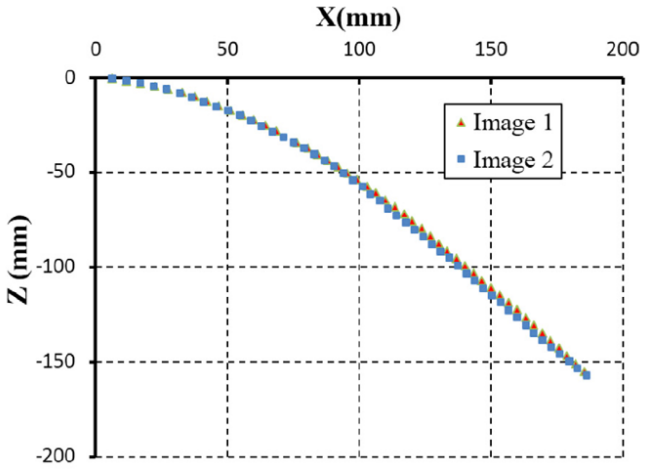

Figure 5-2: *Plot of deflection z against length X from [19] clearly showing a non uniform curvature*

Mechanical Analysis.

5.1.3 Dynamic Mechanical Analysis

Single cantilever Dynamic Mechanical Analysis (DMA) provides an effective testing scenario for the investigation of the adherence of uncured prepreg to the assumptions of engineers bending theory (EBT). DMA applies a cyclic deformation to a small, doubly clamped sample and records the required load to achieve this (Fig. 5-3), whilst controlling temperature with an in-situ environmental chamber. By recording the phase difference between applied stress and recorded strain it is also possible to investigate the elastic/viscous nature of the sample material as its temperature changes [40].

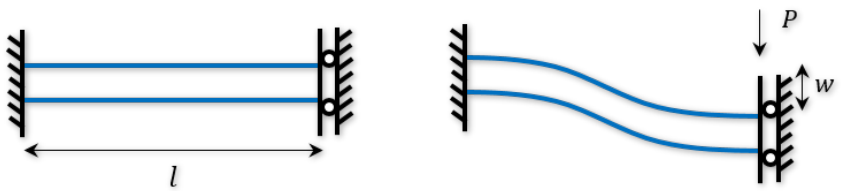

Figure 5-3: *(Left) Initial DMA loading scenario and (Right) deformed shape*

There are several advantages to using DMA to analyse bending behaviour of uncured prepreg when compared to other techniques such as Peirce cantilever, the most obvious being that DMA is a commercially available machine owned by most universities and research orientated companies, with a high degree of control over testing variables such as temperature and deflection, and the capacity for very accurate mea-

surements. Another key advantage is the ability to perform tests over a temperature ramp, allowing the full cure cycle of a piece of uncured carbon fibre to be investigated in a single test. This greatly reduces the testing period when compared to methods which require static temperature testing, such as the interply shear measurements in [95]. For this technique to be valid however we must ensure that the applied shear strain in the sample does not exceed the critical shear strain for the material, i.e. the shear strain at yield, as any further strain increment after this point results in irrecoverable plastic deformation, as per the hardening rule presented in Chapter 3. Considering a typical material response for 8552/AS4 we see that the critical shear strain is typically of the order of 0.1-0.17. If we now consider the shear strain generated in a DMA sample with length ℓ =3mm and an applied deformation of $w = 0.05$mm (Fig. 5-4) we can calculate the shear strain using simple trigonometry.

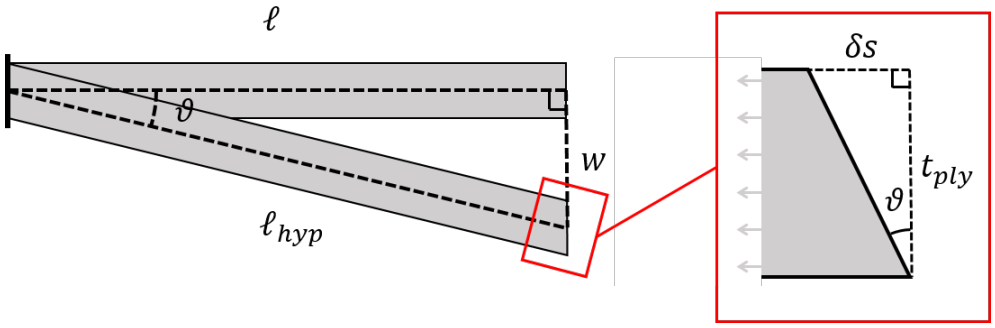

Figure 5-4: *Calculation of shear strain in a sample, assuming zero stiffness in shear.*

As the deflection is small, $\ell \approx \ell_{hyp}$, therefore shear strain γ can be calculated as rev

$$\gamma = \frac{\delta s}{t_{ply}} = tan\vartheta \approx \vartheta \tag{5.1}$$

In order to make a safe approximation we assume a shear stiffness of 0, therefore resulting a maximum possible shear strain for this sample of 0.016, an order of magnitude smaller than the critical shear strain (see results in Chapter 3). This therefore provides confidence in the validity of testing a single sample over a temperature ramp.

A particularly useful feature is the ability for the DMA to unpick the elastic and viscous components of the material behaviour (see Section 5.2). There are however two key limitations with standard DMA when used to investigate uncured prepreg. The first is that DMA calculates the Young's Modulus of a material by assuming Engineers Bending Theory (EBT) which assumes a sample to be infinitely stiff in shear, which as discussed previously is an assumption uncured prepreg clearly does not adhere to [95]. The second limitation is the inability to pressurise a sample during testing, however

the implications of this are limited if we consider results from Chapter 3. The shear strains invoked during bending are very small due to the large length of the sample and the small applied deflection (see Section 5.2). Chapter 3 shows that friction plays a minimal role at these levels of shear strain due the response being dominated by the resin, which can be reasonably assumed to be incompressible.

In this Chapter a method is proposed for adapting the results gathered from single cantilever DMA performed on uncured carbon fibre prepreg, in order that they might consider shear deformation in bending. In Section 5.2 the operating principles of DMA and the Timoshenko Beam Element used to adapt the basic results are discussed. Section 5.3 details the minor adaptations require to allow uncured prepreg samples to be tested along with the test matrix and justification of the investigated variables. In Section 5.4 the amended results are presented and then discussed in detail in Section 5.5. This section also investigates some of the assumptions made in the previous sections in order to fully justify them, before concluding remarks are drawn in Section 5.6.

5.2 Modelling shear in bending

Dynamic Mechanical Analysis (DMA) is a commonly used experimental setup capable of determining the elastic and viscous moduli of a material over a range of temperatures and frequencies. Various different loading scenarios are used. Here, clamped-clamped beam bending is considered for which a sample of length ℓ, height h and breadth b, is clamped at both ends. One end remains stationary, whilst the other end is displaced with frequency $w = w_{max}\sin(\omega t)$ and the force P required to achieve this is recorded (Fig. 5-3. Through viscous effects the force lags a time δ behind the displacement

$$P = P_{\max}\sin(\omega t + \delta) = P_{\max}\cos\delta\sin(\omega t) + P_{\max}\sin\delta\cos(\omega t). \tag{5.2}$$

The rate-independent or elastic part of the force is the in-phase contribution given by $P_e = P_{\max}\cos\delta\sin(\omega t)$, whilst the viscous part is the out-of-phase contribution $P_v = P_{\max}\sin\delta\cos(\omega t)$. The standard DMA software adopts engineers bending theory, which assumes there is no through-thickness shear during bending. This implies that the elastic (storage) and viscous (loss) modulus are given by

$$E_e = \frac{P_{\max}\ \cos\delta\ \ell^3}{3Iw_{\max}} \quad \text{and} \quad E_v = \frac{P_{\max}\ \sin\delta\ \ell^3}{3Iw_{\max}}. \tag{5.3}$$

respectively. Considering Fig. 5-5, we can see that as the peak stress and strain values coincide δ tends towards 0, thus E_v also reduces to 0 and the material has a purely elastic response. As the phase difference increases E_v also increases, whilst E_e

reduces. This behaviour can be represented with a hysteresis loop, in which the area of the curve is indicative of the viscous/elastic state of the material.

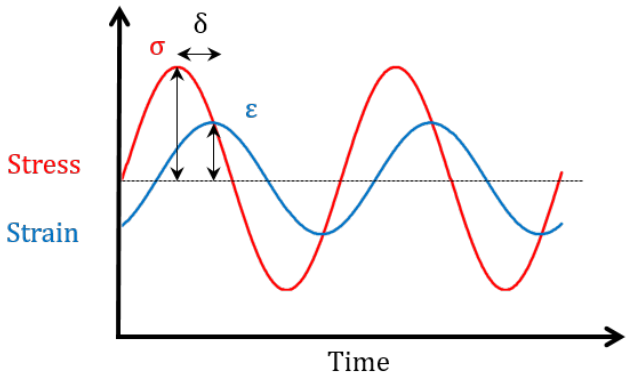

Figure 5-5: *(Left) DMA plot of sinusoidal stress vs strain with phase difference tan δ*

Because DMA calculates Young's Modulus as a material value from the results, one should obtain the same values of modulus regardless of any variations in sample length ℓ. More over if one performed a tensile test to calculate E_e, the answer should be the same. If we now consider three samples of different lengths ℓ we can observed the inability of EBT to capture the bending behaviour of a beam in which shear deformation occurs. Applying the same deflection to beams of different lengths will invoke different degrees of shear deformation, and will thus result in different values of E_e, as shown from some initial testing in Fig. 5-6, the methodology for which is discussed in the next section.

As the imposed deformation remains constant across all samples, the amount of shear deformation invoked changes with sample length. The shorter the sample, the greater the curvature and therefore shear deformation, hence the DMA calculated value of E_e increases with sample length. The plots also suggest a temperature dependent bending stiffness, which is actually due to the resin dominated shear response, as shown later in the chapter. The final confirmation of the unsuitability of EBT is that the value of E_e presented is a factor of 500 smaller than if calculated using the rule of mixtures, in which the individual moduli of the resin (E_m) and fibres (E_f) contribute towards the overall tensile modulus of the material based on the fibre volume fraction, such that

$$E_c = \left(\frac{f}{E_f} + \frac{1-f}{E_m} \right)^{-1} \tag{5.4}$$

where f is the volume fraction of the fibres, such that

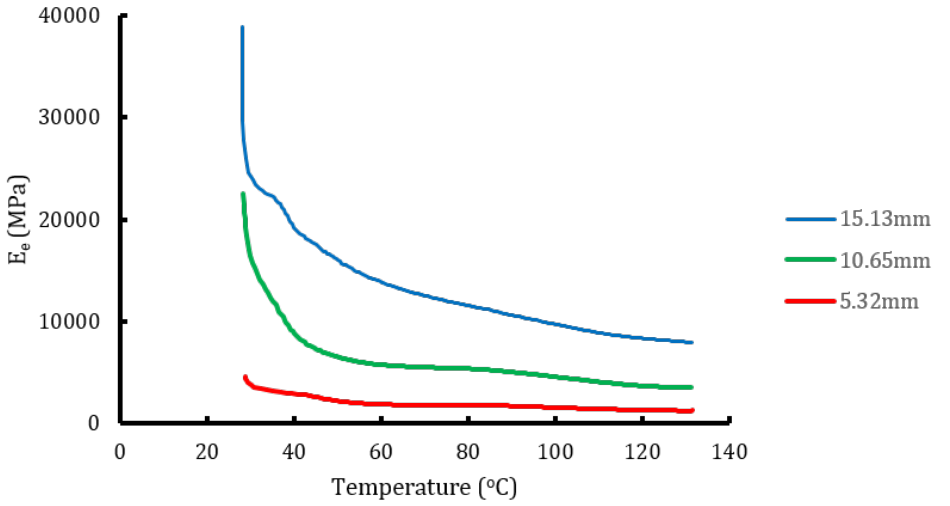

Figure 5-6: *Plots of combined modulus E_e as displayed by the DMA against temperature for eight ply samples of varying lengths, clearly showing that the basic DMA postprocessing suggests a length dependent modulus*

$$f = \frac{V_f}{V_f + V_m} \tag{5.5}$$

For AS4/8552 this gives a modulus of 128GPa.

The key point is that the assumption that no intra-ply shear occurs is invalid. The assumptions of engineers bending theory must therefore be relaxed to first-order shear deformation theory (or Timoshenko beam theory), for which the normal of the mid-surface remains straight but not necessarily perpendicular to the mid-surface, making an angle ϕ to the vertical axis.

5.3 Methodology

Sample preparation for uncured carbon fibre samples is more complex than for typical DMA samples due to the tendency for the sample thickness to reduce under the pressure of the clamps as ths temperature increases. To counter this, samples are mounted with quick curing polyurethane tabs (Fig. 5-7).

The polyurethane is demoldable within half an hour, and when mixed with an additive such as milled carbon fibre or glass microbeads it is sufficiently stiff and thermally stable to provide rigid clamping points. The sample length is therefore measured between the point at which the carbon fibre sample enters the resin tab. The samples themselves are prepared without any consolidation further than the minimal amount

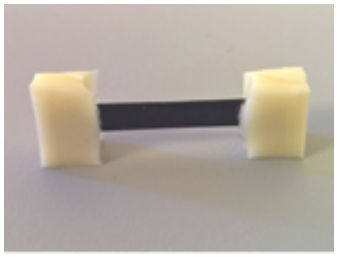

Figure 5-7: *Resin tabbed samples. The sample is inserted into a bath of resin when the viscosity is suitably high in order to prevent the tab bleeding into the sample.*

require to bond them to one another.

Tests were carried out on two materials of four different lengths between 3 and 15mm, for stacks of 1, 2, 4 and 8 plies respectively. The temperature ramp was chosen to run from 30-130°C based on experience from [17], in which it can be observed that an uncured laminate typically reaches its final part thickness prior to the glass transition temperature of the resin, with approximately 250 data points taken along the way. If defects are to occur, it must be during this thickness reduction phase, therefore generating experimental data beyond this point is irrelevant.

As mentioned previously, the deformation mode chosen was single cantilever, with an applied maximum deformation of 0.5mm. This is substantially larger than the typical deformation of 0.05mm employed in DMA, however due to the comparative weakness of the single ply samples it was necessary to ensure that the load results fell within the resolution of the load cell. The maximum shear strain generated in the short samples can be calculated to be 0.012, reducing to 0.005 for the longest sample.

5.3.1 Timoshenko beam element

Timoshenko [56] and Benham and Crawford [55] suggest two potential equations capturing the effects of shear in bending. Each approach considers the effects as an additional linear shear component added to the overall deflection on a cantilever beam, however Timoshenko approaches the problem by balancing loads whereas Benham and Crawford derive it by considering the work done by the applied load. In this type of beam the ability for the layers to shear past one another is governed by a shear modulus, G_{lam}, which controls the angle of the bookend, as shown in Fig 5-8.

Thus as G_{lam} approaches 0, $dw/dx + \theta_x$ approaches 0, causing the normal to rotate and remain vertical. As G_{lam} approaches ∞, θ_x approaches 0 and the calculation reverts to EBT. Moving from a single ply to a small laminate, the bending behaviour becomes further complicated by the presence of a comparatively thick, continuous planes of resin at the interface of the two plies. The shear behaviour of the ply-ply interface has

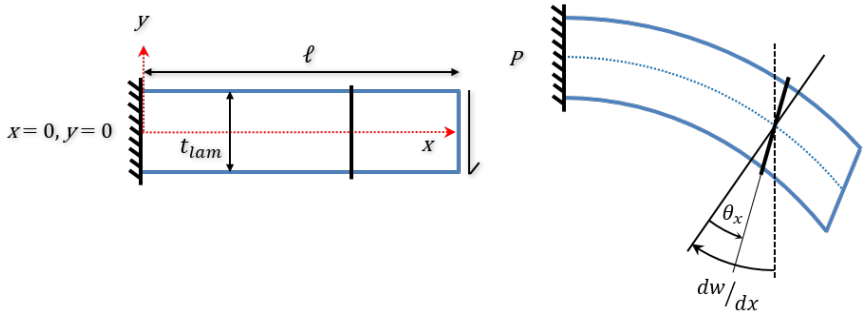

Figure 5-8: *In the deformation of a Timoshenko beam, the rotation of the normal is equal to θ_x, which is not equal to the curvature, dw/dx*

been extensively investigated [95] using a rig designed to slide two plies relative to one another. Due to the nature of the methodology and the material, shear deformation was found to localise almost exclusively to the resin interface after a brief initial period of stiffer, full thickness shear. It can be assumed from this that the apparent bending stiffness of a small laminate will be further reduced on account of these interface regions.

In this scenario the upper and lower faces are free from load and a shearing force P is applied to the end $x = \ell$.

From [56] the deflection at the free end l can be calculated as:

$$w = \frac{P\ell^3}{3E_cI} + \frac{\beta P\ell}{btG_{lam}} \tag{5.6}$$

where β is the linear shear modifier, being 3/2 for a Timoshenko element and 6/5 for a Benham and Crawford element.

The difference in the shear modifiers describes the manner in which shear stress is distributed through the beam. In a Benham and Crawford beam this distribution is parabolic, whereas in a Timoshenko beam the distribution is square. For a single ply of carbon fibre prepreg, the Timoshenko modifier is best suited on account of the structure (see Section 5.5.2).

By combining equations 5.3 and 5.6 we can determine the intra-ply shear stiffness as follows:

$$w = \frac{P\ell^3}{3E_eI} = \frac{P\ell^3}{3E_cI} + \frac{\beta P\ell}{btG_{lam}} \tag{5.7}$$

Rearranging for G_{lam}

$$G_{lam} = \frac{3t^2}{10\ell^2}\left(\frac{E_eE_c}{E_c - E_e}\right) \tag{5.8}$$

From this equation we can see a strong link between the aspect ratio of the sample and shear modulus, therefore achieving the same value of G over several lengths will confirm the validity of the of the shear modifier. Applying this process to the plots shown in the previous section we see this to be true (Fig. 5-9).

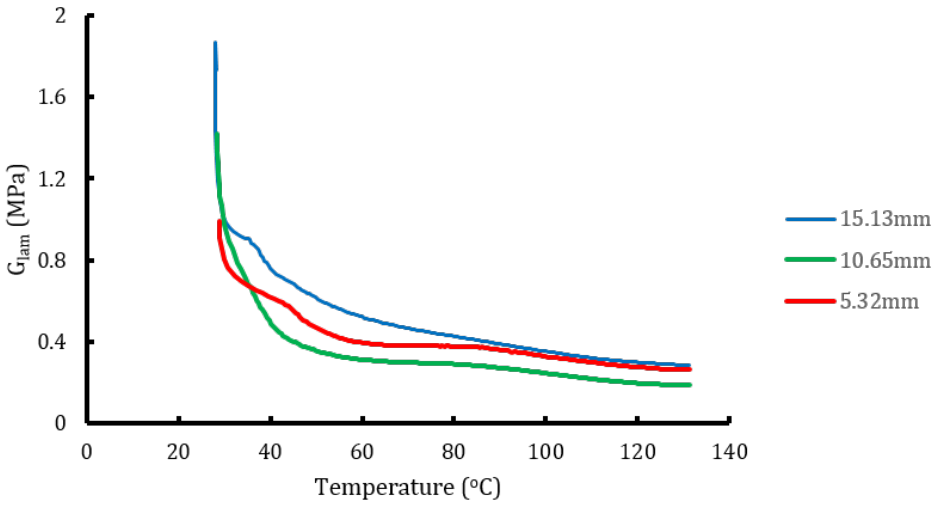

Figure 5-9: *Plots of intraply shear modulus G_{lam} against temperature derived from the results presented in Fig. 5-6*

5.3.2 Laminate bending

Once single ply behaviour has been analysed small laminates consisting of 2-8 plies shall be investigated. From initial testing it can be seen that the effective laminate shear modulus reduces as more plies are added due the increasing number of resin rich interfaces (Fig. 5-11).

In the bending of a single ply it is assumed that the resin rich regions on either side of the ply do not contribute to the bending response in any significant manner. As soon as two plies are stacked together however there exists a plane of weak material in the middle of the structure (Fig. 5-10). Work in Chapter 3 has already shown shear to localise at the interface between two plies when slipped relative to one another, so it can be assumed that the effective shear modulus will reduce. It will not reduce to the values displayed in Chapter 3 however as the fibrous zones must still shear if any deformation is to be achieved, therefore the effective modulus will be determined as a combination of the contributions from the stiff and weak layers.

Knowing the approximate thickness of the interface region and the shear modulus of a single ply we can back calculate the shear modulus of the resin rich interface. The

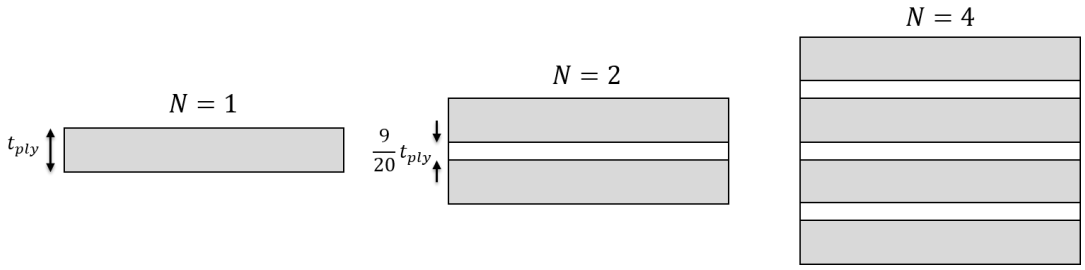

Figure 5-10: *Showing the ratio of interface layers to fibrous layers. The thickness of the resin interface is estimated from S.E.M. imagery*

shear stress can be calculated in the ply and the interface as:

$$\tau = G_{ply}\gamma_{ply} = \frac{G_{ply}\Delta_{ply}}{t_{ply}} = G_{int}\gamma_{int} = \frac{G_{int}\Delta_{int}}{t_{int}} \tag{5.9}$$

where $G_{ply} = G_{lam}$ for a single ply, G_{int} is the shear modulus of the interface, γ_{ply} is the shear strain in the fibrous zone, γ_{int} is the shear strain at the interface, Δ_{ply} is deformation in the fibrous zone, Δ_{int} is deformation at the interface, t_{ply} is the thickness of the fibrous region and t_{int} is the interface thickness such that $t_{int} = 9t_{ply}/25$ (see Section 5.5). Given that the laminate deformation $\Delta_{lam} = \Delta_{ply} + \Delta_{int}$ and the laminate shear strain $\gamma_{lam} = \Delta_{lam}/t_{lam}$, where t_{lam} is the laminate thickness, such that $t_{lam} = Nt_{ply} + (N-1)t_{int}$, we can substitute Eqn. 5.9 such that

$$\gamma_{lam} = \frac{\tau}{t_{lam}}\left(\frac{t_{ply}}{G_{ply}} + \frac{t_{int}}{G_{int}}\right) \tag{5.10}$$

The shear modulus of the laminate is therefore $G_{lam} = \tau/\gamma_{lam}$ and therefore

$$G_{lam}^{-1} = \left(\frac{\alpha_{int}}{G_{int}} + \frac{\alpha_{ply}}{G_{ply}}\right)^{-1} \tag{5.11}$$

where

$$\alpha_{int} = \frac{(N-1)t_{int}}{t_{lam}} \quad \text{and} \quad \alpha_{ply} = \frac{Nt_{ply}}{t_{lam}} \tag{5.12}$$

Rearranging Eqn 5.11 for G_{int} therefore gives:

$$G_{int} = \frac{\alpha_{int}G_{lam}G_{ply}}{G_{ply} - \alpha_{ply}G_{lam}} \tag{5.13}$$

Applying this formula to the results shown in Fig. 5-11 provides the data shown in Fig. 5-12. Due to the temperature aligned data not matching perfectly as the tests progressed individual static points have been selected from the relevant data points in

the respective tests. As discussed in Section 5.5 this technique for unpicking the various moduli of the layers in the laminate has a wide range of potential future applications.

5.4 Results

The average value of intraply shear modulus for different laminates against temperature is displayed in Fig. 5-11, showing the reduction in apparent shear modulus with increasing numbers of interfaces. Each line is the average of at least four results.

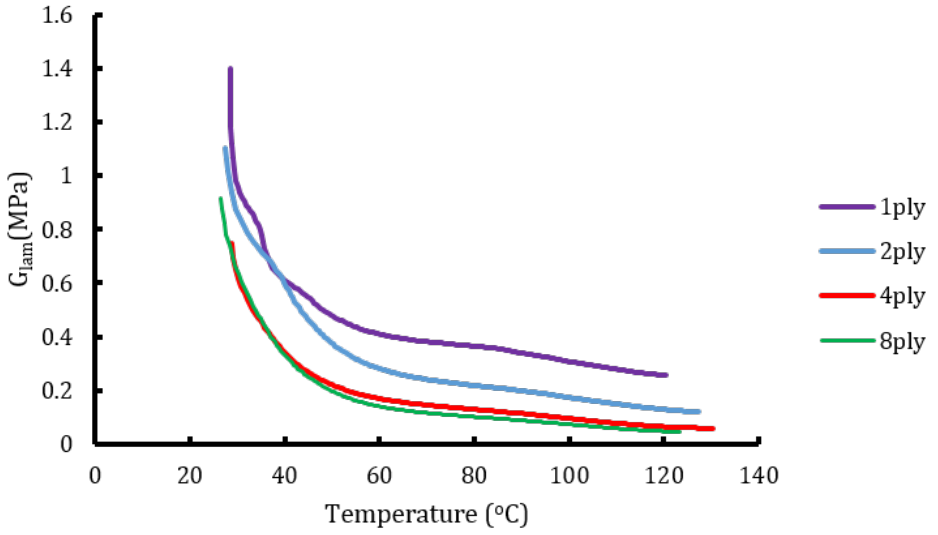

Figure 5-11: *Plots of laminate intraply shear modulus G_{lam} against temperature*

Interply shear modulus G_{int} is plotted against temperature in Fig. 5-12, in both cases reducing with increasing temperature. Also included are values of initial stiffness, K, from the interply shear tests in Chapter 3 to aid the discussion in the next section.

5.5 Discussion

One of the key advantages of DMA is its accuracy and repeatability, a factor which can clearly be seen in Fig. 5-11 and which was common for all samples. This, coupled with quick, simple sample preparation and mounting makes it a very attractive option for investigating bending behaviour. As expected from Fig. 5-6 and the discussion in Section 5.2 intraply shear is a temperature dependent variable, reducing in value as temperature increases on account of the viscous nature of resin. This is also the case for the interply shear results in Fig. 5-12, agreeing with results presented in Chapter 3.

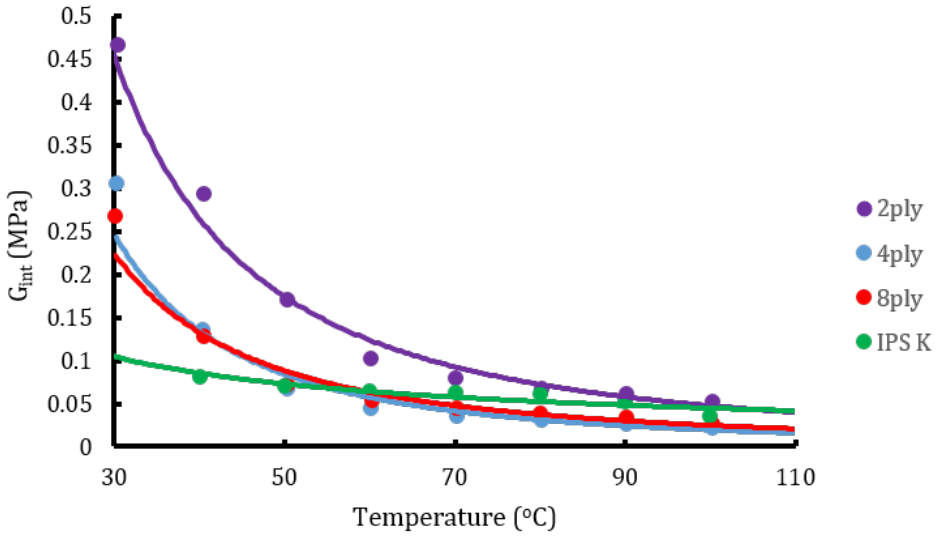

Figure 5-12: *Plots of interply shear modulus G_{int} against temperature including initial stiffness (K) values from Chapter 3.*

It is expected that the 2 ply results will be the least accurate on account of the ratio of fibrous layers to resin interfaces being $n : (n-1)$ and the variability in the interface thickness (see Section 5.5.1). Therefore a 2 ply laminate has a fibre to resin layer ratio of 2:1, whilst a ten ply laminate has a ratio of 10:9, reducing the impact of inconsistencies in the resin interface. The values of G_{int} calculated should be comparable to the values of initial stiffness K presented in Chapter 3, as the strains invoked in the bending tests fall well before the yield strain noticed in interply shear testing. This also reduces the impact of not being able to apply pressure to the samples during testing, as the initial stiffness is observed to be independent of pressure. Figure 5-12 shows a reasonable degree of comparability between the two sets of results, considering the significant difference in methodology and sample size. The K values from Chapter 3 appear almost linear, however this is most likely due to the lack of a 30°C value for this technique. Due to the viscosity of resin being measured on a log scale, and the initial stiffness being resin dominated, it is highly probable that a 30°C value of K would be significantly higher than the value at 40°C, in keeping with the DMA results.

5.5.1 Impact of number and thickness of interfaces

The impact of the number of interfaces is briefly discussed in Section 5.2, where it is noted that the ratio of fibrous regions to interface regions is $N : (N-1)$ on account of the outer resin regions not contributing to the bending response. This goes a long way

towards explaining the non-linear reduction in intraply shear modulus with increasing plies seen in Fig. 5-11, however it is further complicated by the large inconsistency in interface thickness between two plies (Fig. **??**).

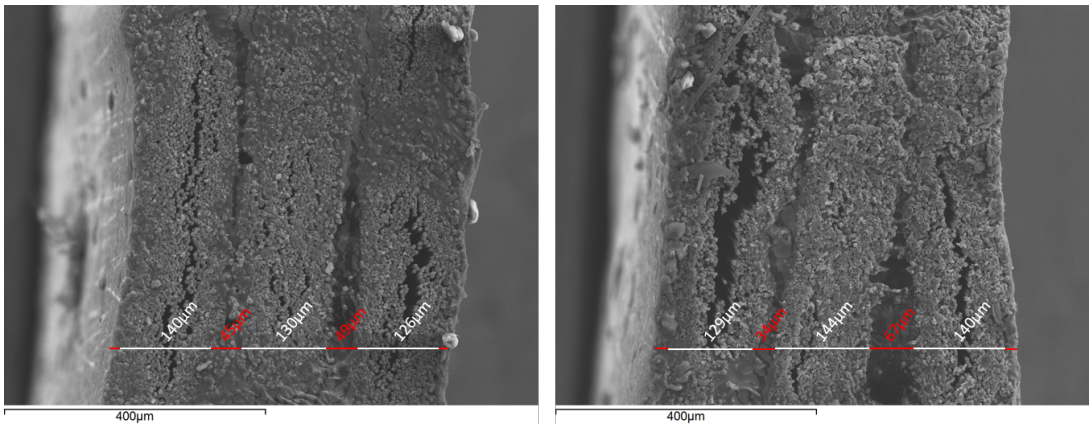

Figure 5-13: *Two S.E.M. images of three plies of uncured 8552/AS4 prepreg, with clear regions of resin, fibre, and small areas of dry core. The material used here was of a lighter GSM than in the earlier testing, hence the reduced ply thickness.*

Consider by way of an example the thicker interface in Fig. 5-13 (Right) which is almost twice the width of the smaller interface. In a sample with a smaller number of layers this has a significant impact on the results. Taking the thicker value and applying it to data gathered at 30°C gives a G_{int} of 0.53MPa, whereas the thin interface gives a value of 0.39MPa. By increasing the number of layers, and by extension interfaces, a more accurate average interface thickness can be obtained for the calculations and the impact of any abnormally sized interfaces on the shear behaviour is lessened.

Although not present to a large degree in the tested material, the presence of a dry core in the fibrous regions of other prepregs is of particular importance when comparing the values of initial interply shear stiffness gathered from DMA with those gathered from the methodology in Chapter 3, in which it is suggested that this value K is the stiffness of the resin interface, which shears as a result of load transferred to it from the bounding rigid fibrous regions. DMA does not apply any pressure to the dry region, and as such, the fibres within it are able to slip freely past one another, with load being transferred as an artefact of surface roughness, geometry and packing density. This means there is potentially a plane of material that is very weak in shear in the middle of each ply, meaning they are no longer rigid bodies in themselves, and will deform to some degree as they transfer stress to the interface, weakening the observed result. In the interply shear testing, the application of pressure leads to a much greater frictional response in the fibrous area, and the manner in which the sample is clamped also restricts movement within the fibre bundle. Future work will aim to investigate

the influence of pressure on the initial stiffness response by individually bagging each DMA sample, and is discussed in more detail in Chapter 7.

5.5.2 Shear modifier

Choosing the correct shear modifier for Eqn 5.6 depends upon the structure of the material being investigated, and the manner in which shear stress is expected to be distributed through the material. In a Timoshenko beam, the shear distribution is square, and therefore maintains a non-deformable normal, compared to a quadratic distribution in a Benham and Crawford element with a non-constant normal rotation through thickness [68]. This shear distribution dictates the shear deformation experienced by the material (Fig. 5-14).

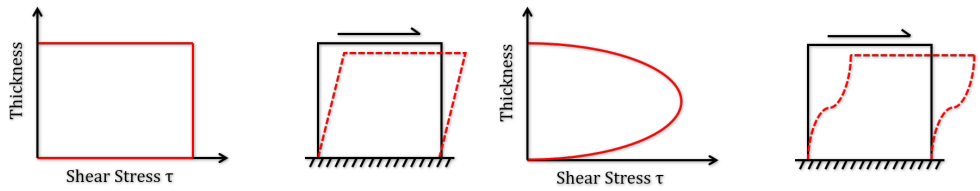

Figure 5-14: *(Left) Timoshenko shear stress distribution and deformation, and (Right) Benham and Crawford distribution and deformation*

If we consider first a 2D cross-section of single ply of prepreg, we have a material comprised of a vary large number of stiff fibres, each separated by a thin weak resin layer. In this instance the approximate distribution is closer to Timoshenko than Benham and Crawford due to the repeating, periodic nature of the contrasting layers. Considering next a two ply stack, the stiff and weak layers are effectively reset, with the ply becoming the stiff layer and the resin interface becoming the weak layer (Fig. 5-15 (Left)) We therefore have a system of just three layers with shear deformation localising to the resin interface. In this instance the Benham and Crawford modifier is better suited, although depending on the contrast in the stiffness of the layers a more stepped distribution might be expected rather than the smooth curve. As we increase the number of plies in the stack the shear stress distribution reverts to a case similar to that of a single ply, thus as $N \to \infty$, $\beta \to 6/5$ (Fig. 5-15 (Right)).

The impact of changing the shear modifier itself is a simple scaling of the results. For example, with the Benham and Crawford modifier Eqn 5.8 becomes:

$$G = \frac{3t^2}{8l^2}\left(\frac{E_e E_c}{E_c - E_e}\right) \tag{5.14}$$

Recalculating a value for G from a 2 ply sample at 40°C we see a change from

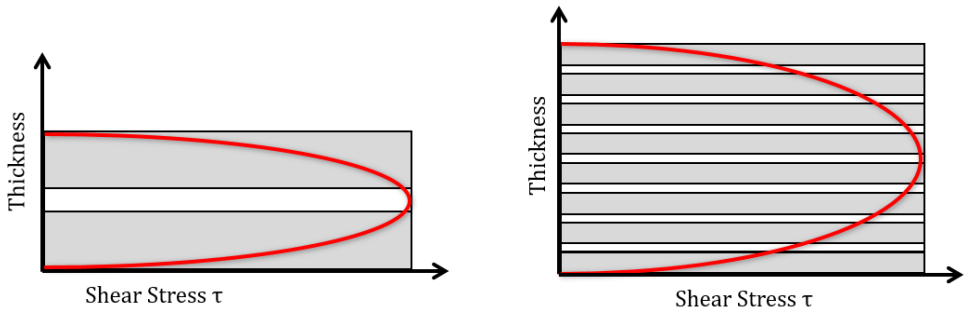

Figure 5-15: *Figure showing the approximate shear stress distribution across (Left) a two ply stack, for which Benham and Crawford is fairly representative, and (Right) an eight ply stack, for which Timoshenko is better suited*

0.412MPa to 0.513MPa. This is a fairly sizeable change, however it should noted that shear stress distribution used by Benham and Crawford is itself not a perfect representation of expected shear distribution in a 2 ply laminate, especially considering the thickness of the interface the contrast in the stiffness of the layers.

Strictly speaking, the prediction provided by Timoshenko is still inadequate, due to the significant difference in the shear stiffness of the ply and the interface [68]. If the shear stress distribution is to be represented to a greater degree of accuracy, a system such as zigzag theory will have to be considered. Zigzag theory is a response to the observed inconsistency between predictions made using Timoshenko beam theory and experimental results, specifically for cured parts [68]. Zigzag theory moves from the single layer assumption of the Timoshenko approach and instead considers a layer-wise approach, in which the kinematic fields of each layer are individually assigned along with constraints to maintain the continuity of the structure [69]. The obvious limitation of this approach is the increased computational complexity, particularly for thick laminates with a large number of variables to consider [70, 71]. The question therefore is whether or not the added accuracy of the layerwise approach is justified considering the inherent inaccuracy in the sample on account of the inconsistency in the interface thickness, and moreover, whether or not there is any point in achieving such a level of accuracy on the microscale, when the multiscale technique for which the parameters are being obtained takes a 'smeared' approximation of the layered structure when running on the coarse scale. Regardless, future work will look to assess the suitability of the layerwise approach before deciding whether or not to adopt it.

5.5.3 Application

The results from DMA do not lend themselves easily to simple prediction of forming parameters, rather they further complicate simple application by making temperature a coupled parameter, much like pressure. Increasing the temperature of the part during forming has already been shown to improve interply mobility, which was originally seen as key to forming a defect free part. Whilst this statement remains true, it must now be balanced against the reduction in bending stiffness which occurs at elevated temperatures. This therefore becomes a problem of optimisation, which requires a representative system model to be able to provide an answer.

5.6 Conclusions and future work

A technique for modifying results gathered from standard DMA to be able to consider shear in bending has been presented and successfully applied. The method itself uses a shear modifier term in which a shear modulus G captures the contribution of shear to bending, whilst the modulus of the material is determined from either rule of mixtures or simple tensile testing. The results highlight the benefits of DMA as a test platform, showing good repeatability and accuracy whilst being easy to set up and run. In order to accurately characterise bending behaviour of uncured prepreg it is necessary to have a detailed understanding of the structure of the material, however this can be achieved readily with S.E.M. imagery.

A limitation of DMA is the inability to apply pressure to a sample during testing, which has been noted in Chapter 3 as a key factor in shear deformation. This is mitigated to some extent by the very small shear strains invoked during the testing, however it could possibly have an impact in the higher temperature range, where the lowered viscosity of the resin might lead to redistribution within the ply. The problem with investigating the bending of a sample which is under pressure is isolating the behaviour of the sample from the material used to apply pressure, this typically being a vacuum bag of some sort, coupled with the small size of the sample and the environmental chamber of a DMA machine.

The results gathered help inform novel process modelling techniques in a number of ways. Firstly, the provision of an intraply shear modulus complements the parameters already gathered in previous work Chapter 3 and allows for the accurate analysis of buckling induced defects. The ability to investigate the same parameter in two very different test scenarios, in this case the interply shear modulus G_{int} (termed K in Chapter 3), also helps build confidence in both the gathered parameters and the methodologies employed.

One aspect of the DMA results which has yet to be considered is the phase difference value tanδ, which describes the viscoelastic nature of the material response. DMA is potentially very versatile in the investigation of the viscoelastic nature, as the testing can perform high and low frequency tests one after another in a single test cycle. The only complication is again converting the loss modulus to a system which considers shear deformation.

5.6.1 Angled plies

If the results gathered in this chapter are to be applied to industrial laminates in any reasonable manner the influence of angled plies must be considered, much as with the interply shear results presented in Chapter 4. The problem with testing angle plies by themselves is the lack of continuous fibres from one end of the sample to the other, resulting in the loss of the elastic contribution of the fibre. This prevents the ability to test the sample in a cyclic manner over a temperature range, which is one of the key benefits of DMA. Fortunately, this limitation can be easily overcome using the same technique that is applied to investigate interply shear stiffness, where the contribution of the stiff fibrous region and weak resin interface are unpicked using Eqn. 5.13. The contribution of an angled ply can therefore be investigated by interposing it between two 0° plies, only in this case values of α_{int}, the 0° ply α_0 and the angled ply α_ϕ must be considered, where

$$\alpha_0 = \left(\frac{N_0 t_{ply}}{t_{lam}}\right) \quad \text{and} \quad \alpha_\phi = \left(\frac{N_\phi t_{ply}}{t_{lam}}\right) \tag{5.15}$$

where N_0 is the number of 0° plies and N_ϕ is the number of angled plies. By extension, $N = N_0 + N_\phi$. Re-deriving Eqn. 5.13 to consider the angled ply therefore gives the intraply shear modulus of the angled ply as

$$G_\phi = \frac{G_{lam} G_{int} G_0 \alpha_\phi}{G_{int} G_0 - G_{lam} G_0 \alpha_{int} - G_{lam} G_{int} \alpha_0} \tag{5.16}$$

An additional complication exists when considering the value of E_c to be used for the bending stiffness. Whilst the tensile modulus of a 0° ply is fairly easy to obtain from a tensile test, determining that of a 90° ply is more complex, for similar reasons to investigating the bending behaviour. Fortunately, by using the tensile test mode available to DMA we can apply the same principles that have been used throughout this chapter to unpick the contribution from an angled ply interposed between two 0° plies. The chief difference between bending and tension is that in the tensile scenario the strain in each component is equal, such that $\epsilon_c = \epsilon_0 = \epsilon_\phi = \epsilon_{int}$, whereas in the bending scenario, the shear stresses are equal. Assuming modulus $E = \sigma/\epsilon$ and stress

$\sigma = F/A$, where A is the cross-sectional area, the strain in each component can be decomposed

$$\epsilon = \frac{F_0}{E_0 A_0} = \frac{F_\phi}{E_\phi A_\phi} = \frac{F_{int}}{E_{int} A_{int}} \tag{5.17}$$

where the area of the 0° fibres is $A_0 = N_0 t_{ply} b$, the area of the angled plies is $A_\phi = N_\phi t_{ply} b$ and the area of the interface is $A_{int} = (N-1) t_{int} b$. Taking the load in the laminate to be the sum of the load in the components, such that $F_{lam} = F_0 + F_\phi + F_{int}$, and letting $\zeta_0 = N_0/N$, $\zeta_\phi = N_\phi/N$ and $\zeta_{int} = ((N-1)t_{int})/N$ and substituting into Eqn. 5.17 gives

$$\sigma_{lam} = \epsilon \left(E_0 \zeta_0 + E_\phi \zeta_\phi + E_{int} \zeta_{int} \right) \tag{5.18}$$

and letting the measured modulus $E_{lam} = \sigma_{lam}/\epsilon$, rearranging for E_ϕ we see that

$$E_\phi = \frac{E_{lam} - E_0 \zeta_0 - E_{int} \zeta_{int}}{\zeta_\phi} \approx \frac{E_{lam} - E_0 \zeta_0}{\zeta_\phi} \tag{5.19}$$

In practice, the contribution of the interface to the tensile response is negligible, and as such ignored. Determining the influence of the angled layers may seem unnecessary at first, given that the tensile modulus is used to calculate the bending stiffness in the previous 0° laminates, however, given the location of the angled plies and the D-matrix term from classical laminate theory, which relates to bending behaviour, we can see that this modulus is not immediately suited [86].

Consider for example two scenarios, firstly a [0,90,0] laminate A, and secondly a [0,90,0,90,0] termed B, and in particular their structure. In the case of laminate A the neutral axis of the beam runs directly through the middle of the weak 90° ply. This means that the bending behaviour of the ply is going to be dominated by the 0° plies either side of it (Fig. 5-16).

From [86] the value of D_{ij}, i.e. the bending stiffness matrix, is best suited relating as it does to curvature which arises due to an imposed moment. This value can be calculated as

$$D_{ij} = \sum_{k=1}^{N} \left(\bar{Q}_{ij} \right)_k \left(t_k \bar{z}_k^2 + \frac{{t_k}^3}{12} \right) \tag{5.20}$$

where $\left(\bar{Q}_{ij} \right)_k$ is the modulus of the k^{th} layer, t_k is the thickness of the k^{th} layer such that $t_k = z_k - z_{k-1}$ where z_k is the distance from the neutral axis to the outer edge of the k^{th} layer, and $\bar{z}_k$ is the location of the centroid of the k^{th} layer from the neutral axis such that $\bar{z} = (z_k + z_{k-1})/2$.

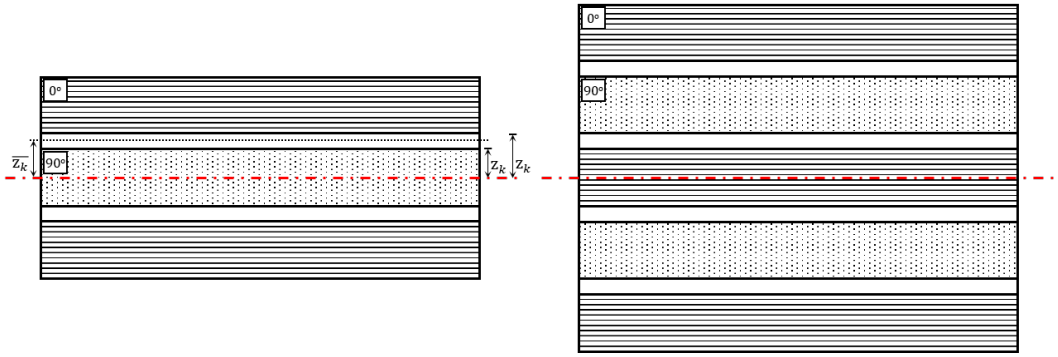

Figure 5-16: *The difference between the RoM and the CLT calculated value of E_c to be used in bending is due to the location of the plies in relation to the neutral axis. In the [0,90,0] laminate on the (Left), the weak 90° ply lies either side of the neutral axis, and therefore contributes very little to the bending response. In the [0,90,0,90,0] scenario on the right, the 90° plies are closer to the edge of the sample, and therefore play a more significant role in the reduction of the modulus.*

Unfortunately the mounting of a tensile specimen in the DMA is more complex than a bending specimen, due to the manner in which load is transferred to the ply from the resin tab. In the bending scenario, the response of the ply is significantly weaker than the stiffness of the resin, and the applied load is compressive. In the tensile scenario, the response of the ply is dominated by the fibre stiffness, which is an order of magnitude greater than that of the resin tab. The response recorded by the DMA is therefore the effective shear modulus of the resin tab (see Fig. 5-17).

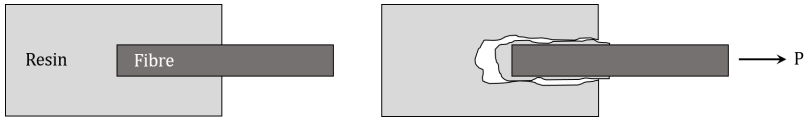

Figure 5-17: *Attempting a tensile test using the methodology described for bending tests will result in a measure of the shear modulus of the resin, rather than the desired tensile modulus of the fibre. The test effectively becomes a fibre pullout scenario.*

For the sake of this example, the tensile modulus of the 90° ply is assumed to be of the same order of magnitude as that of uncured resin, i.e. very small. Applying Eqn. 5.20 therefore gives a value of 122.4GPa for the homogenised laminate $\bar{Q}_{11} = E_c$. This modulus can then be used to calculate G_ϕ at $\phi = 90$ giving 0.427MPa at 30°C, compared to $G_{int} = 0.305$MPa and $G_0 = 0.955$MPa.

Work in Chapter 4 also suggests a change in interface stiffness with angle. To investigate this Eqn. 5.16 can be solved simultaneously for [0,90,0] and [0,90,0,90,0] samples with G_ϕ and G_{int} as the unknowns, on account of the changing ratio of plies to interfaces. This technique clearly provides a very effective manner in which to

accurately obtain values which might otherwise prove experimentally challenging due to the nature of the material, consider that in Chapter 4 it proved impossible to conduct shear tests on angles greater than 45° due to the ply falling apart. Future work will look to conduct a full investigation of the influence of angled interfaces on bending stiffness. In Chapter 7 the possibility of applying this technique to the other test modes available to DMA is discussed, along with the current primary limitation of the technique, the difficulty of testing samples under pressure.

CHAPTER 6

MODELLING COUPLED PARAMETERS AND LAMINATE SCENARIOS

Summary

Inter-ply shear characterisation work has provided a set of process parameters considered to be optimum for forming of a laminate. However, the characterisation tests are by necessity performed on simple flat plates, in which inter-ply shear is forced to occur using an Instron. Whilst this is suitable for determining forming parameters such as temperature, it falls short when considering coupled parameters such as pressure applied to a curved laminate. To remedy this, a laminate scale demonstrator test has been devised, in which the laminate is consolidated into a circular female tool at various temperatures and pressures, in such a manner as to create variable shear strain between the constituent plies. Experimental results suggest that increased pressure improves part formability, contrary to indications from simple shear tests, as the shear stiffness component of the system is relatively small in comparison to the applied bag pressure. Results from the model highlight the importance of accurately modelling the deformation mechanisms involved, with the consolidation law which was applied proving inadequate, resulting in a significant degree of inaccuracy in the results when compared to the experimentally derived values.

6.1 Introduction

Having gathered a number of key parameters and an understanding of the mechanisms governing the material response, the next question is how to use this data to inform design decisions in an industrial setting. Simple application has already been touched on in Chapters 3 and 4, whereby optimum forming parameters such as stacking sequence and rate of deformation can be estimated from the stress/strain traces themselves. This is fairly rudimentary however, and does not account for the coupled behaviour of some parameters. For example, pressure is clearly a key parameter in both consolidation or forming of prepreg laminates, removing air voids, redistributing uncured resin, and providing the force required to conform a flat laminate to a tool with some geometry. In flat, plate-like components it is clear that increased pressure leads to increased consolidation, as no inter-ply shearing action is required. However, in components with non-flat geometry pressure becomes a more complex parameter, as increased pressure also reduces ply mobility as a result of the increased frictional response when fibres interact at the ply interface, as discussed in Chapter 3.

The influence of temperature on the bending response is another prime example of a coupled parameter. Increasing temperature is shown to improve interply mobility, reducing the end-loading on fibres and improving formability. However, at the same time the increased temperature reduces the effective bending stiffness of a laminate by lowering the intraply shear modulus, leaving the plies more susceptible to buckling. In order to investigate these coupled parameters a modelling approach capable of capturing the changing behaviour is required, and one which can be readily experimentally validated.

From an observational perspective, the presence or lack of wrinkles in a part is the easiest way to assess how well it has formed. It is known to be particularly difficult to instigate wrinkle defects in small scale components however, as a key driver for this defect is 'length effect', i.e. the presence of large regions of immobile plies surrounding the geometric region [3, 7]. Wrinkles are also a complex problem to model due to their arising as a result of a buckling instability. In order to assess the coupled effect of pressure a different measure of formability is therefore considered, that being the degree of consolidation achieved in a curved demonstrator. As the sample with non-flat geometry must shear if it is to conform to the tool, any difference in the measured thickness around the part will be due to the manner in which ply mobility is affected by pressure. The tool considered is female in order to ensure the plies are subjected to tensile rather than compressive loads as forming progresses. If the plies cannot slip they will effectively bridge, holding off consolidation and resulting in increased part

thickness. An energy minimisation approach is introduced in Section 6.2 which seeks to balance energy in shear and consolidation against work done by a forming bag. The methodology and tooling dimensions are presented in Section 6.3, with results displayed in Section 6.4. The agreement between the model and the experimental data is discussed in Section 6.5, before finally drawing some conclusions and highlighting areas for further work.

6.2 Modelling consolidation with curvature

6.2.1 Consolidation stiffening

In order to accurately predict the consolidation behaviour of a curved component subjected to pressure, the manner in which a laminate consolidates must be considered. A number of existing process models such as that presented by Hubert et al. [91] consider a composite laminate to be a deformable fibre bed fully saturated with a curing resin, with the compaction behaviour being due to the flow of the resin, implemented using Darcy's law, combined with packing behaviour of the fibre bed. This means compaction behaviour can be broken down into distinct viscous and elastic responses, much like the shear behaviour discussed in Chapter 3. Experimentally characterising consolidation behaviour poses a similar problem to the characterisation of interply shear with regards to the difficulty of isolating the contribution of the individual viscous and elastic components to the overall response. In the case of consolidation behaviour, common practice involves the removal of the resin component in order that the dry fibre might be tested in isolation, with the resulting response being subtracted from the behaviour of a similarly loaded complete composite in order to back calculate the response of the resin. The problem with this approach lies in the fact that the resin greatly alters the manner in which fibre-fibre contact occurs, acting as a lubricating agent and drastically reducing the frictional component of the response.

A more representative test proposed by Hubert and Poursartip [89] allows consolidation testing to be conducted on representative samples of prepreg, without the need for the investigation of the dry fibre response. The fundamentals behind the actual test methodology are fairly simple, using a stepped relaxation test profile, in which a displacement is incrementally applied and held at set intervals, with the load response being recorded (Fig. 6-1 (Left)).

Considering the material to be represented using the Kelvin-Voigt model (see Chapter 2) the stabilised value (i.e. when $d\epsilon/dt = 0$) can be assumed to be the elastic response of the fibre, whilst the initial, stiffer response is due to the viscous resin response, which dissipates as the rate of deformation is removed. A new curve of consolidation

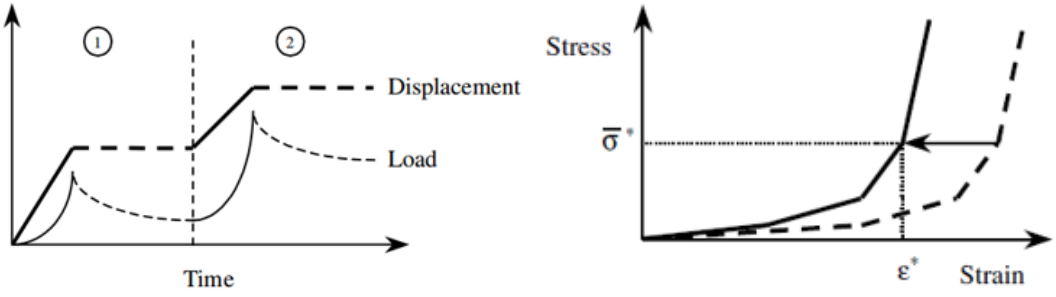

Figure 6-1: *(Left) Incremental deformation is applied then held until the measured load stabilises. (Right) The trace is then shifted to the left to display the elastic component of the stress/strain response. Figures from [89]*

strain vs. normal pressure can then be constructed which captures this elastic behaviour, using a single stress control test to confirm the position of the new curve (Fig. 6-1 (Left)). Dodwell et al. [3] consider a similar approach when looking at a debulk scenario, in which deformation is assumed to be so slow that the viscous contribution of the resin can be considered to be ≈ 0 resulting in a purely elastic response. A power law is then fitted to the consolidation data in which a uniform pressure, q, is applied to the outer layer of a laminate, causing a percentage consolidation, ν. This results in a non-linear stiffening of the laminate as the fibre volume fraction increases such that $q = \nu^2 C$ where C is a consolidation coefficient >0. It has been decided to utilise this power law approach in part due to the simplicity of application, but also due to the fact that the data for 8552/AS4 has already been gathered in [3], eliminating the need for consolidation tests.

6.2.2 Energy minimisation

A simple and effective way of investigating coupled pressure is to apply the principle of minimum energy using the Rayleigh-Ritz method [67] to determine the consolidation strain at either edge of the part. In a curved part, formability is influenced by resistance to shear strain, with Eqns. 3.1 and 3.2 allowing the shear strain required for a part to form to be determined. In order to exaggerate the shear strain one end of the sample can be clamped (Fig. 6-2). Considering the sample below, the maximum shear strain required for the part to form is 0.32 at the free edge applying Eqn. 3.1. Shear strain is assumed to grow in a linear fashion around the part, from 0 at the clamped edge to the maximum value at the free edge. By extension, considering the stress/strain traces shown in Chapter 3, resistance to shear must also grow around the radius, resulting in a non-constant consolidation strain.

Assuming that shear strain increases linearly from 0 at the clamped edge to a maxi-

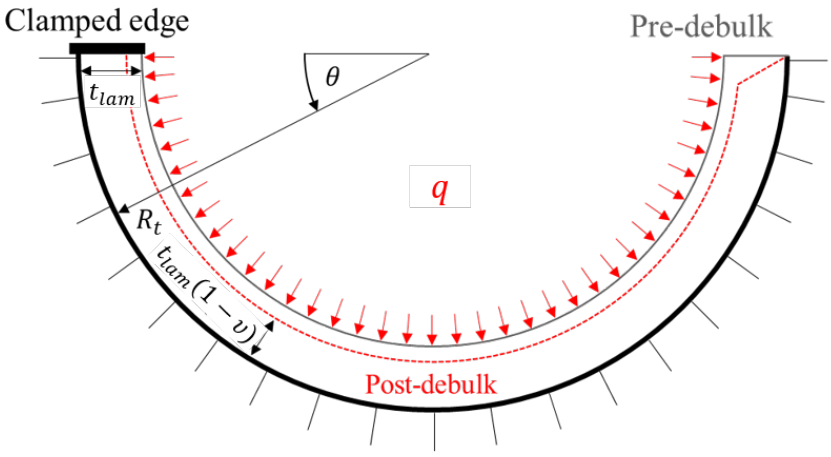

Figure 6-2: *Laminate demonstrator scenario in which shear strain is maximised by clamping the left hand edge.*

mum value at the free edge, the average consolidation strain $\nu(\theta)$ across the component can be calculated as:

$$\nu(\theta) = \nu_1 - \nu_2 \frac{\theta}{\pi} \tag{6.1}$$

where θ is the tool angle and ν_1 and ν_2 are fitted parameters. Therefore, as θ approaches 0, $\nu(\theta)$ approaches ν_1, the maximum consolidation strain. To find ν_1 and ν_2 we can consider an energy minimisation approach, such that the total energy in the system:

$$W = U_C + U_S - w_q \tag{6.2}$$

where U_C is the energy in consolidation, U_S is the energy in shear and w_q is the work done by the bag, such that:

$$U_C = \int_0^\theta \frac{C}{3} (\nu(\theta))^3 t_{lam} R_t d\theta \tag{6.3}$$

where t_{lam} is laminate thickness and R_t is the tool radius,

$$U_S = \int_0^\theta t_{lam} \tau \gamma(\theta)(R_t - t_{lam}) d\theta \tag{6.4}$$

where τ is the shear stress from the logistic function presented in Chapter 3 and $\gamma(\theta)$ is the shear strain, calculated such that:

$$\gamma(\theta) = \nu(\theta)\theta \tag{6.5}$$

and the work done by the bag is:

$$w_q = \int_0^{\theta} q\nu(\theta) t_{lam}(R_t - t_{lam}) d\theta \tag{6.6}$$

Substituting Eqn. 2 into 4, 5, 6 and 7 and integrating through gives the energy in consolidation as:

$$U_C = \frac{(Ct_{lam}R_t)}{3}\left(\nu_1^3\theta - \frac{3\nu_1^2\nu_2\theta^2}{2\pi} + \frac{\nu_1\nu_2^2\theta^3}{\pi^2} - \frac{\nu_2^3\theta^4}{4\pi^3}\right) \tag{6.7}$$

the energy in shear as:

$$U_S = t_{lam}\tau(R_t - t_{lam})\left(\frac{\nu_1\theta^2}{2} - \frac{\nu_2\theta^3}{3\pi}\right) \tag{6.8}$$

and the work done by the bag as:

$$w_q = -qt_{lam}(R_t - t_{lam})\left(\nu_1\theta - \frac{\nu_2\theta^2}{2\pi}\right) \tag{6.9}$$

Applying equilibrium, we differentiate W with respect to ν_1 and ν_2 such that:

$$\frac{\delta W}{\delta \nu_1} = 0 = \frac{\delta W}{\delta \nu_2} \tag{6.10}$$

This gives us two simultaneous quadratics in ν_1 and ν_2 shown below, which can be solved using Maple [61].

$$\frac{\delta W}{\delta \nu_1} = \frac{Ct_{lam}R_t}{3}\left(3{\nu_1}^2\theta - \frac{3}{\pi}\nu_1\nu_2\theta^2 + \frac{1}{\pi^2}{\nu_2}^2\theta^3\right) + \frac{1}{2}t_{lam}\tau(R_t - t_{lam})\theta^2 - qt_{lam}(R_t - t_{lam})\theta \tag{6.11}$$

and

$$\frac{\delta W}{\delta \nu_2} = \frac{Ct_{lam}R_t}{3}\left(-\frac{3}{2\pi}{\nu_1}^2\theta^2 + \frac{2}{\pi^2}\nu_1\nu_2\theta^3 - \frac{3}{4\pi^3}{\nu_2}^2\theta^4\right) - \frac{1}{3\pi}t_{lam}\tau(R_t - t_{lam})\theta^3 + \frac{1}{2\pi}qt_{lam}(R_t - t_{lam})\theta^2 \tag{6.12}$$

The shear stress τ can be calculated from the logistics model presented at the end of Chapter 3, which is informed by the various experimentally derived values of K, K_t and τ_c. This allows a highly accurate calculation of the shear stress around the laminate as the shear strain increases. Although an answer could be derived from a simple, single

step, this would lead to a significant problem with the presented model. When running in a single step the force generated normal to the part effectively remains constant from start to finish. By extension, from our stiffening law this suggests that ν must also remain constant around the part, resulting in a far greater calculated value of ν than would otherwise be expected. In reality the force generated by the pressure q is increasingly split between acting normal and tangentially to the tool, that is to say it must both consolidate the part and drive the shearing mechanism such that $q = \sigma_n + \tau$ (Fig. 6-3). To capture this effect the model must be analysed incrementally for values of applied pressure q, with the minimisation approach being carried out at each point.

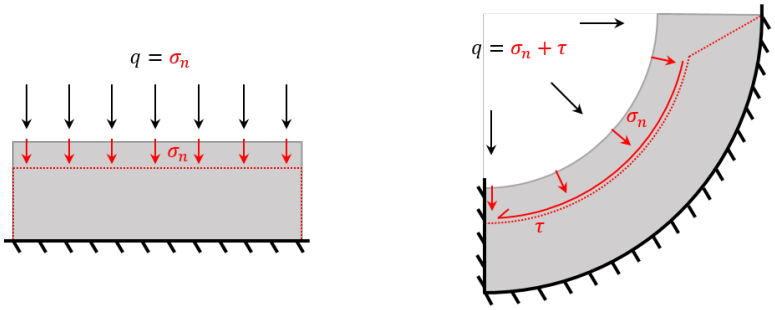

Figure 6-3: *(Left)(Right)*

In order to consider an incrementally changing normal stress σ_n the resistance to shear deformation at values of pressure other than those experimentally investigated must be considered. Thanks to the various individual component models derived in Chapter 3 this is not a challenge, as the experimental data is used to create a set of call in coefficients for each temperature investigated, allowing the prediction of the shear behaviour at any increment of pressure. To improve the accuracy of the results, the data for the 40 and 90°C stress/strain traces was reassessed using the logistics function, with the parameters being used to construct a three dimensional surface showing the evolution of the shear response with increasing pressure and shear strain (Fig. 6-4 (Left)). The other advantage of employing the logistic function is the preference in numerical solutions for a smooth surface, rather than one in which there exist discrete changes in variables, as mentioned in Chapter 3.

This is a very effective way of converting the experimental data into a form suited for modelling input parameters, as it allows for a detailed understanding of the shear response during a complete cure cycle as it undergoes varying control parameters. For example, during a typical cure cycle there exist several pressure 'ramps' as the part moves from initial debulk to final autoclave pressure. Figure 6-4 (Right) shows the changing shear response as the pressure is increased incrementally from 0 to 100 kPa in a linear fashion. Comparing this to a typical stress/strain plot taken with fixed

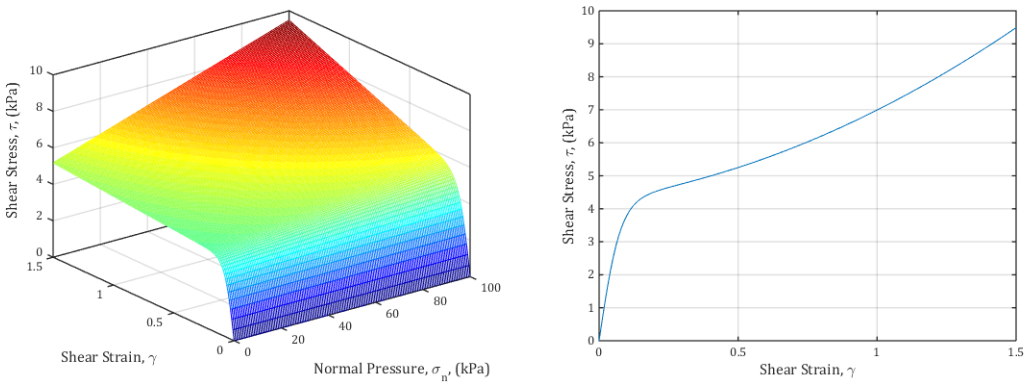

Figure 6-4: *(Left) 3D surface detailing shear stress against strain for an increasing pressure (Right) Stress strain trace taken at a diagonal across the 3D surface, showing changing stress response with incrementally increasing pressure and strain.*

control parameters we see the behaviour to be somewhat different, with a more gradual yield transition and an increasing post-yield gradient, further impairing formability in large shear strain scenarios, although this has a minimal impact on the scenario being investigated here. This is a fairly simple example in which only pressure is changed during a run, however there is nothing preventing modelling of the shear stress response for any non-constant variable in order that the shear response for a fully representative cure cycle might be captured.

6.3 Methodology

In order to validate the model a full scale demonstrator component was required, which could be accurately constructed and measured to allow a thorough comparison of data. This demonstrator was constructed in collaboration Kevin Johnson at the University of Bath, with the work being presented at ECCM 17 [54]. The most accurate means by which to measure part thickness was to use the Co-ordinate Measuring Machine (CMM) at the University of Bath, allowing for thickness scans with an accuracy of 4μm. The process works by first scanning the tool on which samples are constructed, from which a reference plane is constructed. Scans are then taken once a part is laid onto the tool and after every debulk stage. The planes generated from these scans are then overlaid against the reference plane to allow measurement of the thickness.

6.3.1 Tool design

To reduce the risk of any thermal mismatch during cure, the demonstrator tool was itself constructed from tooling carbon fibre, formed on a preliminary aluminium tool.

The dimensions of the tool feature a 180° corner with a radius of 150mm, a length of 700mm and a width of 425mm. A number of key design features have been included to improve both the quality of the part, and the compatibility of the tool with the CMM process. One key design feature is the prominent flange running along the edge of the part (Fig. 6-5). Not only does this stiffen the tool, reducing the risk of warp or deviation from the reference image, it also provides extremely flat surfaces from which the CMM can take an initial (x, y, z) reference plane. To further improve the CMM calibration sockets for four calibration spheres were built into the corners of the tool.

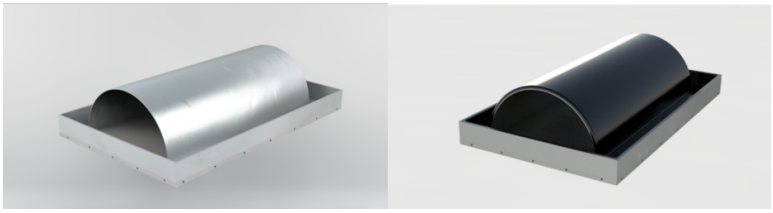

Figure 6-5: *(Left) Male aluminium tool made from a curved sheet and milled baseplate with flanges bolted to the sides. (Right) Tooling carbon is then laid onto the male tool, resulting in a female carbon tool on which tests can be conducted.*

The initial aluminium tool from which the carbon tool is made was constructed from a 12mm base sheet into which the locations of the various features are milled. Aluminium strips were then bolted to the side of the base sheet to create the vertical flanges, and the tool radius, made from rolled aluminium, was seated in groves milled in the base sheet, to ensure the diameter of the feature remained constant. The rolling of the aluminium sheet harbours the most risk of inaccuracy, however scans comparing it to a perfectly calculated cylinder showed variations of less than 1mm, and as results are calculated against the scanned surface of the tool this deviation can be considered insignificant. As mentioned, each corner of the tool has locators into which reference spheres can be mounted. This allows the analysis software to correctly align each scan to the original reference plane even if the tool has been moved from its original position The reference points are constructed around protruding inserts in the aluminium baseplate, machined to ensure they are vertical. Holes cut in the tooling carbon fibre allow it to be laid over these features without requiring deformation of the weave, or variation in the part thickness.

6.3.2 Sample preparation

Ensuring that each sample tested underwent a similar lay-up process was critical to the meaningful comparison of results. To ensure repeatability a number of controls were put in place. A template was constructed for the cutting of plies, ensuring precision

of both size and angle, whilst minimising wastage and reducing the time spent cutting carbon fibre. The material was removed from the freezer 18hrs before cutting to ensure it was fully defrosted. Once the plies were cut they were re-frozen and taken out when required for the lay-up, with 5-6 hours allowed for defrosting with the lay-up itself taking place over several hours. A number of lay-up strategies were investigated before settling on the use of a roller with very little applied force, and a heat gun to promote tack in the material. By minimising the force applied during lay-up the pre-debulk laminate remained fairly thick, thereby resulting in a greater percentage of compaction during the debulk, promoting inter-ply shear and making the formability of the chosen debulk parameters more visible. Each sample was made from 24 plies with three stacking sequences chosen, shown in Table 6.1 below. These stacking sequences were originally chosen as part of a work package being conducted by Kevin Johnson investigating matching stiffness matrices which is not discussed here, however it also allows some discussion of the results presented in Chapter 4 regarding formability of different interface angles.

Sample ID	**Layup**
QI	$[(45/\text{-}45/0/90)_2]$s
60/0	$[60/\text{-}60_2/60/\text{-}60/60/0_2/60/\text{-}60/0_2]$s
30/90	$[30/\text{-}30_2/30/\text{-}30/30/90_2/30/\text{-}30/90_2]$s

Table 6.1: *Test matrix showing stacking sequences investigated*

A key aspect of the sample preparation is the clamping of the left hand edge. This was achieved by applying a strip of quick curing resin to the left hand edge, and placing an aluminium strip above it (Fig: 6-6).

The quick cure resin acts as an adhesive, bonding the plies to one another and the aluminium strip. The resin has sufficient stiffness to hold off the pressure at low temperatures, however initial testing showed that as the temperature approached 180°C the resin began to deform under vacuum. Whilst still sufficiently strong enough to resist the small forming induced load (i.e. inter-ply shear movement), an additional aluminium strip was required to keep pressure off the part. By extending the strip sufficiently over the tool it can be ensured that the strip will not rotate into the part when loaded, as the pressure is acting on a larger area on the supported side than the unsupported side. The debulk itself was carried out either in an oven, when bag pressure of up to 0.1MPa was required, or in an autoclave when pressures greater than 0.1MPa were being investigated. When investigating pressures below 0.1MPa a needle valve was used to adjust the draw on a vacuum pump to ensure a constant pressure and in both instances the part was fully bagged using release film and breather cloth

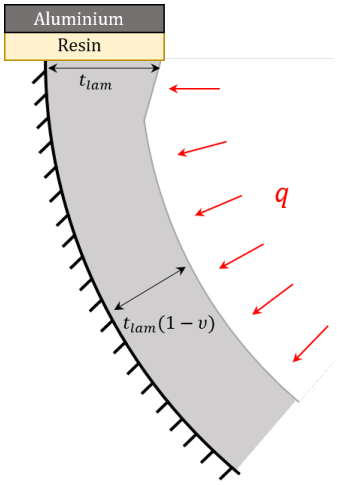

Figure 6-6: *Detail of the clamping set-up using resin to hold the plies and an aluminium strip to withstand pressure. The thickness gradient caused by the clamping results in the bag pressure imparting a small tensile load on the plies, aiding mobility.*

to ensure uniform pressure across the part.

6.3.3 Scanning

In order to assess the thickness of the component measurements were taken along ten lines spaced 35mm apart around the radius of the part with the spacing around the radius being a point every 1mm along a horizontal plane. This means the spacing around the radius was not constant with an effective increase in sampling density in the middle of the part, however this was an unavoidable limitation of the device used. The tool was glued into the rig using a hot melt glue gun each time to ensure it did not move during the measurement process. Measurements made on the reference spheres and flat flange areas ensured that the results taken around the radius could be accurately compared with data gathered from other scans (Fig. 6-7).

6.3.4 Determining test parameters

The forming parameters employed were chosen to provide the largest mismatch in consolidation strain across the part, in order to facilitate data collection. For example, work done in the first report suggests an optimum temperature of 90°C, which has been confirmed by experience in industry. However, running a range of pressures at this temperature through the predictive model showed very little change in end thickness with pressure, as the temperature is such a dominant control aspect that it effectively washes out the influence of pressure, making it harder to accurately predict

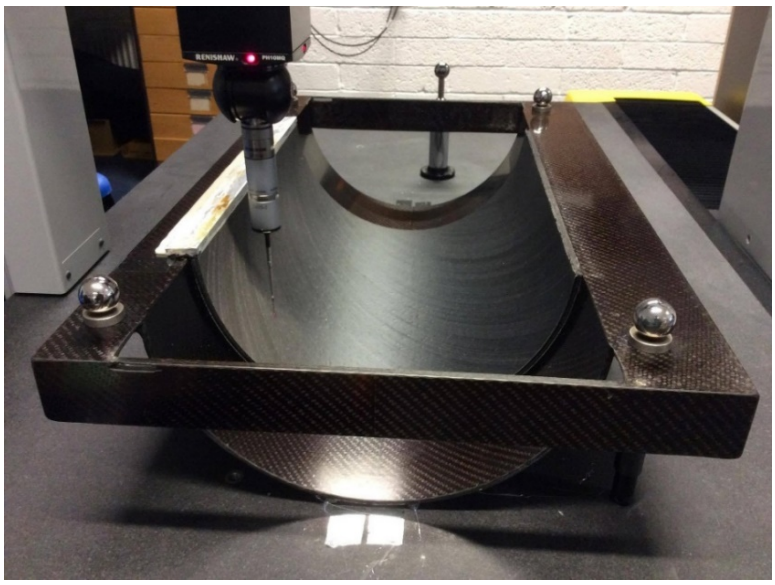

Figure 6-7: *Completed carbon tool with laminate and edge clamping in the scanning rig. Note the reference spheres in each corner.*

the impact on formability. By contrast, running the model at a lower temperature suggests that pressure becomes a far more influential parameter. Two temperatures were investigated, 40 and 90°C at pressures of 0.05, 0.1 and 0.2MPa for the former, and 0.2MPa for the latter. These parameters were tested sequentially on a single sample due to the lay-up being extremely time consuming, and require a large amount of material.

6.4 Results

The predicted and experimental values of ν_1 and the consolidation strain at the unclamped edge, $\nu(\pi)$, at the prescribed forming parameters can be seen in Table 3. Due to the test results being inaccurate at the edges of the part (see Section 6.5 this values are derived from the equation of the trendline applied to the thickness results from the inner region of the part (see Fig. 6-8). At low temperatures the model predicts an improvement in formability with increased pressure, whilst the experimental results show an improved ν at the cost of uniformity of thickness across the part. The model predicts improved consolidation strain at 90°C but with a reduction in uniformity across the part with increased pressure. The experimental values for the 0.1MPa 90°C test were obscured by a large region of bridging that occurred during lay-up. The implications of this are discussed in more detail in Section 5.

Thickness values around the radius of the component for varying pressures immediately after lay-up, at 40°C and at 90°C for both the QI and the 60/0 laminates are

Temp. (°C)	Pressure (MPa)	Predicted		Experimental					
				QI		60/0		30/90	
		ν_1	$\nu(\pi)$	ν_1	$\nu(\pi)$	ν_1	$\nu(\pi)$	ν_1	$\nu(\pi)$
40	**0.05**	0.05	0.04	0.029	0.037	0.029	0.026	0.031	0.008
	0.1	0.069	0.0627	0.036	0.041	0.040	0.035	0.038	0.024
	0.2	0.097	0.091	0.044	0.055	0.053	0.048	0.052	0.033
90	**0.2**	0.157	0.146	0.108	0.082	0.106	0.089	0.098	0.093
cured	**0.7**	-	-	0.109	0.100	0.123	0.117	0.119	0.116

Table 6.2: *Table of results showing consolidation strain achieved at each end of the part*

plotted in Fig. 6-8. The plots typically show an increase in consolidation with increasing pressure, as expected from the model. There are also clear signs of non-uniform consolidation around the part.

6.5 Discussion

6.5.1 Thickness variation traces

The experimental values of ν_1 and $\nu(\pi)$ from the 40°C debulks were calculated relative to the laminate thickness directly after layup. This value itself suffers from slight thickness variations around the tool due to the non-perfect hand layup procedure, which is to be expected. Measurement data for the first 15° of the clamped and free laminate edges were removed due to the inaccuracy of the CMM process in this region, which struggled to properly contact the part at the steep gradient as the part neared vertical orientation. As expected from the methodology and the model prediction, the clamping mechanism itself preventing ply thinning during consolidation, while the lack of edge bars at the free edge allow pressure to act on the ends of the plies, pushing them into the laminate and actually resulting in local thickening at higher temperatures. Due the the significant difference in expected material structure, the 90°C consolidation strains were calculated assuming a constant pre-debulk laminate thickness around the radius using the average thickness value from the pre-debulk trace, in order to allow for a meaningful analysis of the results. The reasoning behind this is that the nature of the resin in the composite is very different at 40 and 90°C. At low temperatures, the resin is very viscous, and behaves almost as a plastic solid. At higher temperatures the viscosity drops dramatically, and it becomes a flowing liquid. This is discussed in more detail in the following section.

The thickness results agree with the temperature findings in Chapter 3, showing 90°C to allow for significantly higher degrees of consolidation strain than 40°C, as a

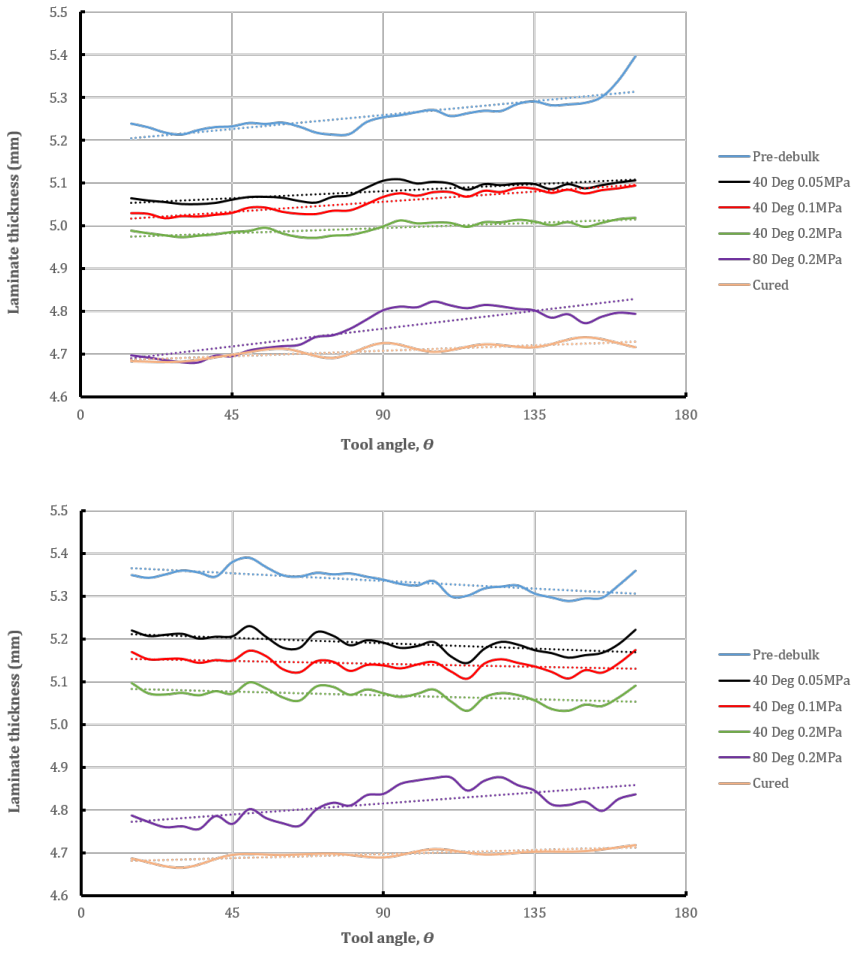

Figure 6-8: *(Top) Plots of thickness around the arc length of the part for the QI sequence after debulking at 40°C and various pressures, showing increased thickness from the clamped edge (0°) to the free edge (180°), and (Bottom) the same tests performed on the 0/60 laminate. Figures from [54]*

result of the resin having a much lower viscosity at this temperature. In fact, the laminate comes very close to final cure part thickness, which is achieved with a much higher pressure of 0.7MPa at a temperature of 180°C.

The model suggests that consolidation strain will slightly reduce around the part. This is not observed for the QI laminate at 40°C, but is apparent for all other cases. The values of $\nu(\pi)$ for the QI laminate appear to suggest an increase in shear strain, suggesting that resistance to shear actually aids consolidation. It is thought that these values are the result of some localised voiding during the lay-up, resulting in artificially easier debulking in that region, and a larger apparent consolidation strain. This seems to be apparent in the thickness trace in Fig 6-8 (Top), where there is a sharp increase

in pre-debulk thickness as the angle approaches 180°, affecting the gradient of the trendline.

The difference in behaviour of the 60/0 and 30/90 laminates when compared to the QI laminate highlights the potential requirement for a stacking sequence-specific consolidation coefficient, with both laminates exhibiting reduced formability, especially in the case of the 30/90 laminate. Considering the work in Chapter 4 this could be due to the increased number of blocked plies, which inhibit through-thickness shear strain, and the lack of any orthotropic interfaces which promote shear. This laminate was actually expected to improve formability, however the benefits of this laminate may only become apparent at very high shear strains, i.e. drape forming, which could not be achieved using this test setup, where the large proportion of angled plies would tend towards some twisting deformation rather than the comparatively stiff inplane shearing. For the 30/90 laminate the reduction in consolidation strain is unsurprising given that the continuous fibres running around a feature, and therefore in the orientation of the shear/slip deformation, have been shown to prevent consolidation if they are unable to slip [7].

When comparing the thickness variations along the tool radius for the different experimental laminates, i.e. Fig. 6-8 (Top) and (Bottom), it becomes apparent that at a 40°C debulk temperature all samples follow a trend set out by the initial pre-debulk thickness distribution. This is even apparent with the QI stack having an initial positive thickness gradient around the tool radius, while the 60/0 laminate is initially negative. The 0.2MPa, 90°C debulk however produces an interesting behaviour where the laminate significantly thickens halfway around the radius towards the free edge. This effect is equally present in all three laminate samples and seems to be a side effect of the bag pressure on the free edge pushing material into a region in the part which has already consolidated and cannot shear further. If a sufficient amount of material is pushed in this manner it is not inconceivable for wrinkles to form. At this temperature and pressure, the QI laminate already reaches final cured part thickness in the first 60° of the tool radius. While having the same thickness distribution around the radius as the QI, the non-standard 60/0 laminate however does not reach cured ply thickness at this stage due to the previously mentioned non-standard stacking sequence characteristics. Despite having different initial average thicknesses and thickness distributions, all samples achieve an identical laminate average thickness of ≈4.7mm after a full cure at 180°C. Both non-standard laminates reach a maximum consolidation strain at cure of 12%. This value exactly matches the initial assumption made in Section 6.2 for the consolidation strain used for calculating the maximum possible shear strain. The QI laminate however only shows a maximum consolidation strain of 10.5%, largely due to

the part being slightly more consolidated during the lay-up.

6.5.2 Comparison of predicted and experimental values

By relating the experimental values of consolidation strain (Table 6.2) at either edge of the part to those calculated using the model derived in Section 6.2, we can assess both the impact of stacking sequence on the formability of the component and the accuracy of the energy minimisation model. Considering the experimental thickness traces, in particular the non standard laminates, we can see that whilst the general trend of the change in consolidation strain around the tool is similar, the calculated values of consolidation strain are significantly higher than the experimentally obtained values. This is due in part to the nature of the power law used to represent consolidation stiffening being highly inaccurate outside its fitted data range, discussed in greater detail in Section 6.5.3, and in part due to the potential difference in porosity in the curved laminate demonstrator and the flat laminates from which the consolidation law was fitted. The consolidation law applied, drawn from the works of Hubert et al. and Dodwell et al. [16, 17], considers only the response of the elastic fibre bed, assuming a fully impregnated system in which there exists only resin and fibre. Realistically, resistance to consolidation is therefore an artefact of the viscosity of the resin, and the permeability of the fibre bed as its packing density increases (see Section 6.2), with the consolidation itself occurring as the fibre bed adjusts to achieve optimum packing density. Considering the SEM images presented earlier however we can see that an uncured laminate contains a significant amount of air trapped not only between the plies, but also within the fibre tows themselves (see Fig. 1-1). These air pockets or voids mean the fibre volume fraction of the laminate could be significantly lower on account of the additional thickness, meaning the effective consolidation strain achievable is greater. It is thought that the level of porosity in the curved laminate is significantly reduced during layup when considering the lay-up regimes employed in [54] and [17] respectively. The use of a roller and a small degree of applied heat by Johnson et al. [54], necessary to promote adhesion in the curved tool, most likely resulted in a significant reduction in interlaminar voiding, and even the tow core porosity.

The pressure required to remove the air is a function of the viscosity of the air and the permeability of the fibre bed; air obviously being significantly less viscous than resin at any temperature, and the permeability of the fibre bed, this being at a maximum value at the start of the process. The pressure required to achieve reduction in thickness due to removal of air can therefore be assumed to be an order of magnitude weaker than that required to force resin flow, suggesting the calculated consolidation stiffness to be significantly weaker than one might expect for a fully impregnated sys-

tem, hence the apparent over-prediction from the model. Attempts at considering the more detailed consolidation model presented by Hubert [92] further highlight the importance of understanding the initial fibre volume fraction and the manner in which it changes throughout the test. Changes of just 1% in volume fraction can result in up to a 25% increase in consolidation strain achieved. A simple approach towards combating this could be to simply shift the curve presented in Fig. 6-1 depending upon the value of fibre volume fraction to alter the effective stiffness of the response. Unfortunately, more significant problems exist with the consolidation law applied in this Chapter.

6.5.3 Consolidation laws and resin flow

A significant cause of inaccuracy in the energy minimisation model presented in Section 6.2 lies in the power law used to represent consolidation stiffening. Whilst a power law is reasonably accurate over the range of data to which it is fitted, problems arise when it is used to predicted behaviour at higher pressures on account of the structure of carbon fibre prepreg. Consider for example a single dry fibre subjected to full autoclave pressure (i.e. 0.7MPa). Because of the exceptionally high elastic modulus of the fibre, usually around 230GPa, this small pressure will elicit a strain of just 0.003, whilst a more process representative pressure of 0.2MPa will generate a strain of < 0.001. Considering that a full laminate typically consolidates by around 20%, and that resin in its liquid form can be assumed to be incompressible, the consolidation must be due to three mechanisms; evacuation of trapped air from between the plies, increased packing density of the fibre bed, and the redistribution of resin from the surface of the ply to the dry core.

Assuming the repacking of the fibre bed to be relatively weak as a response (see Section 6.2), the 'stiffness' of this response is therefore highly dependent on the permeability of the laminate, but is yet significantly less than the stiffness of carbon fibre. As a result of this, it stands to reason that once the ply is fully wetted and the fibre bed is at its optimum packing density, no further consolidation will be able to occur. This suggests a limit to the maximum attainable consolidation strain, or at the very least a transitional point from a very weak response to a very stiff one. For this reason the power law, and the continual increase in consolidation strain which it predicts (Fig. 6-9 (Left)), does not represent the expected behaviour of a laminate. A more representative approach which maintains the simplicity of the power law would be to fit a hyperbolic function of the form $y = a/(b - \nu)$ to a set of data from consolidation testing (Fig. 6-9 (Right)).

This function would therefore result in a hard limit to the maximum attainable consolidation strain, albeit at the cost of additional computational complexity, whilst

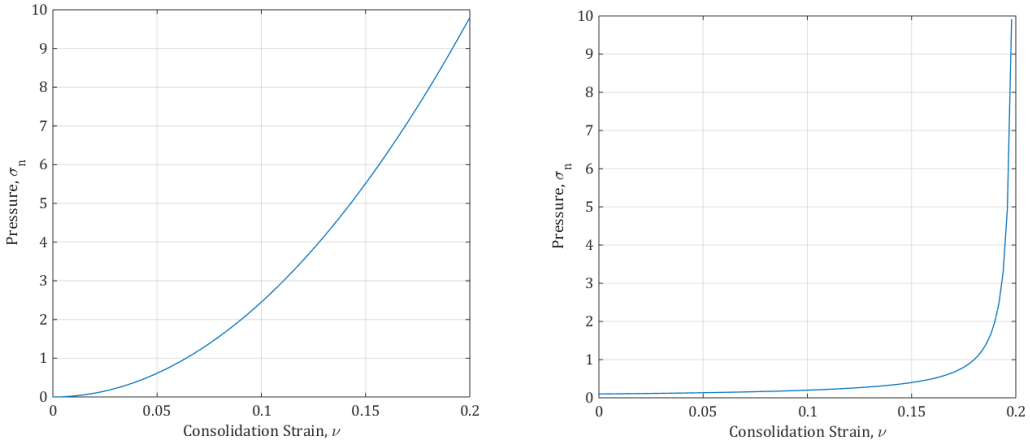

Figure 6-9: *(Left) Consolidation stiffness behaviour fitted to a power law, suggesting a continual increase in consolidation strain with increasing pressure, and (Right) the same behaviour fitted to a hyperbolic law, suggesting some limit to the maximum attainable consolidation strain.*

being able to represent the extremely weak response when drawing air from the laminate in the initial stages of consolidation. This is the basis of the approach adopted by Hubert [92], who also considers the influence of fibre volume fraction and fibre waviness, as mentioned in the previous section.

The key problem with both the power law considered and a hyperbolic approach is that it models only the elastic behaviour of the fibre bed. To truly represent the behaviour in consolidation and the manner in which it is affected by temperature, pressure and the reinforcement architecture, a system which considers resin flow must be considered. Needless to say, these models are significantly more complex than the entirety of the model presented in the Chapter, and are already incorporated in the novel process modelling technique in development. If we consider the manner in which the experimental data for this model is generated (see Section 6.2 and Fig. 6-1) we come to the conclusion that the normal stress σ_n which generates consolidation is significantly under-represented, as a large part of the resistance to consolidation must come from the stress required to force the resin to flow through the fibre bed. This in turn leads to a significant reduction in the level of shear stress generated on account of the highly pressure dependent value τ_c. This in turn explains the fairly minimal difference in consolidation strain around the part as predicted by the model and the generally high level of consolidation strain expected, as the plies are fairly mobile. Whilst it was originally hoped that the relatively slow deformation experienced during a debulk might mitigate the omission of the resin based shear response, it unfortunately appears that resin flow must indeed be represented accurately as per the work of Hubert

[92] if values of consolidation strain are to be predicted.

6.5.4 Clamping and tension

An interesting side effect of the clamping mechanism used during the debulk was the potential for it to impart a tensile load upon the plies. As the clamped edge is prevented from thinning, it creates a gradient into the debulked region, as shown in Fig. 6-6. This effectively redirects the bag pressure, so that it is no longer acting normal to the tool in this thicker region, rather, some component of if the pressure is acting in the plane of the ply, imparting a tensile load (Fig. 6-6). Naturally this angle itself requires some length change if it is to be achieved, increasing the required shear strain across the part. It is not known if this increase in required shear strain has a greater detrimental effect on the formability than the positive implications of the tensile load it generates; however, it is an area of considerable interest for future work.

6.6 Conclusions and future work

The suggestion from initial material characterisation tests that increased pressure during debulk could lead to reduced thickness loss in geometries with some curvature has been disproved using a rigorous new methodology to produce a curved laminate scale demonstrator. These tests have shown that increased pressure always results in an increase in consolidation strain in the component. Experimental results have shown some indication of the coupled nature of pressure in a curved component however, as increasing pressure does result in less uniform consolidation across the part, as plies in areas which must undergo large shear strains if they are to conform to the geometry are hindering by the increased pressure. This shear component is significant enough to have a visible effect on the thickness of the component, but not strong enough to hold it off completely.

A simple energy model has been implemented incrementally in order to give some indication of the consolidation strains expected around a component as it forms at some temperature and pressure. The accuracy of the model is subject primarily to the complexity of the consolidation and shear laws used within it, which must be updated to consider porosity in an uncured laminate if accurate values of consolidation strain are to be achieved. Whilst the model does hint towards the influence of resistance to shear in the forming of curved components, the unsuitability of the consolidation law used hinders the accurate representation of the mechanics at play.

Continuing work will look to improve the accuracy of this model, whilst keeping it as simple as possible, as the Cosserat model in development is far better suited to

modelling not only the complexity of the material problem, but also a wider range of component geometries. Whilst the model presented in this Chapter will never be as effective as a similar Cosserat model, it is felt that there is still some value to a comparatively simple system by which forming parameters can be quickly assessed. In order to achieve this, some consideration must be given to resin flow and the manner in which fibre volume fraction changes during consolidation.

6.6.1 Edge effects

One particularly interesting behaviour observed in the samples is a tendency towards thickening in the middle of the radius at higher temperatures. This appears to be the result of a second mechanism, which exists due to the lack of edge bars on the free edge. Pressure acting in plane on the plies at free edge appears to effectively promote mobility, with the undesirable effect of pushing excess material into a region which is under pressure and therefore immobile, a similar mechanism to that which generates wrinkles around corner radii. This also results in a rounded edge to the laminate as the upper plies shear more than those closer to the tool, rather than the sharp angle that occurs when shear strain between plies is uniform throughout the laminate. This behaviour confirms the importance of edge bars, and also confirms the notion that letting the plies slip too freely makes them more susceptible to wrinkling, thus requiring that a balance must be struck to ensure plies only slip the desired amount. In practice this would mean selecting a slightly lower temperature than the apparent minimum value from the characterisation tests. This influence of edge bars can be simply investigated by effectively including them as an additional test variable in future work.

CHAPTER 7

CONCLUDING REMARKS AND FUTURE WORK

Summary

This thesis highlights the importance of accurate characterisation methods and the value of modelling the results, even in a heuristic sense, when analysing the data and building an understanding of the mechanisms behind the material response. Simple models such as Coulomb friction are incapable of adequately representing the complex nature of uncured carbon fibre prepreg, and even classic viscoelastic models fall short due to the high contrast between the fibre and the resin response, and the changing dominance of the fibre or resin behaviour over a range of processing variables. Before concluding this thesis a number of key areas of future interest are defined.

7.1 Future work

7.1.1 Interply twist

Interply twist is a hugely important mechanism in the forming of laminates in which there exist plies laid orthogonally to one another. As explained in Chapter 4, the application of any load not aligned with or perpendicular to the fibres will result in some degree of rotation, resulting in some degree of both inter and intraply deformation, not unlike the response in bending. Work by Hallander et al. has already observed orthogonally aligned interfaces to improve formability, however the mechanics of this behaviour have yet to be investigated in detail for non-woven materials in high pressure forming scenarios.

As with interply shear, there exists a problem when considering quite how to characterise this behaviour. The work of Larberg et al. adapts the bias extension test, commonly used for woven materials, to be used with a [±45]s laminate, observing the material to behave in a manner similar to its woven counterpart up to a point, before splitting and coming apart. Unfortunately, due to the lack of any consolidation pressure this test is not suitably representative of the boundary conditions expected in a consolidation scenario, or even double diaphragm forming. The most obvious technique would be to attempt to utilise some form of vacuum bagging to provide an exact replica of the loading scenario experienced in a debulk. Naturally this adds to the complication of determining the contribution of the bagging material to the load response in order that it might be subtracted, however, due to the very small shear strains experienced during consolidation this should be a minor issue.

Another potential route of investigation is the adaptation of a rotational rheometer. Covering the top and bottom plates of a rheometer could allow the imposition of interply twist in a controlled manner, similar to the interply shear testing. The primary limitation appears to be that most rheometers are not designed to apply significant levels of torque, or even consolidation pressure. As such it will most likely be necessary to simply use the rheometer design as a blueprint for the development of a custom built rig.

Investigating the experimental characterisation of interply twist for uncured carbon fibre prepreg is be a key component of a wider EPSRC funded research program titled ADAPT, to be conducted by the author.

7.1.2 Advanced Dynamic Mechanical Analysis

The adaptation of DMA to allow the investigation of composite materials in bending opens up the possibility of using this technique to accurately investigate a wide range

of material properties. Building on the work presented in Chapter 5, there are several aspects which can be considered to improve applicability and confidence in the results. As shown at the end of the chapter, the investigation of the influence of angled plies is quite feasible, and one aspect of the future work will be to complete bending tests on a range of different angles.

A mode of particular interest for the model presented in Chapter 6 is compression, as it will allow for the generation of a high fidelity data to fit the new hyperbolic consolidation stiffness model against. In the DMA setup, a small sample is sandwiched between a stationary plate and a second plate attached to the load cell, and a fixed load or deformation applied. Due to the highly plastic nature of uncured prepreg in compression it will not be possible to perform a cyclic analysis as per bending stiffness, however the minimal set-up time and control over the applied load and deformation still makes this an attractive alternative to previous tests conducted using an Instron. The only possible limitation is the sample size. Work by Dodwell et al. has observed the tendency for excessive consolidation at the edge of a plate in the fibre direction, due to the high permeability in the fibre direction allowing the resin to flow easily from the edge part. As the sample is very small, this, could result in an abnormal degree of consolidation when compared to a larger sample. An easy solution to this can be found in extending the sample beyond the clamping plates and tabbing the edges however.

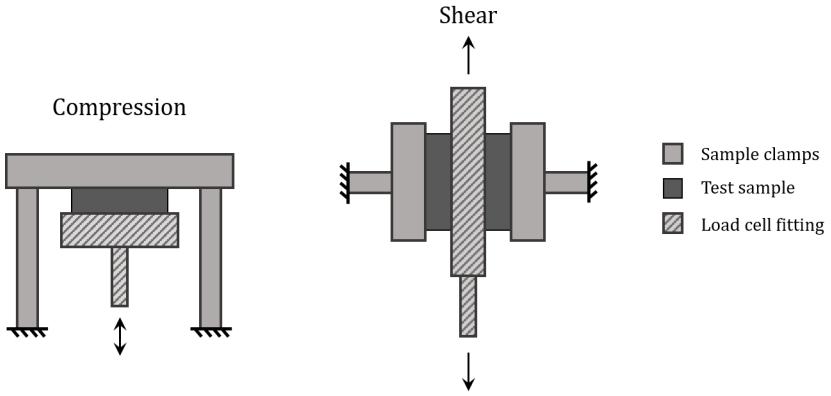

Figure 7-1: *(Left) Compression mode for DMA in which a sample is compressed against a fixed constraint and the resulting load measure (Right) Shear mode, in which two blocks of sample material are held against a central plate which is then excited in such a way as to provoke shear deformation in the samples.*

It is also possible to assess the shear response of a sample using the DMA, in a manner not dissimilar to the methodology presented in Chapter 3. Two small identical blocks of the sample material are arranged between the outer clamps, with a central plate attached to the load cell separating them. This central plate is then excited in

a cyclic nature and the load response recorded. An obvious limitation of the standard setup is the lack of control over the confining pressure applied to the sample, however, if this pressure can be regulated it would provide a test scenario capable of testing the plastic hardening behaviour presented in Chapter 3 via a repeated load - unload test loop, along with the general viscoelasticity of the material response.

The principal limitation of the DMA methodology employed at present is therefore the inability to apply a consolidation pressure to the sample. As such, it suffers from the common problem of not adequately representing the debulk process, and a change in the potential frictional behaviour of the dry fibre core. As noted in the conclusion of Chapter 5 this could result in the artificial lowering of the apparent resin stiffness in the interlayer when compared to the values calculated in Chapter 3. This is due to the the fibrous region no longer acting as a rigid body, as is assumed in the interply shear testing in Chapter 3. The problem is therefore one of finding some manner in which to apply pressure to a DMA sample. Two simple approaches exist, the simplest being the application of some consolidation pressure to the sample prior to testing to achieve a higher level of consolidation, and the complete wetting of the fibres, although this would not allow the lower temperature ranges to be investigated in a representative manner, and there would be a risk of the plies 'unbedding' during the test. The best approach would appear to be to individually vacuum bag each sample using a small envelope bag and a hot sealer, before mounting the samples in resin tabs as per the methodology presented in Chapter 5. This would be an improvement upon the previous approach, as the vacuum would be applied to a cold sample, and would allow a constant application of pressure during the test. Several limitations are immediately apparent however, chief of which would be that the vacuum would not be continually 'pulled' during the test, preventing the removal of air from the dry fibre core as the resin is consolidated, meaning that the air would have to remain within the bag somehow. A less significant problem exists in that the sample preparation would become significantly more time consuming, although this could be offset by bagging and sealing several samples at once.

7.1.3 Gaussian process regression

A problem common to the majority of characterisation tests, and experimental work in general, is the widely accepted requirement of repeat tests to confirm the results of the first round of testing. This practice becomes problematic when the test methodology is particularly time intensive, or if the test matrix requires the investigation of a large number of parameters. A more efficient and intelligent approach is to utilise some form of design of experiments or supervised learning to build from a simple baseline test

matrix [63]. In this way, the accuracy of the results can be analysed against how well they fit predicted function rather than their error about a stationary, repeated point. A technique commonly chosen is Gaussian process regression due to its increased flexibilty when compared against linear regression type approaches [65, 66], albeit at the cost of increased computational cost and reduced ease of use [64].

In a simple linear regression case, a function $f(x)$ is fitted looking to minimise the sum of the squares of the error when comparing the function to the data. The fitted function is built from a series of spline basis functions, which are straight lines. The curve is therefore effectively a series of gradients which can be 'smoothed' by the application of a roughness penalty.

Gaussian process regression, or kriging, improves on this by fitting Gaussian distributions to the data points again looking to minimise the square error as per linear regression methods, but also optimise the length scale of the Gaussian distribution of the data. The process then interpolates between the known data points, with the resulting points being governed by the covariance of the original data. The interpolation therefore runs through the means of the Gaussian confidence integrals (see Fig. 7-2), with the region of least confidence being selected as the parameters desired for the next experiment. This new data point is then fed into the model and the process repeated until the desired level of confidence is achieved across the whole data set.

Two approaches to data analysis, the first assumes the observed data points to be perfectly known, i.e. there is zero error in the values (Fig. 7-2 (Left)). As a result of this no prediction intervals exist around these points. The second and more suitable approach is to assume the data points to be noisy, as per the plot shown in Fig 7-2 (Right). In this case it is theoretically possible for the process to suggest an exact repeat of a previous test case, however the overall trend is likely to be more representative [62].

The application of this process in combination with an informed initial test matrix will allow for a greatly reduced test program for future materials whilst retaining confidence in the obtained data, and can be applied to data from any of the characterisation techniques previously presented. An additional advantage of GPR is the ability to perform cross-validation in order to assess the sensitivity of your data. This is achieved using the'Leave one out' approach, whereby you remove a single data point at a time and record the change in the LSE between the old and new curves, allowing you to determine confidence bounds for your data set.

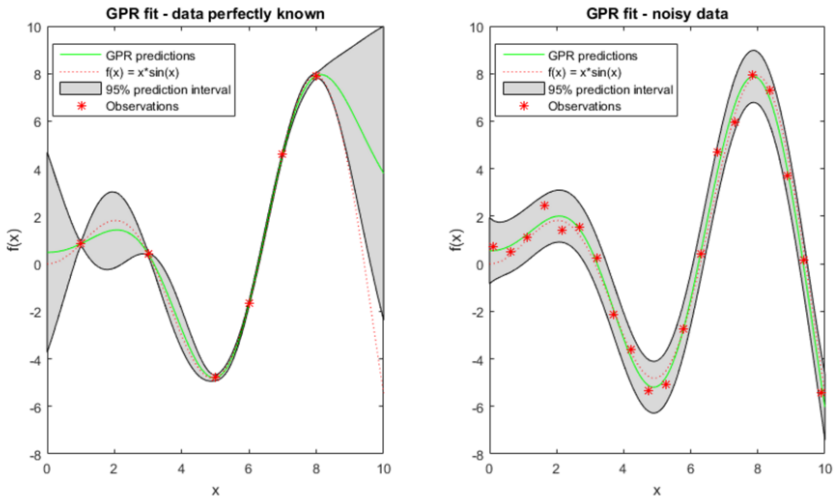

Figure 7-2: *(Left) GPR for perfectly known data points and (Right) for data assumed to be noisy. The predicted test parameters are defined to sit in area of least accuracy. Image from [62]*

7.1.4 Resin flow, interface thickness and porosity

One of the major assumptions made in all calculations of shear behaviour presented in this work is that interface thickness remains constant throughout the test run. This is a reasonable assumption for the results presented in Chapter 5, due to the absence of a consolidation pressure, however, for the results presented in Chapter 3 and 4 the applied pressure will lead to a reduction in interface thickness, which is even acknowledged as being a potential cause for parts of the observed behaviour. The degree to which this interface changes will most likely vary depending on the generation of carbon fibre. The fully liquid nature of the resin in 2nd generation prepreg will presumably allow the interface to reduce to a minimal thickness, however the thermoplastic particles in a 3rd generation prepreg will dictate the minimum thickness of the interface (see Fig. 2-6 in Chapter 2). Following the argument in Chapter 3 justifying choosing ply thickness as the value used to derive shear strains, the change of thickness at the interface will not have a significant impact on the results, however it remains an area of interest, particularly when considering the influence of the changing resin content that exists at the interface during the forming process.

When consolidating a laminate, a significant portion of the observed thickness loss is a result of excess resin at the interface either redistributing towards dry regions in the fibre core, or flowing from the edge of the part. Consolidation is therefore a resin flow dominated behaviour, and as such can be modelled as the flow of liquid resin through a porous fibrous material [85]. This can be simply represented using Darcy's

law, which suggests the flow rate to be proportional to the pressure gradient, modified by coefficients of permeability and viscosity. The principal complication is that neither viscosity nor permeability remain constant over the forming process, the former as a result of changing temperature and cure state, and the latter as a function of the increasing packing density of the fibres as the air is drawn from between the plies. This a problem which causes problems even for established flow models in F.E. packages such as ABAQUS [84], and requires the development of component specific code. The development of a flow model capable of predicting the consolidation behaviour based on viscosity and permeability is an attractive prospect, given that the only other alternative is to conduct an extensive experimental program. Young et al. propose a model studying three-dimensional resin flow building on the work of Gutowski and Dave [85, 87, 88] with a view to expanding the techniques developed for laminates built from a single orientation of unidirectional prepreg to consider cross-ply and even woven laminates. Future work on consolidation and shear behaviour will most likely use this work as a starting point.

The vast majority of work conducted on resin flow and consolidation only looks to simulate the resin flow in laminates in which the fibrous reinforcement remains stationary transverse to the applied pressure. Any work in this area must therefore consider some manner in which to experimentally assess resin flow in a system undergoing shear deformation. Work by Poursartip et al. [83] traces resin flow by 'tagging' a layer of resin within a laminate with bromine or chlorine, elements which register well with various forms of elemental analysis, allowing for a quantitative measure of resin flow. The challenge with using a technique such as this is that in order to ascertain the degree to which an interface is shearing and whether a dislocation occurs at the interface, any form of tagging must be sufficiently distinct that the relative movement of the resin in a single interface can be assessed. One potential option would be to apply a different trace element to each ply at the interface, and to apply the element to a distinct region rather than the entire ply. The validity of this approach also depends on the resolution of the elemental analysis technique employed. The intention would be to use one of the elemental analysis techniques available to S.E.M., with Poursartip et al. [83] suggesting the use of Wavelength dispersive (WDX) over Energy dispersive (EDX) X-ray spectroscopy on account of its improved sensitivity and resolution.

Further investigation will look to analyse the degree of porosity in an uncured laminate post lay-up, as this can have a significant impact on the degree of consolidation achieved during debulk. Due to air evacuation being a significantly weaker mechanism than resin flow, this can lead to current saturated models under-predicting the level of consolidation strain achieved when compared to experimental scenarios. The chief

challenge lies in developing a repeatable method by which porosity might be achieved during lay-up, and then measuring the effective thickness of the porous zones. An attractive option is the use of a load cell mounted within a Computerised Tomography (CT) scanner. In this manner, the porosity of a small laminate might be analysed post lay-up, and after incrementally applied load steps.

7.2 Concluding Remarks

This thesis creates the foundations of a characterisation regime capable of decomposing the complex behaviour of uncured carbon fibre prepreg laminates as they are subjected to various manufacturing induced loads into a set of definable parameters, for use either in novel process modelling applications or as simple metrics by which to assess the formability of a given prepreg. The test methods employed in this work are pre-existing, with the interply shear rig being very similar to those of Larberg [10] and Wilks [32], and Dynamic Mechanical Analysis being a long established technique with a commercially available test rig. The novelty in the work therefore comes from the analysis of the data, and in particular the development of a heuristic model capable of unpicking the results so that the contribution of the fibre and the resin might be better understood, whilst providing vital input parameters for advanced process modelling techniques. For example, the role of friction in determining interply mobility was originally considered as having a local minimum at some point over a temperature range [10], however the new model presented in Chapter 3 suggests that friction consistently rises with temperature, with the resistance to shear at lower temperatures being resin dominated.

This trend typically continues through the interply shear results, with the lower temperature response being resin dominated before transitioning to a more frictional, fibre dominated behaviour as the resin redistributes away from the interface under the effects of lowering viscosity and increasing pressure. A phenomenon of particular interest is the strain hardening observed post yield. It is thought that this in part to do with the resin at the interface flowing and reforming, and also due to the plies beginning to intermesh under the effects of pressure. The angles ply results in Chapter 4 support this hypothesis, with hardening decreasing with increasing interface angle. The mismatch in angle not only prevents intermeshing between plies, but also theoretically reduces the ability of the resin to flow at the interface. Tests conducted on a third generation prepreg also support the flow hypothesis, showing a very different behaviour in the region where flow is expected to be most influential on account of the restrictive thermoplastic particulate reinforcement. This behaviour is particularly important in large

shear strain forming scenarios, as the incremental resistance to deformation increases the risk of severe defects such as wrinkles and bridging. The overall conclusion from these chapters is that by manipulating processing parameters such as temperature, rate of deformation and pressure, you can improve interply mobility and reduce the risk of defect formation. The results in Chapter 4 also point towards the possibility of optimising stacking sequence for manufacture rather than just performance.

In Chapter 5 the bending behaviour of single plies and small laminates is investigated, in order that wrinkle formation might be better understood. As with interply shear, resin plays a large role in the bending of carbon fibre prepreg, however in order for the material to shear, some degree of intraply shear must now occur. To investigate this parameter the simple Engineers Bending Theory approach used by Dynamic Mechanical Analysis was successfully altered to consider an additional Timoshenko shear modifier. The intraply shear modulus results are an order of magnitude larger than the initial interply stiffness results from the previous Chapter, as expected on account of the structure of the material. Moreover, by observing the apparent decrease in intraply shear modulus in laminates of more than one ply, it was possible to back-calculate an approximate interply shear stiffness, which agreed well with the results gathered from the interply shear rig, providing confidence in the results gathered by both techniques. The results gathered from this chapter are vital in the prediction of wrinkle formation, as they provide the modelling parameters necessary to predict whether or not the forming induced stresses will result in the buckling of plies.

The final chapter addresses the problem of predicting coupled parameters, focusing on pressure as an example. A coupled parameter in this context is one which improves one aspect of forming, but has a negative impact on another. For example, increased pressure improves the achievable percentage consolidation, but also reduces interply mobility by amplifying the frictional response. The problem thus becomes one of optimisation, and in this example is investigated using a relatively simple energy minimisation approach, using the logistic function proposed at the end of Chapter 3 to inform the model. Comparison of the modelling results against a rigorous experimental program conducted simultaneously showed as similar trend in consolidation stiffness around the corner, however it also showed a significant over-prediction in obtained values of consolidation strain, due to unsuitable assumptions made in the consolidation law employed. There was some evidence of reduced formability in the form of thickening around the radius of the part however, confirming the negative influence on formability of resistance to shear deformation.

Overall, the presented work has served to provide a solid foundation in characterising the fundamental behaviour of uncured carbon fibre prepreg in shear and bending.

The development and application of even relatively simple heuristic models has allowed a detailed analysis of how the individual components of the composite work together to create the overall response to shear and bending, allowing the tailoring of forming parameters and processes, along with the design of the laminate itself, in order to minimise the risk of defect formation.

APPENDIX A

EFFECTS OF PARTICULATE THERMOPLASTIC REINFORCEMENT ON INTERPLY SHEAR RESPONSE

Experimentation in Chapter 3 has focused on a single material, 8552/AS4. This is a second generation material, in which the resin matrix is predominantly thermoset, with solved thermoplastic resin added to improved toughness. The material was chosen partly due to it still being widely used and readily available, but also due to it acting as the precursor for a range of modern third generation prepregs consisting of a baseline resin system called M21 and some fibre. As discussed in Section 2.1.3 third generation prepregs have an additional particulate thermoplastic resin at the surface to limit resin flow, improving uniformity of resin distribution in the final part. Work by Larberg et al. [10] noted third generation prepreg to be significantly more resistant to interply shear than a second generation prepreg, warranting further investigation.

As part of a work package conducted for GKN aerospace, interply shear testing was conducted on a proprietary derivation of M21 in this case coupled with an IM7 fibre, in order that optimal manufacturing conditions might be confirmed for a consolidation process. Analysing these results using the model presented in Section 3.4 should provide some insight into the stiffer response, as well as confirming the process and model for a different material. As with 8552/AS4, the test program investigates the influence of

temperature, rate and pressure at the interface between two 0° plies.

The test methodology is identical to that described in Section 3.5, along with measures taken to ensure accuracy and repeatability of tests.

A.0.1 Results

Figure A-1 (Left) displays the critical shear stress τ_c against temperature, showing a minimum value at 80°C. Figure A-1 (Right) shows strain hardening parameter, H, against temperature, reaching a minimum at a temperature of 60°C.

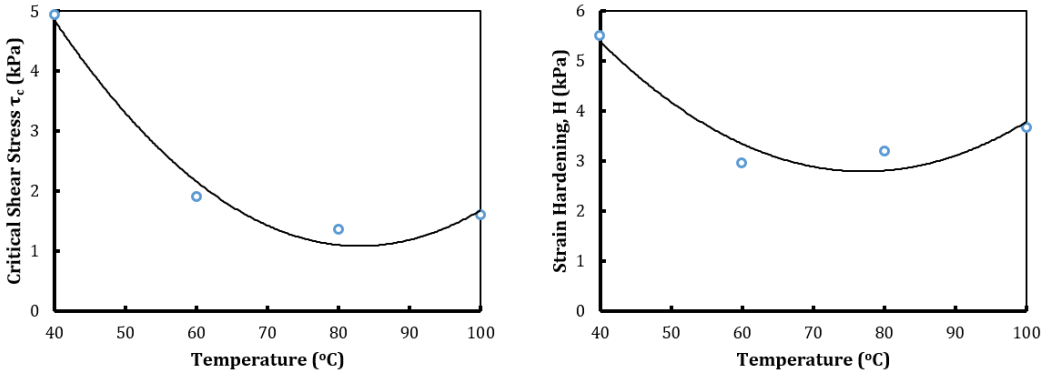

Figure A-1: *(Left) Plot of critical shear stress, τ_c, against temperature and (Right) Plot of strain hardening parameter against temperature.. Test conducted at rate $R = 0.1mm/min$ and normal pressure, σ_n, of 75kPa.*

The values of coefficient of friction, μ, and joint strength, j, calculated for each temperature are displayed in Table A.1. Typically, μ increases with temperature whilst j decreases. Table A.2 displays values of coefficient of viscosity, η, and rate independent modulus, S, for each temperature. Both values clearly reduce with temperature.

Temperature (°C)	**Rate (mm/min)**	μ	j **(kPa)**
40	0.1	0.017	3.82
60	0.1	0.018	0.59
80	0.1	0.021	0.12
100	0.1	0.022	0.02

Table A.1: *Values of coefficient of friction and joint strength for each temperature at a rate of 0.1mm/min. Each value was calculated from a number of different pressures [1].*

Temperature (°C)	η (MPa.s)	S (kPa)
40	12.02	39.47
60	6.32	24.63
80	3.00	15.64
100	3.22	13.88

Table A.2: *Coefficient of viscosity, η, and rate independent modulus, S, for the tested temperatures. Tests conducted at a normal pressure of 75kPa.*

A.0.2 Discussion

Inter-ply Yield

Critical shear stress is a vital parameter when considering slip in a laminate, denoting the point at which a laminate stops shearing as a relatively stiff single mass and instead deforms by the slipping of the constituent plies relative to one another with a significantly reduced stiffness. From a forming perspective this is of particular importance as a low critical shear stress will greatly improve the formability of the part. From Fig. A-1 we can see that the minimum value of τ_c is reached at 80°C. This finding has been corroborated with experience gathered at GKN Aerospace during the production complex components. Results gathered on 8552/AS4 suggested a slightly higher temperature of 90°C for that particular material, which is in keeping with the difference in rheology for the two materials, with M21 having a lower viscosity at 80°C than 8552.

Breaking down the value of τ_c using the Mohr-Coulomb equation we can see that μ increases with temperature whilst j decreases (Table A.1). The hypothesis presented in Section 3.7 is that this is due to the behaviour being resin dominated at lower temperatures when a thick band of resin exists at the ply interface, before becoming fibre dominated at higher temperatures when the resin redistributes to the fibre core as its viscosity lowers. Interestingly, the values of μ obtained for M21 are significantly higher than those for 8552 at lower temperatures. This suggests that the thermoplastic particulate reinforcement, which remains solid at processing temperatures, has a significant impact on the material behaviour, causing the response to be much more pressure dependent. The reduction in j values when compared to 8552/AS4 (0.12kPa at 80°C compared to 1.33kPa for 8552) is in keeping with the altered rheology of the material, with M21 being designed for use at lower temperatures than 8552, improving speed of production. The effects of this are also apparent when looking at the viscoelastic parameters, η and S. As with the results for 8552 both values decrease as temperature increases, however the drop in viscosity is significantly more rapid, whilst the values of elastic modulus are slightly larger. This change is modulus is most likely due to the rigid particulate reinforcement sitting in the resin layer stiffening the material response.

Strain Hardening Parameter

The change in the strain hardening parameter with temperature is the chief difference between the results for M21 and 8552. Figure 3-21 shows a peaked behaviour with a maximum value between 60 and 70°C. By contrast, M21 has an inverted behaviour, with a minimum value reached between 60 and 80°C. In Section 3.7 this behaviour is attributed to the viscosity of the resin. At low temperatures the resin is sufficiently viscous to allow a physical de-bond at the interface after yield. When the viscosity of the layer reduces, it starts to flow. This could allow some reformation of the joint, requiring it to be yielded again. As the viscosity lowers further the resin redistributes to the fibre core, thus reducing this tendency for joint reformation. By design the thermoplastic reinforcement alters this behaviour, specifically restricting resin flow during cure.This would prevent joint reformation at the optimum temperature range, reducing hardening. The increase in hardening with temperature seen after the minimum point is reached is consistent with the theory that hardening can also appear as a result of fibre intermingling, which increases as the resin redistributes to the fibre core. Whilst the fibres in a third generation prepreg are unlikely to come into contact, the particulate reinforcement itself will become increasingly embedded in the fibres, resulting in a different form of intermingling. With the exception of the strain hardening parameter, the general trend of results presented for M21 are not dissimilar to those for 8552, with the differences observed being expected as a result of the change in material composition and the rheology of the resins. The point of minimum resistance to yield is identified as one of the key parameters for forming, regardless of shear strain expected. For M21 this occurs at 80°C, and can be further improved by minimising rate of deformation and applied pressure, although pressure control can have coupled effects, as it is the principal driver for the forming mechanism, as is discussed in greater depth in Chapter 6.

REFERENCES

[1] J. S. Lightfoot, M. R. Wisnom and K. Potter. A new mechanism for the formation of ply wrinkles due to shear between plies, Composites, Part A 2013. 49:139-147.

[2] P. Hallander, M. Akermo, C. Mattei, M. Petersson and T. Nyman. An experimental study of mechanisms behind wrinkle development during forming of composite laminates, Composites Part A 2013. 50:54-64.

[3] T.J. Dodwell, R.Butler, and G. W. Hunt. Out-of-plane ply wrinkling defect during consolidation over an external radius, Composites Science and Technology 2014. 105:151-159.

[4] T. J. Dodwell. Internal buckling instabilities in layered media, Philosophical Magazine - Instabilities Across the Scales IV. 95 (28-30):3225-3243. DOI:10.1080/14786435.2015.1034221

[5] N. Ersoy, T. Garstka, K. Potter, M. R. Wisnom, D. Porter and G. Stringer. Modelling the spring-in phenomenon in curved parts made of a thermosetting composite, Composites Part A 2010. 41:410-418.

[6] A. R. A. Arafath, R. Vaziri and A. Poursartip. Closed-form solution for process-induced stresses and deformation of a composite part cured on a solid tool: part I - flat geometries, Composites Part A 2008. 39:1106-1117.

[7] T. A. Fletcher, R. Butler and T. J. Dodwell. Anti-symmetric laminates for improved consolidation and reduced warp of tapered C-sections, Advanced Manufacturing: Polymer and Composites Science. Accepted 2015.

[8] P. Boisse, N. Hamila, E. Vidal-Salle and F. Dumont. Simulation of wrinkling during textile composite reinforcement forming. Influence of tensil, in-plane shear and bending stiffnesses, Composites Science and Technology 2011. 71(5):683.

[9] N. Ersoy, K. Potter, M. R. Wisnom and M.J. Clegg. An experimental method to study the frictional processes during composites manufacturing, Composites Part A 2005. 36A:1536-1544.

[10] Y. R. Larberg and M. Akermo. On the interply friction of different generations of carbon/epoxy prepreg system, Composites: Part A 2011. 42:1067-1074.

[11] J. L. Gorczyca-Cole, J. A. Sherwood and J. Chen. A friction model for thermostamping comingled glass-polypropylene woven fabric, Composites Part A 2007. 38:393-406.

[12] G. W. Stachowiak and A. W. Batchelor. Engineering Tribology 2000, Butterwoth-Heinemann.

[13] W. Wieleba. The statistical correlation of the cefficient of friction and wear rate of PTFE composites with steel counterface roughness and hardness, Wear 2002. 252 9-10:719-719.

[14] A. Johnston, R. Vaziri and A. Poursartip. A plane strain model for process-induced deformation of laminated composite structures, Journal of Composite Materials 2000. 35:1435-1469.

[15] G. S. Springer. Resin flow during the cure of fiber reinforced composites, Journal of Composite Materials 1982. 16:400-410.

[16] P. Hubert, A. Johnston, A. Poursartip and K. Nelson. Cure kinetics and viscosity models for hexcel 8552 epoxy resin, International SAMPE symposium and exhibition 2014. 2341-2354.

[17] T. J. Dodwell, S. Erland and R. Butler. A Cosserat continuum model for uncured composite laminates with applications to ply wrinkle formation, 20^{th} International Conference on Composite Materials, Copenhagen, July 2015.

[18] K. Potter. In-plane and out-of-plane deformation properties of unidirectional preimpregnated reinforcement, Composites Part A 2002. 33:1469-1477.

[19] B. Liang, N. Hamila, M. Peillon and P. Boisse. Analysis of thermoplastic prepreg bending stiffness during manufacturing and of its influence on wrinkling simulations, Composites Part A 2014. 67:111-122.

[20] K. Potter. Understanding the origins of defects and variability in composites manufacture, 17^{th} International Conference on Composite Materials, Edinburgh, July 2009.

[21] G. Slayter. Method and aparatus for making glass wool, U.S. Patent 2,133,235 A, Issued November 11, 1933.

[22] K. L. Loewenstein. The manufacturing technology of continuous glass fibres, New York, Elsevier scientific, 1973.

[23] Aviation research and analysis report AR-2007-021, Fibre composite aircraft - capability and safety, Australian Transport Safety Bureau, 2008.

[24] High performance carbon fibres, National Historic Chemical Landmarks. American Chemical Society. Retrieved April 26, 2014.

[25] R. Bacon. Filamentary graphite and method for producing the same, U.S. Patent 2,957,756, Priority date March 18, 1958.

[26] R. B. Millington and R. C. Nordberg. Process for preparing carbon fibres, U.S. Patent 3,294,489 A, Priority date December 19, 1961.

[27] W. J. Cantwell and J. Morton. The impact resistance of composite materials - a review, Composites 1991. 22 (5):347-62.

[28] P. Harrison, M. J. Clifford and A. C. Long Shear characterisation of woven textile composites: a comparison between picture frame and bias extension experiments, Composites Science and Technology 2003. 64(10-11):1453-1465.

[29] A. S. Milani, J. A. Nemes, X. T. Pham and G. Lebrun. The effect of fibre misalignment on parameter determination using picture frame test, 14^{th} International Conference on Composite Materials, San Diego, July 2003.

[30] A. C. Long. Composites forming technologies, First Edition, Woodhead Publishing Limited, Cambridge, England.

[31] A. M. Murtagh. Characterisation of shearing and frictional behaviour in sheet-forming of thermoplastic composites, University of Limerick, 1995. PhD Thesis.

[32] Wilks CE. Processing technologies for woven glass/polypropylene composites, University of Nottingham, 2000. PhD Thesis.

[33] P. Scherer and K. Freidrich. Inter- and intraply-slip flow processes during thermoforming of CF/PP laminates, Composites Manufacturing, 1991. 2(2):92-96.

[34] C. Mack and H. M. Taylor. The fitting of woven cloth to surfaces, The Journal of the Textile Institute, 1956. 47:477-488.

[35] K. Potter. Beyond the pin-jointed net: Maximising the deformability of aligned continuous fibre reinforcements, Composites: Part A, 2002. 33:677-686.

[36] Y. R. Larberg, M. Akermo, and M. Norrby. On the in-plane deformability of unidirectional prepreg, Journal of Composite Materials, 2011. 0(0):1-11.

[37] J. Wang, R. Patton and J. R. Page. The Draping of woven fabric performs and prepregs for production of polymer composite components, Composites Part A, 1999. 30:757-765.

[38] C-L. Lai and W-B. Young. Modelling Fiber Slippage during the Preforming Process, Polymer Composites, 1999. 20/4:594-603.

[39] Y. R. Larberg. Deformability of Unidirectional Prepreg Materials, KTH Engineering Sciences, 2009. PhD Thesis.

[40] Dynamic Mechanical Analysis (DMA), A Beginner's Guide, PerkinElmer Inc, 2008.

[41] S.V. Lomov, I. Verpoest, M. Barburski and J. Laperre. Carbon composites based on multiaxial multiply stitched preforms. Part 2. KES-F characterisation of the deformability of the preforms at low loads, Composites Part A, 2003. 34(4):359-370.

[42] A. K. Pickett, G. Creech and P. de Luca. Simplified and advanced simulation methods for prediction of fabric draping, Revue europÃ©enne des Ã©lÃ©ments, 2005. (6):677-691.

[43] N. Lammens, M. Kersemans, G. Luyckx, W. V. Paepegem and J. Degrieck. Improved accuracy in the determination of flexural rigidity of textile fabrics by the Peirce cantilever test (ASTM D1388), Textile Research Journal, 2014. 84(12):1307-1314.

[44] R. H. Plaut. Formulas to determine fabric bending rigidity from simple tests, Textile Research Journal, 2015. 85(8) 884-894.

[45] S. G. Advani and E, M. Sozer. Process modeling in composites manufacturing, Marcel Dekker, Inc, 2002.

[46] Y. R. Larberg, M. Akermo and M. Norrby. On the in-plane deformability of cross-plied unidirectional prepreg, Journal of Composite Materials, 2012. 46(8):929-939.

[47] S. N. Monteiro, K. G. Satyanarayana; A. S. Ferreira, D.C. O. Nascimento, F. P. D. Lopes, I. L. A. Silva, A. B. Bevitori, W. P. Inacio, J. Bravo Neto and T.G. Portela. Selection of high strength natural fibers, Revista Materia, 2011. 15(4):488-505.

[48] M. Nielsen, A. T. Rhead and R. Butler. Structural efficiency via minimisation of elastic energy in damage tolerant laminates, ECCM $16-16^{th}$ European Conference on Composite Materials, Seville, Spain, $22-26^{th}$ June, 2014.

[49] N. G. McCrum, C. P. Buckley and C. B Bucknall. Principles of Polymer Engineering, Oxford University Press, 1988.

[50] D. Roylance. Engineering Viscoelasticity, Department of Materials Science and Engineering, Massachusetts Institute of Technology, 2001.

[51] M. A. Meyers and K. K. Chawla. Mechanical Behaviour of Materials, Cambridge University Press 2nd ed., 2009.

[52] Generating a Stribeck curve in a reciprocating test (HFRR/SRV-type test), Application Note #1004, Bruker Nano Surfaces Division, Campbell, CA, USA. Accessed 16/06/2016.

[53] D. Zhu, J. Wang and Q. J. Wang. On the Stribeck curves for lubricated counterformal contacts of rough surfaces, Journal of Tribology, 2015. 136(2)

[54] K. Johnson, S. Erland and R. Butler. The influence of fibre angle and resin properties on consolidation of curved laminates, ECCM $17-17^{th}$ European Conference on Composite Materials, Munich, Germany, $26-30^{th}$ June, 2016.

[55] P. P. Benham, R. J. Crawford and C. G. Armstrong. Mechanics of engineering materials, Harlow : Longman 2nd ed, 1996.

[56] S. P. Timoshenko and J. N. Goodier. Theory of elasticity, London : McGraw-Hill 3rd ed, 1970.

[57] F. T. Peirce. The "handle" of cloth as a measurable quantity, Journal of the Textile Institute Transactions, 1930. 21(9):377-416.

[58] S. P. Haanappel, R. H. W. ten Thije, U. Sachs, B. Rietman and R. Akkerman. Formability analyses of uni-directional and textile reinforced thermoplastics, Composites Part A, 2014. 56:80-92.

[59] V. Koissin. New evaluation method for Peirce cantilever test results, Leuven and Texcomp 11 Conference.

[60] T. Dodwell. Multilayered folding with constraints University of Bath, 2011. PhD Thesis.

[61] Maple 18, Version 18.02, Build ID 991181, 20/10/2014

[62] Gaussian process regression models, MathWorks Documentation R2016a, http://uk.mathworks.com/help/stats/gaussian-process-regression-models.html Accessed 25/08/2016

[63] E. Burnaev and M. Panov. Adaptive design of experiments based on Gaussian processes, Third International Symposium, Statistical Learning and Data Sciences. Egham, UK, April $20 - 23^{th}$, 2015.

[64] A. A. Giunta and L. T. Watson. A comparison of approximation modeling techniques: polynomial versus interpolating models, AIAA-98-4758

[65] S. M. Batill, J. E. Renaud and X. Gu. Modeling and simulation uncertainty in multidisciplinary design optimization, AIAA-2000-4803

[66] V. V. Fedorov. Design of spatial experiments: model fitting and prediction, Handbook of Statistics, Elsevier, Amsterdam, 1996. 515-553.

[67] E. H. Mansfield. The bending and stretching of plates, International Series of Monographs in Aeronautics and Astronautics, Solid and Structural Mechanics Divions, Vol. 6. Pergamon Press, 1964.

[68] A. Tessler. A refined zigzag beam theory for composite sandwich beams, Journal of Composite Materials, 2009. 43:1051-1081.

[69] D. Liu and X. Li. An overall view of laminate theories based on displacement hypothesis, Journal of Composite Materials, 1996. 30(14):1539-1561.

[70] C. T. Sun and J. M. Whitney. Theories for the dynamic response of laminated plates. AIAA Journal, 1973. 11(2):178-183.

[71] M. Di Sciuva. An improved shear-deformation theory for moderately thick multilayered anisotropic shells and plates, Journal of Applied Mechanics, 1987. 54:589-596.

[72] J. Sun, M. Li, Y. Gu, D. Zhang, Y. Li and Z. Zhang. Interply friction of carbon fiber/epoxy prepreg stacks under different processing conditions, Journal of Composite Materials, 2013.

[73] L. K. Grunenfelder, T. Centea, P. Hubert and S. R. Nutt. Effect of room-temperature out-time on tow impregnation in an out-of-autoclave prepreg, Composites Part A, 2013. 45:119-127.

[74] T. Centea, L. K. Grunenfelder and S. R. Nutt. A review of out-of-autoclave prepregs - material properties, process phenomena, and manufacturing considerations, Composites Part A, 2015. 70:132-154.

[75] S. Thomas, C. Bongiovanni and S. R. Nutt. In situ estimation of through-thickness resin flow using ultrasound, Composites Part A, 2008. 69:3093-3098.

[76] S. Thomas and S. R. Nutt. Temperature dependence of resin flow infusion (RFI) process by ultrasound imaging, Applied Composite Materials, 2009. 16:183-196.

[77] T. Centea and P. Hubert. Modelling the effect of material properties and process parameters on tow impregnation in out-of-autoclave prepregs, Composites Part A, 2012. 43:1505-1513.

[78] L. K. Grunenfelder and S. R. Nutt. Air removal in VBO prepreg laminates: effects of breathe-out distance and direction, Proceedings of the 43rd International SAMPE Technical Conference. Fort Worth, TX: Society for the Advancement of Material and Process Engineering; 2011.

[79] J. Kratz and P. Hubert. Anisotropic air permeability in out-of-autoclave prepregs: effect on honeycomb panel evacuation prior to cure. Composites Part A, 2013. 49:179-91.

[80] J. Kratz, T. Centea and P. Hubert. Air permeability of out-of-autoclave honeycomb structures during processing. Proceedings of the 26th Annual Technical Conference, American Society for Composites

[81] MATLAB and Statistics Toolbox Release 2015b, The MathWorks, Inc., Natick, Massachusetts, United States.

[82] W. Young. Resin flow analysis in the consolidation of multi-directional laminated composites, Polymer Composites, 1995. 16(3):250-257.

[83] A. Poursartip, G. Riahi, L. Frederick and X. Lin. A method to determine resin flow during curing of composite laminates, Polymer Composites, 1992. 13(1):58-65.

[84] X. Yan. Finite element modeling of consolidation of composite laminates, Acta Mechanica Sinica, 22(1):62-67

[85] Handbook of composites, Second edition. Chapman and Hall, London, 1998.

[86] A.T. Nettles. Basic mechanics of laminated composite plates, NASA Reference Publication 1351, 1994.

[87] R. Dave, J. L. Kardos and M. P. Dudukovic. A model for resin flow during composite processing: part 1 - general mathematical development, Polymer Composites, 1987. 8(1):29-38

[88] R. Dave, J. L. Kardos and M. P. Dudukovic. A model for resin flow during composite processing: part 1 - Numerical analysis for unidirectional graphite/epoxy laminates, Polymer Composites, 1987. 8(2):123-132.

[89] P. Hubert and A. Poursartip. A method for the direct measurement of the fibre bed compaction curve of composite prepregs, Composites Part A, 2001. 32:179-187.

[90] P. A. O'Connell and G. B. Mckenna. Encyclopedia of Polymer Science and Technology. John Wiley and Sons, Inc.

[91] P. Hubert, P. Vaziri and A. Poursartip. A two dimesional flow model for the process simulation of complex shape composite laminates. International Journal for Numerical Methods in Engineering, 1999. 44:1-26.

[92] P. Hubert. Aspects of flow and compaction of laminated composite shapes during cure. University of British Columbia, 1996. PhD Thesis

[93] J. Sjollander, P. Hallander and M. Akermo. Forming induced wrinkling of composite laminates: A numerical study on wrinkling mechanisms. Composites Part A, 2016. 81:41-51.

[94] L. Liu, B. Zhang, D. Wang and Z. Wu. Effects of cure cycles on void content and mechanical properties of composite laminates Composite Structures, 2006. 73:303-309

A.1 Personal Works

[95] S. Erland, T. J. Dodwell and R. Butler. Characterisation of inter-ply shear in uncured carbon fibre pre-preg, Composites Part A, 2015. 77:210-218

[96] S. Erland, T. J. Dodwell and R. Butler. Inter and intra-ply shearing of uncured carbon fibre laminates, ECCM $16-16^{th}$ European Conference on Composite Materials, Seville, Spain, $22-26^{th}$ June, 2014.

[97] S. Erland, T. J. Dodwell and R. Butler. Viscoelastic inter-ply slip in uncured laminates: Experimental characterisation and modelling, ICCM $20-20^{th}$ International Conference on Composite Materials, Copenhagen, Denmark, $19-24^{th}$ July, 2015.

[98] S. Erland, T. J. Dodwell and R. Butler. The influence of fibre angle and resin properties on uncured interply shear, ECCM $17-17^{th}$ European Conference on Composite Materials, Munich, Germany, $26-30^{th}$ June, 2016.